

**Optimal Sub-Pixel arrangements and coding for
ultra-high resolution three-dimensional OLED displays**

by

Zhivko Yordanov

A doctoral dissertation submitted as partial fulfilment
for the award of the academic degree of

Doctor of Engineering Sciences
(Dr.-Ing.)

Faculty of Electrical and Computer Engineering
of the University Kassel

2007

Supervisors:

1. Prof. Dr.-Ing. Siegbert Hentschke
2. Prof. Dr. Ivo W. Rangelow
3. Prof. Assen Nedev

Examination Board:

1. Prof. Dr.-Ing. Siegbert Hentschke
2. Prof. Dr. Ivo W. Rangelow
3. Prof. Dr.-Ing. Josef Börcsök
4. Prof. Dr.-Ing. Wolf-Jürgen Becker

Day of the Oral Examination:

27 July 2007

*To my wife and my daughter,
to whom I promised this a few years ago.
They fully supported me to conclude it
during weekends and holidays.
I promise I will not do anything like this again!*

*To my parents,
who would have liked to see it finished.*

Table of Contents

1. INTRODUCTION	9
1.1 GENESIS	9
1.2 AIMS AND OBJECTIVES	11
1.3 SUMMARIES AND LAYOUT OF THESIS	13
1.4 SUMMARY	13
2. BACKGROUND THEORY AND LITERATURE REVIEW	15
2.1 DIFFERENT PRINCIPLES OF 3D IMAGES PRESENTATION	15
2.2 CURRENT CONDITIONS OF THE STEREOSCOPIC DISPLAY TECHNIQUE	21
2.3 WHY OLED?	23
2.4 PRINCIPLE OF MULTI-VIEWER AUTOSTEREOSCOPIC 3D DISPLAY	24
2.4.1 <i>Parallax barrier stereogram</i>	25
2.4.2 <i>Optical lens array</i>	28
2.4.3 <i>Viewing zones in a 3D image of pixels, formed by optical plate</i>	30
2.4.4 <i>Image depth ranges, achievable with parallax barrier mask and lens arrays</i>	36
2.5 PSYCHOLOGICAL BASICS OF THREE-DIMENSIONAL PERCEPTION	38
2.6 SUMMARY	42
3. DEVICE COMPONENTS, DESIGN AND PROCESSING.....	43
3.1 INTRODUCTION AND USES OF ORGANIC LIGHT EMITTING DIODE (OLED)	43
3.1.1 <i>Introduction</i>	43
3.1.2 <i>Structure of an OLED</i>	45
3.1.3 <i>Working principle of OLED</i>	46
3.1.4 <i>Comparison between LED and OLED working principles</i>	48
3.1.5 <i>OLED display technologies</i>	51
3.2 INTRODUCTION AND USES OF INDIUM-TIN OXIDE (ITO).....	57
3.2.1 <i>Patterning ITO</i>	58
3.2.2 <i>Spin-On Method</i>	58
3.2.3 <i>Photolithography</i>	59
3.2.4 <i>Etching of ITO</i>	60
3.2.5 <i>Metallization and Ohmic Contacts – Lift-off Process</i>	62
3.2.6 <i>Measurement and Analysis techniques</i>	64
3.3 LENS-RASTER GLASSES	66
3.4 SUMMARY	67
4. MULTIPERSPECTIVE MIXING ALGORITHM. DIGITAL AND BINARY 3D SUB-PIXEL ARRANGEMENTS.....	68
4.1 MULTIPERSPECTIVE MIXING ALGORITHM.....	68
4.2 DIGITAL AND BINARY 3D SUB-PIXEL ARRANGEMENTS.	69
4.2.1 <i>Controlling through pixel illumination</i>	69
4.2.2 <i>Controlling through distribution of pixel parts</i>	71
4.2.3 <i>Controlling through dynamic pixel size variation</i>	73
4.3 SUMMARY	77
5. PREPARING OF WORKING SAMPLES AND HOUSING. MEASUREMENTS AND ANALYSIS	78
5.1 PREPARING OF WORKING SAMPLE	78

5.1.1	<i>Sample for determination of the maximal Achievable resolution</i>	78
5.1.2	<i>Sample for determination of the structure homogeneity and reliability</i>	90
5.1.3	<i>3D-Sample – sub pixel arrangements</i>	92
5.1.4	<i>Pixel arrangements with using of additional passive layer</i>	96
5.2	ADVANTAGES, PROBLEMS AND LIMITATIONS.	97
5.3	HOUSING AND CONTROL OF OLED DEMONSTRATORS.	98
5.4	SUMMARY	99
6.	OPTIMISATIONS OF THE VISUAL QUALITY AND SUGGESTIONS FOR FUTURE DEVELOPMENT	100
6.1	ACTIVE MATRIX ORGANIC LIGHT EMISSIVE DIODE	100
7.	3D IMAGE CODING FOR REAL TIME TRANSMISSION - SUGGESTION FOR CODING ALGORITHMS	103
7.1	INTRODUCTION TO MEDIA CODING ALGORITHMS.....	103
7.2	CODECS WITH QUALITY DAMAGE.....	104
7.3	CODECS WITHOUT QUALITY DAMAGE	105
8.	CONCLUSIONS	106
9.	APPENDIXES	108
	REFERENCES	125

1. Introduction

1.1 Genesis

Information display technology is a rapidly growing research and development field. Resolutions of TFT displays are increasing rapidly and the flat panel liquid crystal display market has grown from 29 Billion US\$ in 2002 to 52 Billion US\$ in 2006. However, for Multi View three dimensional applications higher resolution through increased number of pixels are needed, because – in comparison with the traditional 2-dimensional representation, there is a further dimension, the depth. Using state-of-the-art technology, optical resolution can be increased dramatically by organic light-emitting diode - since the light emitting layer is very thin, under 100nm. The main question is what pixel size is achievable technologically? The next generation of display will consider three-dimensional image display. In 2D¹, one is considering vertical and horizontal resolutions. In 3D² or holographic images, there is another dimension – depth. Because of the specific location of the human eyes (positioned horizontally), the “depth” dimension can be estimated in the horizontal plane. The major requirement is the high resolution horizontal dimension in order to sustain the third dimension using special lenticular glass or barrier masks, separate views for each eye. These lenses separate many perspectives to the eyes of the observer. The high-resolution 3D display offers hundreds of more different views of objects or landscape. The optical principle of three-dimensional representation of objects is based on a lenticular structure of vertical cylindrical lenses. This technology can be used in many fields: medicine (distance 3D consultations and operations, 3D observing diagnostics etc.); data visualization (CAD³/CAM⁴ design, chemical and genetic molecular modelling, biology etc.); entertainment (3D movie, 3D games, 3D imaging); military (visual demonstrations of strategic deployment, volumetric simulations of training flight, in-progress tactical operation development. etc.); cartography and meteorology (geographic information systems, weather forecasting, volcano and earthquake modelling, eruption predictions, etc.); industry (3D precise modelling of engine

¹ Two-dimensional

² Three-dimensional

³ Computer Aided Design

⁴ Computer Aided Manufacturing

details, space and aircraft design simulations, etc.); architecture (interior and exterior design, structural analysis, building modelling etc.). Currently there are some technologies for presenting the information in three-dimensions:

- **Holographic Method**

Conventional holograms are made by splitting a laser beam into two, reflecting one of the resulting beams (aptly named the "object" beam) off the object, recombining the two and exposing the result on a piece of photographic film. The interference between the two sub-beams produces a pattern on the film which when developed and illuminated reveals a three-dimensional picture of the original object. The process is long, complicated and requires the use of expensive high-powered lasers, making it impractical for widespread commercial use. Unfortunately it also results in holographic images of limited size, colour, quality and viewing angle.

- **3D Pixels (voxels)**

Series of algorithms transform 3D data in format, which reproduces them in three dimensions. Subsequently, the projector represents this data with frequency in the range of 5000 sequences/sec on the rotating screen inside a transparent sphere. As a result, human eyes can observe 3D image. However, this technology offers very small images with eight colours and not very good brightness or contrast.

- **Stereoscopic Method.**

There are two main types:

1. First, that uses glasses (colour filters, polarizing filters, and shutter glasses). Depending on the type of equipment the quality is relative. From very bad – in colour filters to excellent in glasses with polarization filter. All of them have one general disadvantage – the observer needs additional glasses or device mounted on the head for separating the perspectives.

2. The second type is the so-called **Autostereoscopic Display** and works without the use of additional glasses – holographic screen, lenticular glass, or barrier masks. To create a 3D image, the left and right eye must see slightly different images. The available autostereoscopic 3D screens use series of fine vertical bars or lenses to direct the two images correctly onto each eye. These technologies are more useful because they allow the creation of large size images, without glasses and there are no limitations on colours. This work is

devoted to creating a very-high resolution three-dimensional display based on the autostereoscopic display type without the use of additional glasses.

A very strong candidate for the realization of such type of 3D displays is the OLED⁵ (Organic Light-Emitting Diodes) technology. OLEDs have potential to be a key technology for information displays in the future. The display technology presented in this work promises to bring into use bright colour 3D flat panel displays in a unique way. Unlike the conventional TFT⁶ matrix, OLED displays have constant brightness and colour, independent from the viewing angle i.e. the observer's position in front of the screen. A sandwich (just 0.1 micron thick) of organic thin films between two conductors makes an OLE Display device. These special materials are named electroluminescent organic semi-conductors (or organic photoconductors (OPC⁷)). When electrical current is applied, a bright light is emitted (electrophosphorescence) from the formed Organic Light-Emitting Diode. Usually for OLED an ITO⁸ layer is used as a transparent electrode. Such types of displays were the first for volume manufacture and only a few products are available in the market at present. The key challenges that OLED technology faces in the application areas are: (i) producing high-quality white light (ii) achieving low manufacturing costs (iii) increasing efficiency and lifetime at high brightness. Looking towards the future, by combining OLED with specially constructed surface lenses and proper image management software it will be possible to achieve 3D images.

1.2 Aims and Objectives

The main goal is to develop a technology platform of lightweight, portable, and flexible 3D flat panel display with passive matrix, that provides easy to read visual imagery, vibrancy in colour and low power consumption. In addition, it is also a aim to develop a working sample that demonstrates the principle. The display is autostereoscopic, i.e. it must work without additional mounted equipment on the observer's head. As a source technology, I have taken advantage of earlier

⁵ Organic Light Emissive Diode

⁶ Thin Film Transistor

⁷ Organic Photoconductors

⁸ Indium Tin Oxide

experiences of the Institut für Periphere Mikroelektronik – University of Kassel, based on one hundred perspective half-holographic picture. In order to increase the visual quality and improve the comfortable multi-user observation, a rearrangement of the pixel sequence has to be made. These 3D display samples are based on a 3" inch sized glass base. The department Institut für Nanostrukturtechnologie und Analytik – University of Kassel has the capacity to work with silicon or glass up to 3.5 inches. The OLED deposition is possible in Fraunhofer Gesellschaft Golm.

The process has to undergo some new research steps because the OLED technology is very different in its nature of a well known TFT. For fulfilment of high-quality 3D picture, pixel arrangement can be very easily modified. Having in mind this goal at first, the best possibilities have been investigated and then optimized.

As a very first step, wafer design with test structures was initiated, based on ITO layers. These wafers are thick with polymer coating. With the aid of these samples the highest possible resolution, homogeneity of the emitted light and the possibility for contacting with conductive layer is determined. For this purpose glass plates, based on indium-tin-oxides (ITO) electrodes are used. Before procuring etching masks, the physical borders of the quality of the obtained picture have to be analysed. There are some fundamental limitations in the quality of the conductive layer, owing to physical limitations of photolithography, etching-process and homogeneity and crystal structure of the ITO material. These limitations can be determined through optical and electrical measurement and evaluation of the test fields. Finally the OLED deposition requirements have been checked for the achieved screen resolution. On the basis of the collected information it is necessary to make a second test series. If it is necessary, some corrections in the etching process must be carried out. With the second wafer series, the results for homogeneity and quantity of the errors in ITO and OLED layers have been ascertained. The results from these two series of samples have been important before undertaking the subsequent steps.

The second step is developing and program special algorithms for arrangement of the subpixels on the layer. Ahead of the algorithm there are some important requirements. Some of its parameters are as follows:

- Mixture of different observers' perspectives;
- Generate the pixel / subpixel sequence from the mixed scene;

- Generate an optimized script for the software, generated lithography mask;
- Assure possibility for easily changing the parameters of the scene: lens raster parameters, pixel parameters, observer's distance, etc;
- Speed.

Following the manufacture of the first samples the results have been analysed and an estimation of the successful pixel combination have been made. For achieving a very high colour pixel resolution, further enhancements are necessary. In order to study the resolution limits, test samples have been designed and produced by applying a polymer organic material.

1.3 Summaries and Layout of Thesis

In the second chapter of the thesis, background theories along with relevant literature survey have been presented. Then chapter three follows which gives a description of the specific components in OLED displays (ITO wafers, polymers, contacting etc.) and the specifics of mixing and coding algorithms of pixel displacement for high resolution 3D displays. The chapter also contains a thorough description of all the processing steps involved in the fabrication of the device. Chapters four and five deal with the steps of designing and examining the first set of experimental prototypes. These are the results concerning the physical limitations of the technology processes – lithography on ITO and polymer. In chapters six and seven are given some suggestions for the improvement of the achieved visual quality and the special features of the 3D displays used in *application specific* devices. Finally there is an introduction of compressing algorithms for decreasing volume of 3D image data stream. The different ways for image size without quality loss are observed. Chapter eight presents the conclusion for the work and list of suggestions are given.

A list of used relevant literature and publications are given in Appendix part.

1.4 Summary

This chapter presented the genesis of the three-dimensional displays and the aims and objectives of this PhD work.

2. Background theory and Literature Review

2.1 Different principles of 3D images presentation

Stereoscopic film and static pictures have been a reality for many years on the market. In most cases these are devices using additional glasses on the observer's head. Given below is a brief description of a few basic and often used 3D image principles.

- **Polarizing^{9 10 11 12 13} sheets.**

These devices separate the perspectives exactly, according to the left or right eye. Usually there are either horizontal-vertical or diagonal polarizing sheets, and the user wears polarized glasses that distribute the correct view to each eye (Fig. 2.1). Polarizing filters can also be attached to glass-mounted slides. Incorrect positioning of the projectors in relation to the screen can cause keystone, where the image is trapezoidal shaped due to foreshortening, resulting in vertical parallax. If more than one projector is used, for example, orthogonal polarizing filters are placed in front of each projector and both left and right eye images are projected onto a non-depolarizing screen simultaneously. Hence, the technique is time-parallel. The audience wears passive glasses in this case. Using more than one projector always brings with it the difficulties of adjusting the images. L/R¹⁴ views may be correctly registered; there must be minimal luminosity differences, minimal size differences, minimal keystone, minimal vertical parallax, minimal ghosting, and so forth.

⁹ Principles of Optics, 7th edition, M. Born & E. Wolf, Cambridge University, 1999, ISBN 0-521-64222-1

¹⁰ Fundamentals of polarized light : a statistical optics approach, C. Brosseau, Wiley, 1998, ISBN 0-471-14302-2

¹¹ Field Guide to Polarization, Edward Collett, SPIE Field Guides vol. FG05, SPIE, 2005, ISBN 0-8194-5868-6

¹² Polarization Optics in Telecommunications, Jay N. Damask, Springer 2004, ISBN 0-387-22493-9

¹³ Optics, 4th edition, Eugene Hecht, Addison Wesley 2002, ISBN 0-8053-8566-5

¹⁴ Left / Right

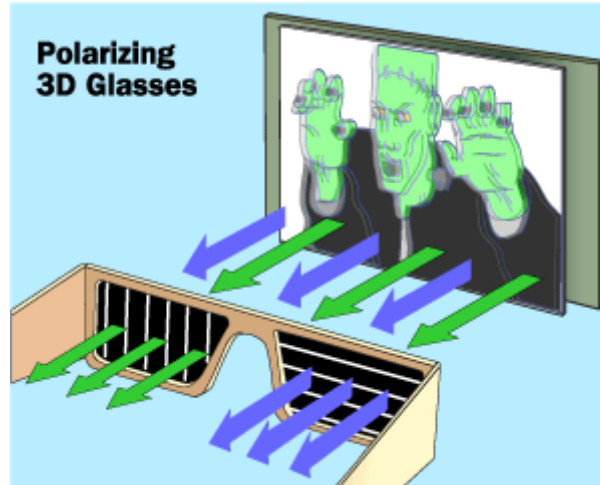


Fig. 2.1 3D viewing method, using polarizing glasses

- **Anaglyphs¹⁵.**

The anaglyphic method has been in use for years to represent stereo pairs and it was a salient technique in old 3D movies and comic books. Coloured filters cover each eye, red/green, red/blue or red/cyan filters being the most common. One eye image is displayed in red and the other one in green, blue or cyan so that the appropriate eye sees the correct image (Fig. 2.2). Since both images appear simultaneously, it is a time-parallel method. The technique is easy to produce using simple image processing techniques and the cost of viewing glasses is very low. Greyscale images are most common. Pseudo colour or poly-chromatic anaglyphs are becoming more common. If correctly done, anaglyphs can be an effective method for presenting stereo images, but with relatively low colour and contrast quality.

¹⁵ Method of encoding a three-dimensional image in a single picture by superimposing a pair of pictures

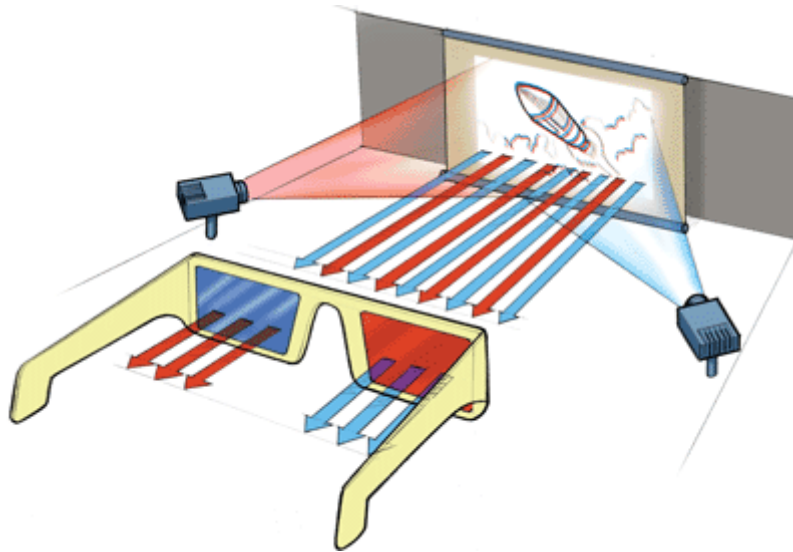


Fig. 2.2 3D viewing method, using a red-blue anaglyph

- **ChromaDepth¹⁶.**

Chromostereoscopy is a phenomenon in optics commercialized by Richard Steenblik [3]. The technique originally used double prism-based glasses, which slightly deflects different colours in an image, laterally displacing the visual position of different - colour regions of the image in different amounts. The prisms are oriented in opposite directions of each eye, thus presenting different images to each eye and creating a stereo pair. The produced chromo stereoscopic glasses, found in the market under the name of ChromaDepth 3D, utilize a unique micro optic film that performs the same optical function as double prism optics without the attendant weight and cost. Images designed for viewing with the help of the ChromaDepth 3D Glasses use colour to encode depth information. A number of colour palettes have been successfully employed, the simplest of which is the RGB on Black palette: on a black background red will appear closest, green in the middle ground, and blue at the background. Reversal of the optics results in the opposite depth palette: BGR on Black. A peculiar feature of the ChromaDepth 3-D process is that the user does not have to create a stereo pair. A single ChromaDepth 3-D colour image contains X, Y, and Z information by virtue of the image contrast and the image colours. The

¹⁶ <http://www.chromatek.com/>

observed by the user stereo pair is created by the passive optics in the ChromaDepth 3-D Glasses. The basic limitation of the ChromaDepth 3-D Process is that the colours in an image cannot be arbitrary if they are to carry the image's Z dimension, so the method will not work on arbitrary images. The best effects are achieved with images that are specifically designed for the process as well as with natural images, such as underwater reef photographs, that have natural colouring fitting in the required palette.

- **Vectographs¹⁷.**

Edwin Land introduced Polaroid's Vectograph process in 1940. The earliest Vectograph images used widely were black-and-white polarizing images formed by iodine ink which applied image wisely to opposite oriented polyvinyl alcohol (PVA) layers laminated to opposite sides of a transparent base material. The iodine forms short polymeric chains that readily align with the oriented polymeric molecules and stain the sheet. The chemistry is analogous to that of uniformly stained iodine polarizers, such as Polaroid H-sheet, used in polarizing filters for stereo projection and in 3D glasses used for viewing stereoscopic images [8].

In 1953 Land demonstrated three-color Vectograph images formed by successive transfer of cyan, magenta, and yellow dichroic dyes from gelatine relief images to Vectograph sheet. Unlike StereoJet digital inkjet printing described below, preparation of Vectograph colour images required undertaking long, critical photographic and dye transfer steps. Although the process produced excellent images, it never made its way to the market.

- **Field Sequential Devices.**

There are many manufacturers of active and passive glasses systems. The shutter transition occurs within the vertical blanking period of the display device and is all but invisible. The main advantage of such shutters is the dynamic range, which is the ratio of the transmission of the shutter in its open and closed state (Fig. 2.1). The transmission of the shutters is

¹⁷ Kind of stereoscopic technology that uses polarized glasses to view a three-dimensional photographic image embedded in a plastic sheet

commonly 32%, but because of the 50% duty cycle the effective transmission is half of that. Their transmission should be neutral and impart little colour shift to the image under view. The field of view (FOV) varies also. Ninety-seven degrees is the regular one. SGI¹⁸ can operate at a speed of up to 200 fields per second.

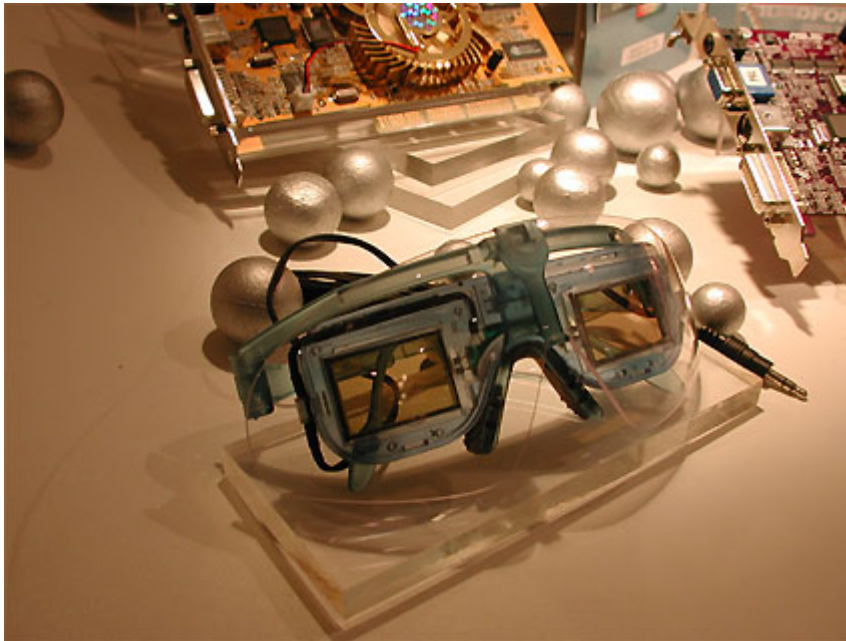


Fig. 2.3 3D viewing method, using PC shutter-glasses

Passive systems have a lower dynamic range than active eyewear systems. The phosphor afterglow on the CRT¹⁹ causes ghosting, or image cross talk, in this type of system. In order to minimize the time that the modulator is passing an unwanted image, electrode-segmentation can be used. The modulator's segment changes state moments before the CRT's scanning beam arrives at that portion of the screen. As a consequence of this action the modulator changes state just as the information is changing. This increases the effective dynamic range of the system and produces a high quality stereo image.

¹⁸ Silicon Graphics, Inc.

¹⁹ Cathode Ray Tube

The personal computers not supplied with a stereo sync output, can use the above-and-below format. The left image is placed on top half of the CRT screen and the right image on the bottom half, thus reducing the resolution of the image. Now, the stereo information is a reality but it needs an appropriate way to send each L/R image to the proper eye. One way to achieve it is to connect an external unit to the computer's monitor connector and intercept the vertical sync signal. When there is an option the unit adds an extra vertical sync pulse halfway between the existing pulses. The result causes the monitor to double again the original rate. This in effect stretches the two images to appear on the whole screen and show field sequential stereo.

- **The Sanyo Display.**

The Sanyo display uses LC technology for both image presentation and a parallax barrier [11]. Since the thermal expansion coefficients are the same, registration is maintained in different operation conditions. They call the parallax barrier part of the display the "image splitter". It uses two image splitters, one on each side of the LC (image presentation) panel Fig. 2.1.

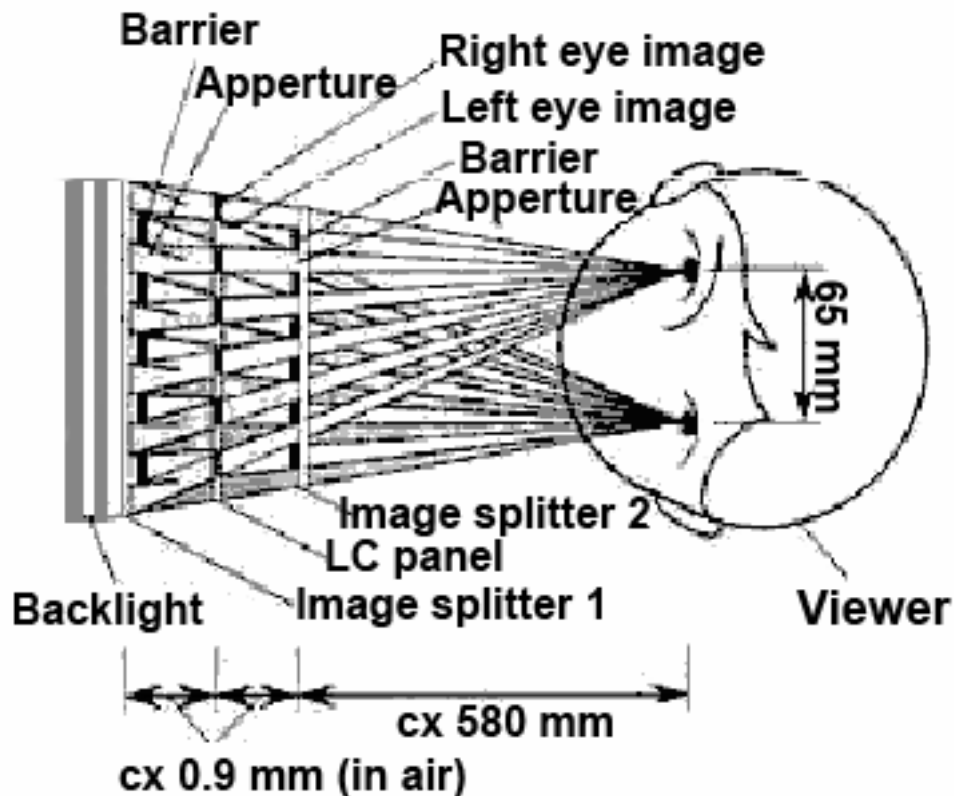


Fig. 2.4 A double image splitter

On the splitter on the backlight is evaporated two thin film layers; aluminium and chromium oxide. Etching provides the vertical stripes. The stripe pitch is slightly larger than twice the dot pitch of the LC panel.

The viewer-side splitter is a low-reflection layer. The stripe pitch is slightly smaller than twice the dot pitch on the LC image presentation panel. Each slit corresponds to a column of the LC panel. It is claimed that the technique produces no ghosting.

2.2 Current conditions of the Stereoscopic display technique

3D display methods have long attracted the attention of a lot of researchers. Although their current application is yet limited to certain industrial or medical applications, advertisements and home entertainment are among the potential application-consumers in the future. Most of them are classified as autostereoscopic displays, which do not require special 3D glasses, but

nevertheless restrict the location of the observers and the field of viewing. One of the methods suggests controlling the viewing field with relation to the position of the observer's head. A multi-viewpoint application is also possible by increasing of images spatially. With these multi-view points, the image will change with the observer's head following it, thus meeting the requirements of motion parallax to some degree.

When a lenticular²⁰ lens is combined with a colour LCD that has the RGB vertical stripe arrangement, chromatic separation will occur even if the observation point is correct. To solve this problem, a display using a mask with a special chequered pattern has been developed [12]. An input image of this display is a superimposed image with lateral stripes rather than one with vertical stripes. Pictures of such a kind are compatible with video software used in the field-sequential method.

A display with a parallax barrier is also applied to stereoscopic imaging. However, it is more difficult with this method to secure necessary brightness than with the display using lenticular lens array. Several improvements to resolve this problem have been made. In one example [13], a slip barrier is placed between the liquid crystal panel and the backlight side. It is reported that this arrangement increased the brightness on both sides by 1.4 times.

A new development of an experimental stereoscopic LCD using this parallax barrier is the system [16], which uses two joint LC panels, one serving as an image display plane and the other one as a slit barrier. Since slit barrier patterns can be freely controlled with this structure, we can have an arbitrary number of viewing points from two eyes to multiple viewing points. It is also possible to make the barrier mask or the screen's image follow the movement of the head, and to display 2D images at full resolution by removing the barrier altogether. There are certain ways to reduce moiré and crosstalk, including a double-barrier structure with a LC panel in between by means of a type of 3D display panel with a head-tracking system [17].

At Heinrich-Hertz Institut, Germany a variety of autostereoscopic displays are being developed [19], including projection systems and flat panel displays using a lenticular glass screen. Making the pitch of the lenticular sheet correspond to each colour of subpixel²¹ of RGB rather than to every single pixel can eliminate the

²⁰ Single convex lens that magnifies light through a prism effect

²¹ Handles a single color channel

chromatic separation, which occurs because of the RGB vertical stripe arrangement in an LCD. These stereoscopic displays use head-tracking systems according to their purpose.

2.3 Why OLED?

In recent years, organic light-emitting devices have made tremendous progress. They are now making their progress as the leading innovation among lots of technologies under development for next generation flat panel displays. The OLEDs have many advantages compared to other flat displays – TFT and STN²².

Some of them are:

- With simple construction
- Thin
- Better viewing angle (more than 160°)(Fig. 2.5)
- Saturated emissive colours
- Low power consumption
- Plastic can be used as a substrate

²² Super-twisted nematic

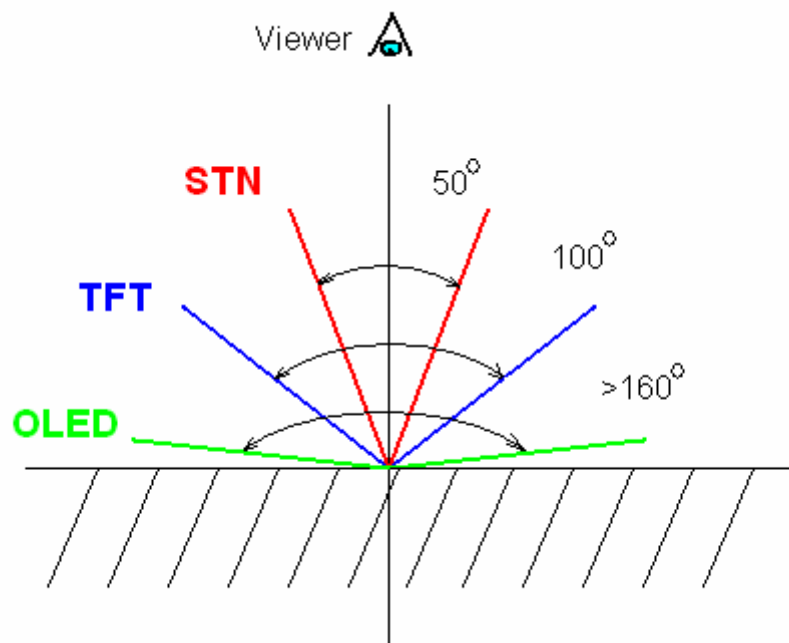


Fig. 2.5 Viewing angle of different flat panel technologies

Another big advantage of OLEDs is the time of reaction of the pixels.

2.4 Principle of multi-viewer autostereoscopic 3D display

On a flat panel with very high resolution (display or printout) with an accurate pixel arrangement under precise positioning, the lenticular lens raster can achieve multi-perspective **Autostereoscopic** display. The term autostereoscopy is usually made use of to refer to a system that enables stereoscopic images to be viewed without the help of a stereoscope, additional devices at the head or some other similar devices. In fact, all such systems do contain some kind of optical device that enables the 3D image to be reconstructed, but the essential difference between an autostereoscopic system and a conventional two-image one is that the optical aid is incorporated into image or the screen, rather than being used in the form of a separate item worn or handled by the observer. Free viewing is rather different because there is no certainty that a particular spectator will be able to see a 3D image, if he has not practised the techniques required.

2.4.1 Parallax²³ barrier stereogram

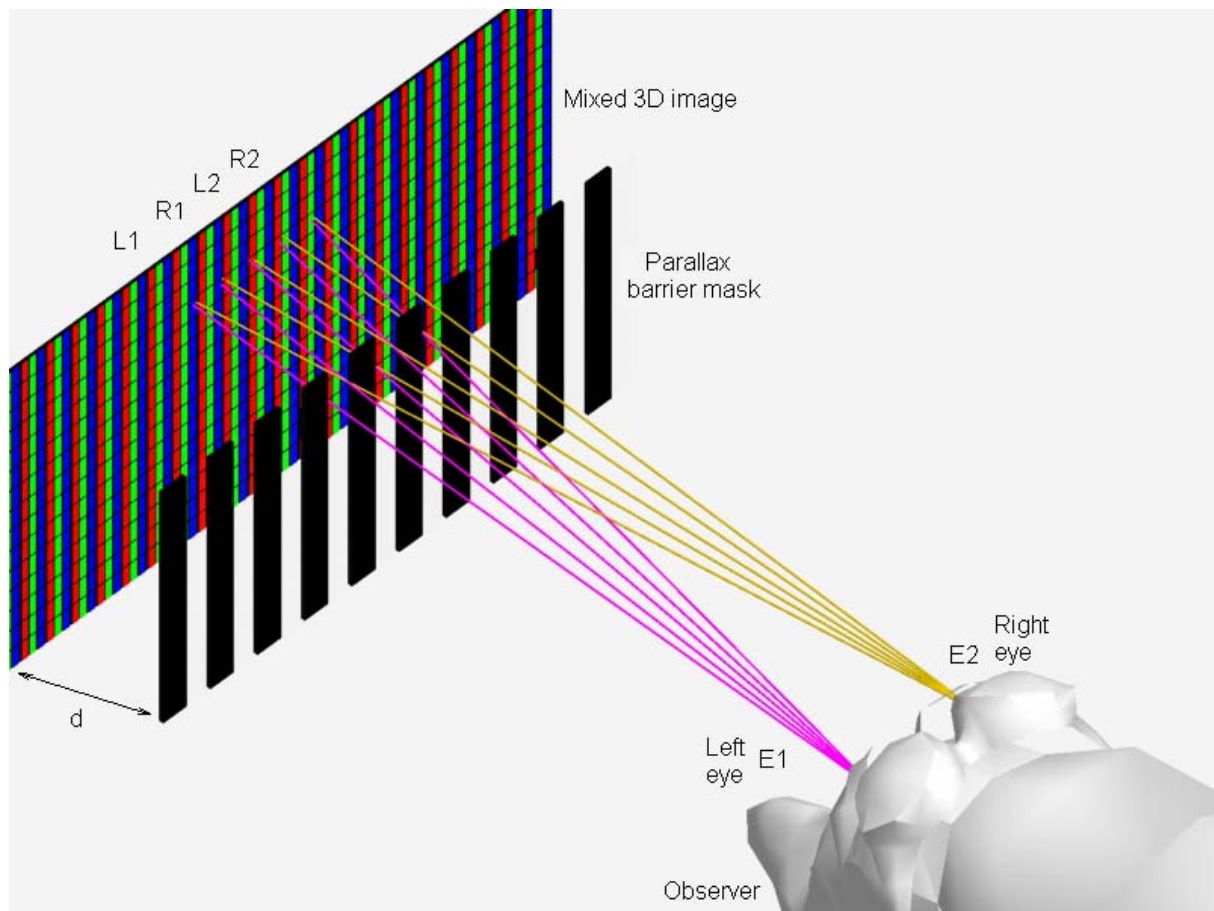


Fig. 2.6 The raster principle. With correct positioning of the parallax barrier mask in front of the composed image of alternating left and right stripes, each eye can see only the correct image.

The simplest principle to get a multi-user autostereoscopic image is to use raster barrier mask in front of one high-resolution display with correct displacement of the pixel raster (Fig. 2.6) [27]. Such type 3D display forms the basis of the majority of autostereoscopic viewing systems. Raster is a term borrowed from the world of television, where it is the term used to define the pattern of horizontal lines, traced by an electron beam as it scans the screen. CRTs are not workable because usually the geometry of the picture is irregular and the measures are individual for each different device. Technically it is more suitable and the results are better by using TFT, plasma, or OLED displays. These displays have exactly placed pixel

²³ The change of angular position of two stationary points relative to each other as seen by an observer, due to the motion of an observer.

matrixes. In stereoscopy, it refers to a vertical grid screen placed in front of a picture that is constructed from narrow vertical strips, arranged alternately from the left and right images. The raster consists of a series of separate parallel vertical slots, or is in the form of a transparent sheet ruled with opaque vertical lines (Fig. 2.6) and it is placed at a precise distance, close to the strip picture. This arrangement allows the left eye of the spectator to see only the left image strips of the composite image and the right eye the alternating right image strips. Thus each eye can see a “complete” and correct image. However, the very presence of the grid spoils the images because neither of them is truly complete. Between the strips of either image there are a corresponding number of gaps (where the grid slats mask the strips of the other image). For better resolution, the number of strips needs to be as large as possible; this is akin to the improvement in the quality of TV images that occurred when the old PAL (625 lines) was changed to HDTV²⁴ (1080 lines). Those types of 3D displays create only view zones with horizontal parallax. With properly designed raster which is with a very small spacing to match up with a finely divided components image, the individual lines will not be resolved and the image will appear continuous, as is the case with TV images, or normal photos. It also helps if the picture is relatively large to allow it to be viewed at a greater distance.

The other disadvantage is that the correct viewing of the stereoscopic image is often only possible from certain fixed viewing positions. Moving away from these positions could result in each eye noticing the incorrect image or parts of both images, which would spoil the effect, or give a pseudoscopic 3D image. Pseudoscopic means that the respective images on the screen for the left and right eyes are exchanged.

The composite image constructed in the way described above is also known as a **parallax barrier stereogram**.

So far it has been assumed, as depicted in Fig. 2.6, that the raster is a regular one with respect to the gap width, as shown in Fig. 2.9. In this way, extra picture element strips can be located directly behind each slat to provide additional viewing positions. The extra strips could simply be duplicates within a single group, but they might be made from images taken from slightly different viewpoints. As an observer moves his head from one viewing position to the next,

²⁴ High-definition television

there will be subtle changes to the images. This can enhance the perception of the total 3D image, replicating, somewhat roughly, the changes that occur as the head moves when looking at real objects.

The disadvantage of increasing the slat/gap with ratio is that less light is reflected from the image to the observer, and the picture appears darker and dull. To preserve the original resolution of the picture, both slat and gap widths have to be reduced to the picture element strip width. For example, suppose a parallax stereogram is constructed with ratio 6:1 of slat/gap width as in Fig. 2.9. If the original 1:1 raster has been made from picture strips of 0.6 mm width, say, then the new version would have to be made from 0.1 mm width elements to maintain the gap spacing of 0.6 mm. This represents a resolution of 1.67 lines/mm.

Making a parallax stereogram by physically cutting photographs into 0.6 mm or, worse, 0.1 mm strips and reassembling them is clearly out of the question; therefore precise optical methods are required. The cutting method could, however, be used for special display purposes, using very large prints intended to be viewed at relatively long distances, but it is a tedious method and even in this case, some means of producing the alternative strips optically would be easier.

Fig. 2.6 gives clue to a possible method if we re-interpret the main features. Imagine two projectors at E_1 and E_2 , the one at E_1 projecting the left image and that at E_2 the right image. By placing a raster as shown (a transparent sheet with black lines) in front of a film, which replaces the composite print, we can capture the correct strip sequence directly onto the film with one exposure. This can be viewed with the same raster correctly in place, to give a correct 3D image.

With a 6:1 slat/grip ratio raster (or any other ratio) several exposures have to be made, each from a different viewpoint. Fig. 2.9, re-interpreting the fact in a similar manner, illustrates this concept.

Elaborations of these principles have been used mostly for projection and direct 3D viewing in cinema, mainly as experimental trials of autostereoscopy. None has succeeded in making a permanent impact in the public domain, though successful results have been achieved [20]. Much work has been directed into the designs of raster to ensure that all the members of a fairly large audience can correctly observe the 3D images.

2.4.2 Optical lens array

Replacing the parallax barrier mask by the **optical lens plate** offers a better improvement in the quality of autostereoscopic images. The single viewpoint problem associated with simple grid raster is eliminated, and acceptable resolution can be achieved. An autostereoscopic lenticular print consists of a composite strip photograph, often produced by a precession optical printer onto photographic paper or high-resolution display which has a thin transparent plastic coating in the form of many parallel semi-cylindrical lenses (Fig. 2.7).

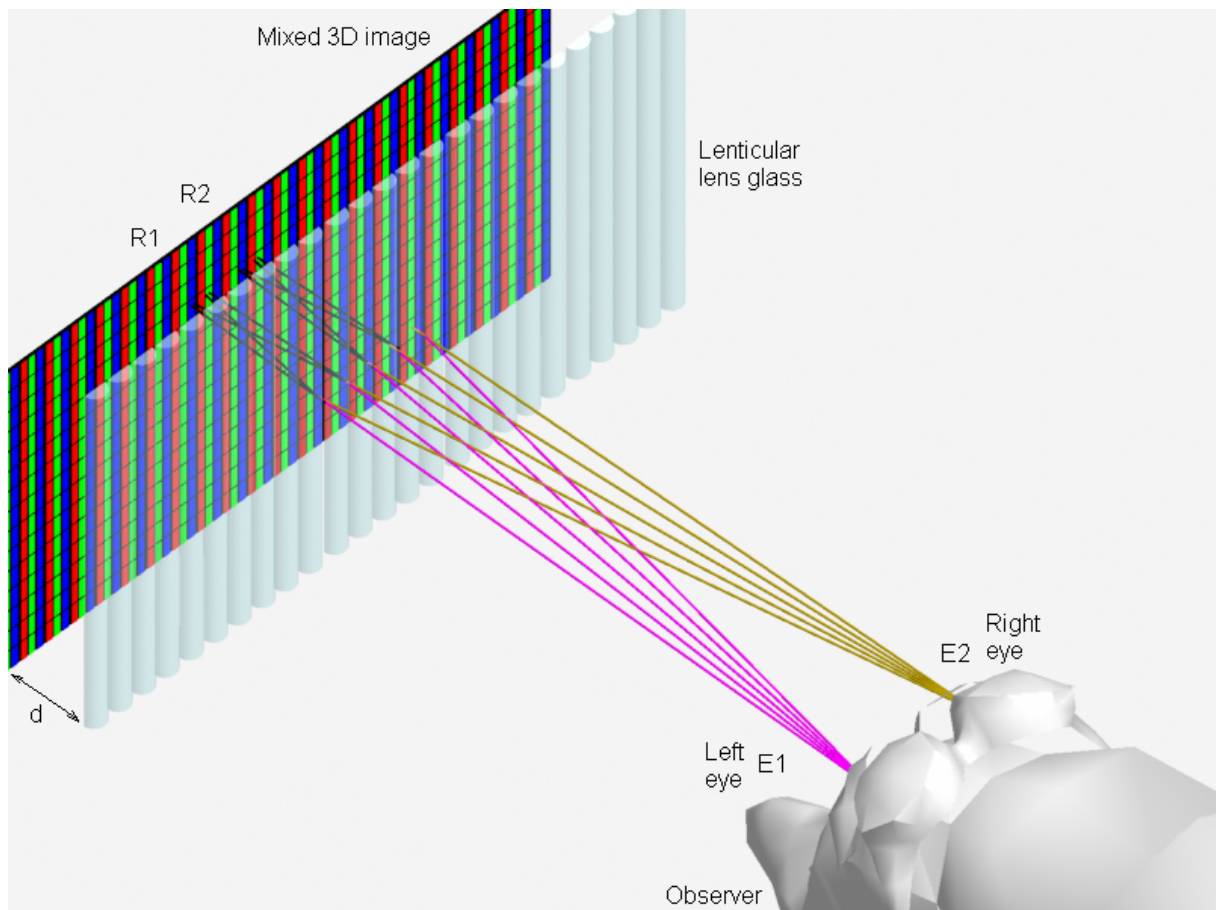


Fig. 2.7 System, that uses lenticular lens glass. With correct positioning of the lens glass in front of a mixed 3D scene, each eye sees only the correct image.

At normal viewing distances the ribbed surface can just about be discerned, so there is little apparent loss of quality compared to the standard – non-stereographic image.

Each semi-cylindrical lens directs the two eyes of an observer sight lines to different image strips (left and right as appropriate) located behind the lenticular screen Fig. 2.8.

Moving the head sideways when looking at the print makes for different left and right image strips to be viewed. There may be a slight jump in the continuity of viewing the picture as the viewpoint is changed from one position to another, several times as the head is moved, and part of the image may momentarily appear pseudoscopic. However, the overriding effect makes it easy to view 3D image for which there is no critical viewing position. The slight changes in the image that are observed as different strips coming into view, give an impression of looking around the subject, as occurs when viewing real objects while moving the head slightly. With a continuous lateral head movement one will detect occasional relative movements between foreground and background that can enhance the perception of the total image.

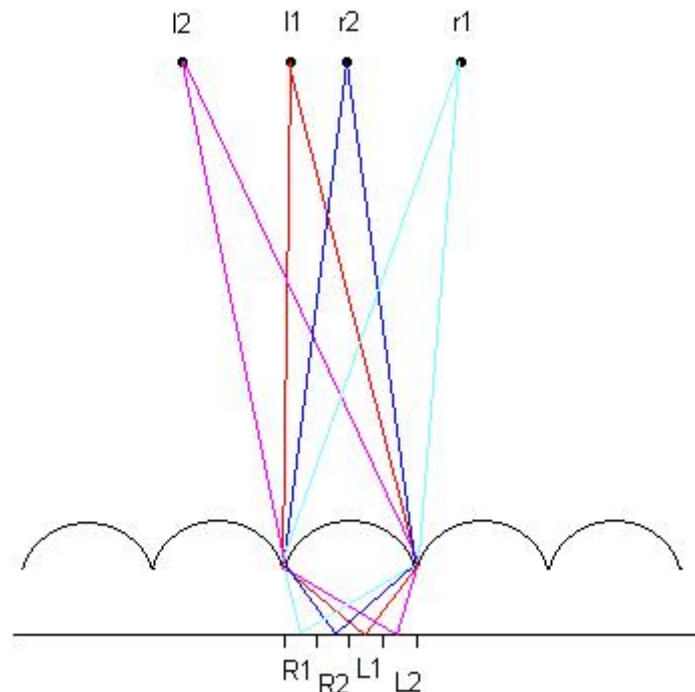


Fig. 2.8 A lenticular print enables the observer to see the image correctly from many positions. With the eyes at $l1$ and $r1$, pixels $L1$ and $R1$ are seen. From $l2$ and $r2$ the observed pixels are $L2$ and $R2$.

The optical lens plate is the most well-developed stereoscopic viewing plate at present, however, image clarity, and viewing zone uniformity are limited. The parallax barrier plate is not much different from the lenticular; however, it has another problem of low image brightness. The microlens array plate has so far not strictly defined standard form of manufacture and has limited resolution.

2.4.3 Viewing zones in a 3D image of pixels, formed by optical plate

In designing 3D imaging systems with a lenticular or parallax barrier mask, if the position of each viewing section is known, pixel locations of each view image can be defined for a given optical mask by backtracking the rays from the image because each optical element of the plate magnifies pixels aligned under or above it.

The correlation between the multi-view image pixels and their corresponding viewing zones are given in Fig. 2.9 and Fig. 2.10. They depict how the viewing zone is divided into K equal sections by K different view images numbered 1 to K from left to right. Each view image is assumed to consist of 5 pixels numbered 1 to 5 , aligned in the horizontal direction. Fig. 2.9 shows a point light source array with a one-dimensional image mask in front of it. The array consists of 5 equal point light sources specified by a colour point.

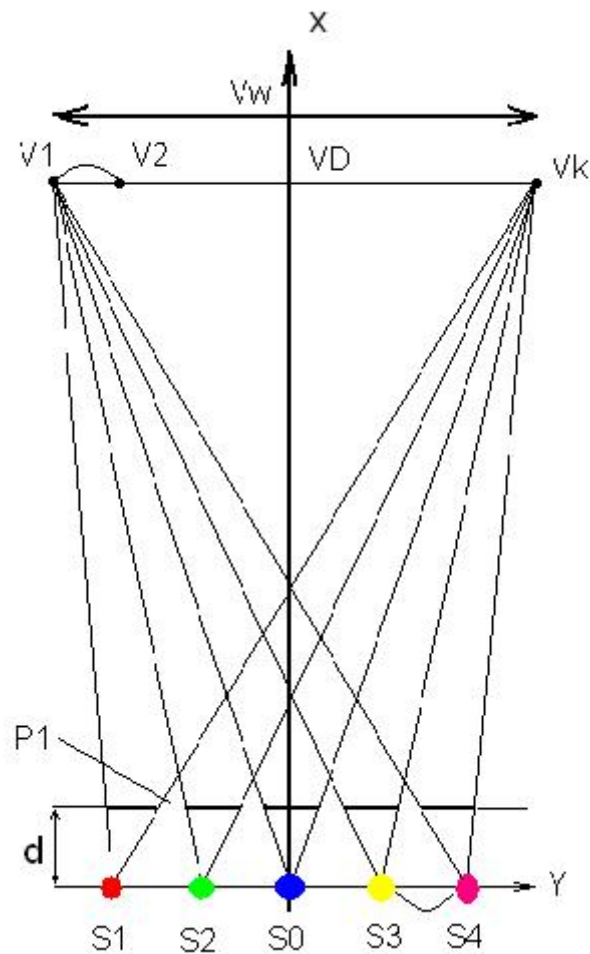


Fig. 2.9 Viewing zone forming by the point light source array.

Each source is defined by $S1$, $S2$, $S0$, $S3$ and $S4$ and aligned along the y -axis with a distance between neighbouring sources, p . In Fig. 2.9, Fig. 2.10, let us assume that $S0$ is in the origin of the x and y -axes, and the viewing zone with a width Vw , is located at a distance in the x -axis direction from $S0$ and is segmented into K equal size sections corresponding to K different view images. $V1$ and Vk specify left and right edges of the viewing zone, respectively, and they are symmetric along the x -axis. $V1$ and $V2$ define the viewing-zone section $V S1$ for the view image No.1, $V2$ and $V3$ $V S2$ for the view image No.2 and Vk and $Vk V Sk$ for the view image No. K . When lines are drawn from each PLS²⁵ to $V1$ and Vk , these lines divide the horizontal line at position A into 5 equal sections. The position A is defined as that of the first intersection points between these lines.

²⁵ Point Light Sources

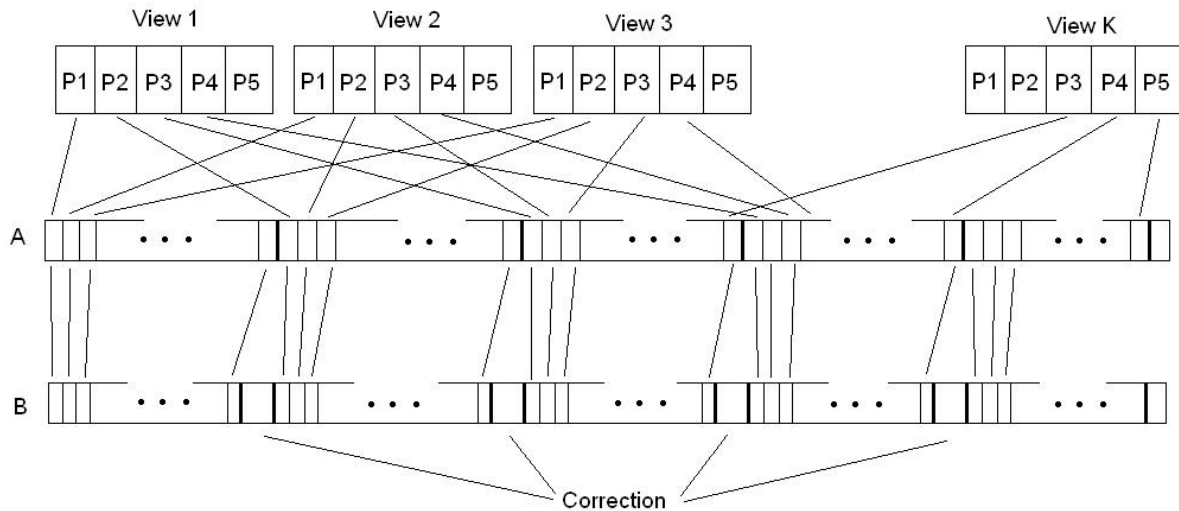


Fig. 2.10 Pixel arrangement in image mask.

For the horizontal line at position B, it is segmented into 5 equal sections with blank region between each of them. These blank regions have the same size and transmit no light from the PLS to viewing zone. The position B can be any arbitrary location in-between positions A and PLS. When VS_1 , VS_2 ... and VS_K have the same size, if lines are also drawn from each PLS to V_2 , ... and V_K , these lines again divide each of the 5 equal sections into K equal subsections. The relative location of each subsection in each section is the same as that of the corresponding viewing zone section in the viewing zone, and the subsection size is proportional to its corresponding viewing-zone section size. Hence, the one-dimensional image mask at positions A and B should have the same structure as the viewing-zone line at V_d .

Fig. 2.10 shows the pixel arrangement in the mask. In the mask, each section functions as a pixel cell. If each section and the K subsections are identified by numbers 1 to 5 and 1 to K from left to right, respectively, in the same way as the viewing zone section, it can be said that the N th ($N = 1$ to 5) pixel from the L th ($L = 1$ to K) view image fills the L th subsection of the N th section. Each section is illuminated by its corresponding PLS. To make this kind of mask, a **very high-resolution display** is needed. A good candidate for such a type of display is the OLED display.

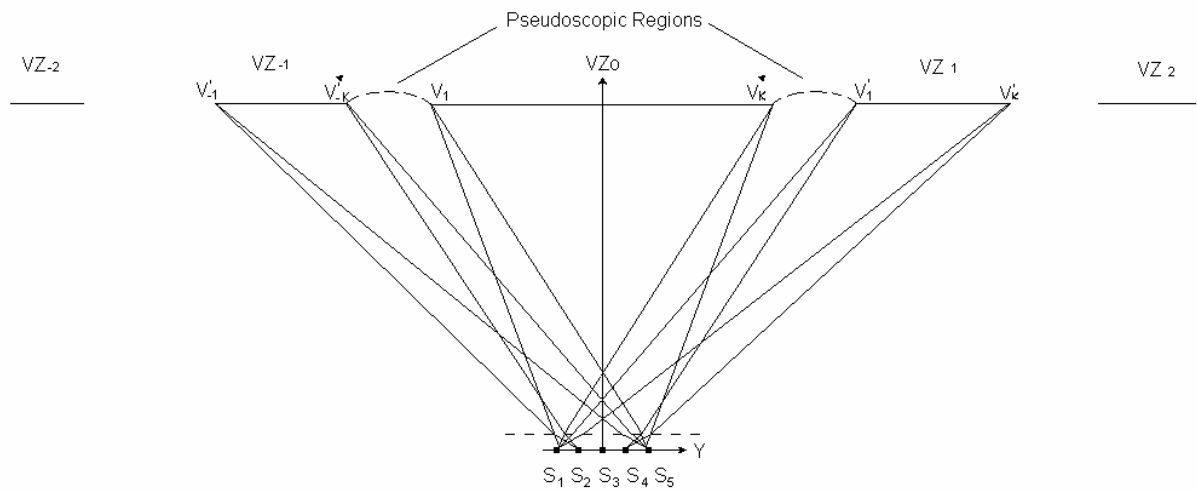


Fig. 2.11 Viewing zones created by illuminating adjacent segments of the image mask

If the mask at position B is distanced from the PLS array, by the similar triangle correlation, the widths of each session, W_s and each blank region, W_b are calculated as is shown by the formula,

$$W_s = \frac{dV_w}{Vd} \quad (2-1)$$

$$W_b = P - \frac{d}{Vd}(P + V_w)$$

In (2-1), $W_s + W_b$ represent the width of the mask corresponding to P , i.e. the distance between neighbouring light sources. It is given as,

$$W_s + W_b = p \left(1 - \frac{d}{Vd} \right) \quad (2-2)$$

When the mask is located at A, $W_b = 0$, then d and W_s are calculated as,

$$d = \frac{pVd}{(Vw + p)} \quad (2-3)$$

$$Ws = \frac{pVw}{Vw + p}$$

The size of each subsection in each section is given as Ws/K . The sizes of viewing-zone sections, $VS1$, $VS2$, ..., and VS_k can not be more than our eye distance to eliminate the chances of putting the viewer's two eyes in the same viewing zone section. If the eye distance is assumed to be 65mm, the viewing-zone width Vw can be more than $(65 \times K)$ mm. The viewing-zone size increases linearly in proportion to K .

The viewing zone specified by $VZ0$ in Fig. 2.9, Fig. 2.10 is not the only viewing zone for the configuration. It is just one of the only viewing zones for configuration. It is just one of the viewing zones, located at the centre. There will be many other viewing zones with a size Vw along the extended line of $V1 \ K1$ due to PLS illumination to other section of the mask. For example, the illumination of the mask sections 2 and 1, and 4 and 5 by PLS $S0$ will create viewing zones $VZ-1$ and $VZ-2$ and $VZ1$ and $VZ2$ respectively as shown in Fig. 2.11

The gap between each viewing zone has a size of $Vd \ Wb / d$. Hence, when $Wb = 0$, i.e. the image mask is in position A, there is no gap between the neighbouring viewing zones. In the border regions between neighbouring viewing zones, there will be an abrupt view-image change from view No 8 to No 1. Hence, the depth of the perceived image will be replaced, i.e. the perceived image will be pseudoscopic. This pseudoscopic viewing region can be diminished by increasing the gap between neighbouring viewing zones with more than our eye distance, i.e. $Vd \ Wd / d > 65mm$.

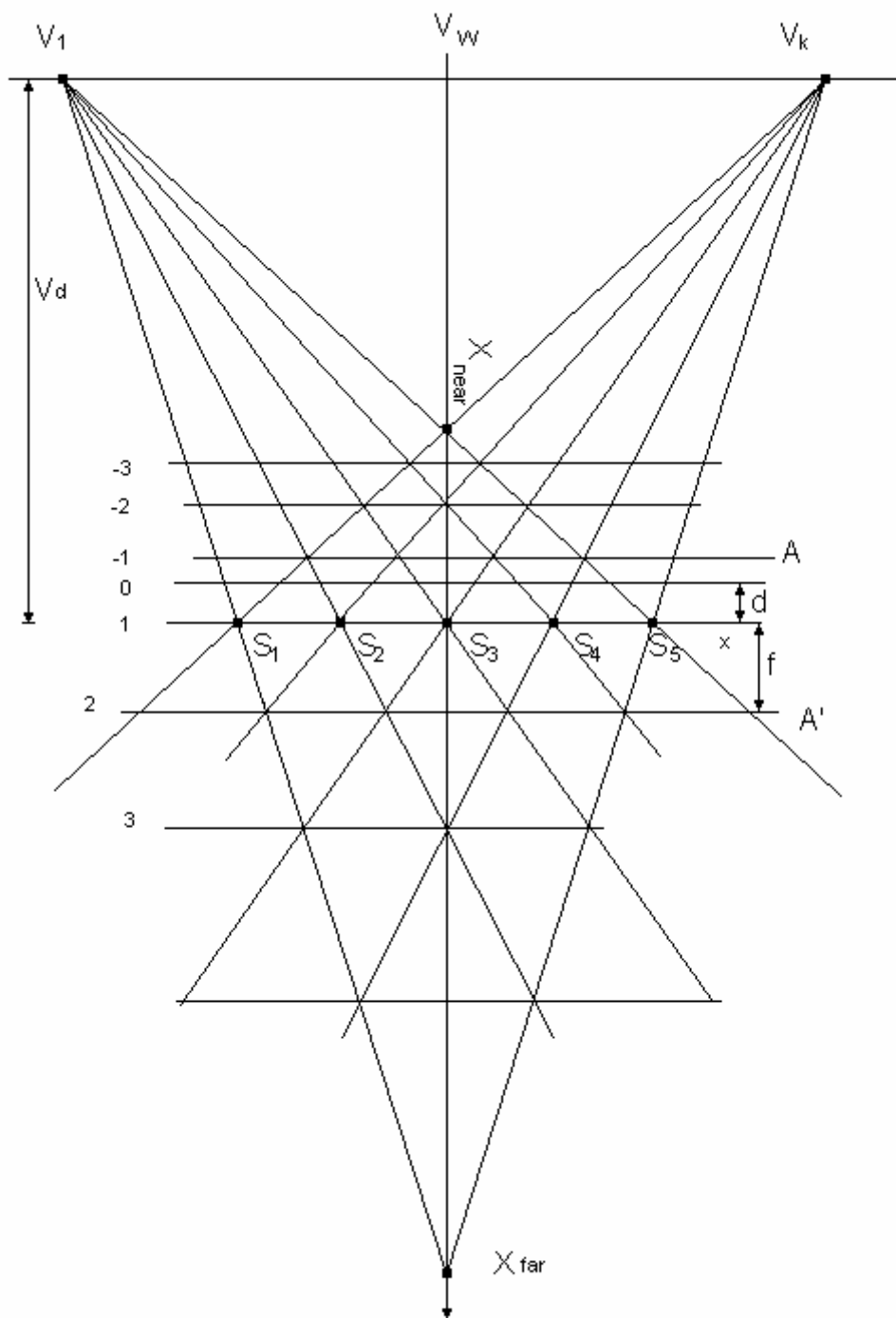


Fig. 2.12 Placement the depth levels in 3D image.

Fig. 2.12 is an extended view of Fig. 2.9. If 'f' is the distance between the PLS array and the line connecting crossover points at position A', it is given as,

$$f = \frac{pVd}{(V_w - p)} \quad (2-4)$$

In this case, the distance between neighbouring crossovers points, W's is calculated as,

$$W's = \frac{pV_w}{V_w - p} \quad (2-5)$$

W's and Ws in (2-3) have the following correlation:

$$W's = W_s \frac{V_w}{V_w - p} \quad (2-6)$$

Since triangles made of connecting each PLS and the line sections in positions A and A' are similar to each other, changing the line sections in positions A to A' will not make any difference from geometrical point of view, if the sections in position A are magnified by $V_w/(V_w-p)$ times and rotated 180° .

2.4.4 Image depth ranges, achievable with parallax barrier mask and lens arrays

In Fig. 2.9 and Fig. 2.10, the viewing zone size V_w should be bigger than our eye distance to adopt many view images. However, since viewers can adjust their eyes to any pair of viewing zone sections, their eye can distance apart and it is possible to consider that V_1 and V_k represent the pupil positions of a viewer's eyes. In this case, the lines connecting intersection points of lines from neighbouring points, lines from points of two distanced apart points and many

others, will provide a means of determining the obtainable image depth for the autostereoscopic imaging systems.

Since the intersection points are virtual points, which can be discerned simultaneously at both $V1$ and $V'k$, these points will work as volume picture elements in the construction of the stereoscopic images. For the generality of the analysis as is shown in Fig. 2.12, it is assumed that there are n PLSs at position $X0$, and the positions of lines connecting the intersection points that are the same distance from the PLS array are specified by $x \pm j$ ($j = 0, 1, 2, 3, \dots, n-1$). Then $x \pm j$ is defined as,

$$x \pm j = V_D \cdot \frac{\pm jp}{V_W \pm jp} \quad (2-7)$$

In (2-7), V_D and V_W correspond to viewing distance and viewer's eye distance, respectively. Since the most protruding image point, i.e. the nearest image point to the viewers, x_{near} is when $j = -(n-1)$, x_{near} is defined as,

$$x_{near} = V_D \cdot \frac{-(n-1)p}{V_W + (n-1)p} \quad (2-8)$$

Since $S=(n-1)p$ is the width of the display screen, the theoretically permitted maximum image protrusion is represented as $V_D \times S / (V_W + S)$. This correlation shows that the maximum image protrusion allowed for the autostereoscopic imaging system is almost equal to the viewing distance. When, V_D , V_W , and S are assumed as 1m, 6.5cm and 50cm, respectively, the protrusion is calculated as 88cm. This protrusion is too large to be observed easily and without any efforts by viewers. The protruded image depth for viewing the stereoscopic images comfortably is different for different people. However, empirically, it will be more comfortable for the viewers if the image protrusion does not exceed one third of the viewing distance. To make this value, S should equal $0.5V_W$. In this sense, S will present the parallax between left and right eye images but not screen size. Hence, it can be said that the parallax should not exceed one half of our eye distance for comfortable viewing of the protruded stereoscopic images.

From (2-8), the distance between two adjacent lines connecting the intersection points, d_D is calculated as,

$$d_D = \frac{pV_D V_W}{V_W^2 + (2n-3)pV_W + (n^2 - 3n + 2)} \quad (2-9)$$

If d_D is larger than our depth sensitivity at a given viewing distance, viewers will perceive discrete depth images. To make images with a smooth depth, the distance between each PLS, i.e. p and V_D should be smaller. In this case, the volume picture elements become finer.

The farthest image point, x_{far} is infinity when $V_W = (n-1)p$, otherwise x_{far} equals to $x_{n-1}(j = n-1)$. That is,

$$x_{far} = \frac{(n-1)p}{V_W - (n-1)p}. \quad (2-10)$$

Equation (2-10) works only for the case of $V_W > (n-1)p$ because when $V_W < (n-1)p$, $x_{far} > V_D$. The possible minimum and maximum image depths behind the screen are given as f in (2-4), i.e. $n=2$ case and infinity, respectively. Equations (2-8) and (2-10) show that $(n-1)p$ represents the parallax and as for the image depth it is linearly proportional to the viewing distance V_D .

In both lenticular and parallax barrier cases, multiple views of a scene can be included making for motion parallax as the viewer moves his/her head from side to side creating what is called **panoramagram**. Recently, parallax barrier liquid-crystal imaging devices have been developed that can be driven by a microprocessor and are used to view stereo pairs in real time without any glass.

2.5 Psychological basics of three-dimensional perception

Three-dimensional images provide a strong sensation of reality because they bear depth information and this is what makes the best distinction between them and 2D images.

There are many cues used by the brain to estimate depth in a visual scene. All of them we can separate in two main groups: the information is generated from both eyes and the information is gathered by different psychological cues.

- **Accommodation.** When viewing distant objects in the lens the eyes are in a relaxed state. As the eye focuses on nearer objects, the muscles surrounding the lens are activated to accommodate its shape and focus the image on the retina.

- **Convergence.** This phenomenon is observed when the eyes rotate in their sockets about a roughly vertical axis (assuming the head is upright) to allow the lines of sight of both eyes to move towards each other. Both these peculiarities and principles combined with the many years' experience gained, give us our sense of depth, the relative distance of objects in view at a particular moment. This sense of depth, it must be stressed, is a relative rather than an absolute one. All the same, one can develop a skill of estimating distances with some degree of accuracy.

Accommodation and convergence tend to work together, because viewing an object at a given distance will require so much of the use of each effect, thus we need a muscular action for focusing and eye-sighting of the correct amount to cause the two lines of sight to intersect at the observed object. However, the two are not permanently linked and they can function independently. This can be demonstrated by considering a stereogram viewed in a conventional stereoscope. The stereogram itself will be located at approximately 40 mm from the stereoscope's lenses (of 40 mm focal length) and light rays from all parts of the image will penetrate the eyes in a more or less parallel way. This means that the eyes will be focused at infinity for every feature within the image. However, the eyes will converge as normal for objects at different distances, just as they would if viewing the actual scene. Thus the eyes converge while maintaining constant focus, a situation that is not encountered in a normal vision.

The convergence eye movement and accommodation function perform an important role in gazing and the pursuing the visual target into depth. The accommodation function is controlled by the alternating thickness of the crystalline lens. The refractive power exists not only in the lens, but also in the cornea, and all through the optical path. The accommodation plays a role in giving a clear sight

image to detectors on the retina. The convergence eye movement carries out the role of setting the gazed-at-target to the fore for cognition of the object.

In the human visual system, the accommodation function or the convergence eye movement can detect the distance of a visual target. Although an object in front or behind the point of gaze is reflected to different positions on the retina of the right and left eyes, only one object is presented near the gazed-at-point. This phenomenon is underpinned by the existence of binocular disparity detection cells in the visual cortex. Single vision is caused in the periphery of the point of gazing, and this range is called Panum's fissional area.

The human eye can usually accommodate to an object when the viewing distance is less than about 2 m. This means that a three-dimensional image display that produces only binocular disparity, i.e. a stereoscopic display, is inadequate for natural viewing.

These factors must be exactly observed before projecting a very high-resolution 3D Autostereoscopic sample. This is indispensable because the diagonal of the sample is limited to 2.2 inch i.e. it is relatively small and this means that it must be observed from a relatively short distance – about 30cm. Human eyes and brain at such a distance are very irritable and any inadequacy between the different reception cues will make it impossible to achieve 3D effect.

- **Binocular disparity.** This phenomenon means a difference in the images projected on the left and right eye retinas in the viewing of a 3D scene. It is the salient depth cue used by the visual system to produce the sensation of depth, or stereopsis. Any 3D display device must be able to produce a left and right eye view and present them to the appropriate eye separately.

- **Motion parallax.** This phenomenon is observed when an observer is in motion and the visual sense surrounding the person is represented as a drifting image on the retinas of the observer's eyes. The drift speed on the retina depends on the relative distance of a given object from the image. If the object is close to the observer, the drift speed of this object on the retina will be faster than when the object is further away from the observer. It is a well-known fact that this relative motion of the visual image on the retina, known as motion parallax, is used by the visual system to generate sensation of depth [21], [22]. This is one of many cues

used by brain to estimate depth in a visual scene that does not require information from both eyes.

There are also some purely psychological factors for receiving the depth information.

- **Linear perspective** refers to the change in image size of an object on the retina in inverse proportion to the object's change at a distance. Parallel lines moving away from the viewer, like the rails of a train track, converge to a vanishing point. As an object moves further away, its image becomes smaller, an effect called perspective foreshortening. This is a component of the depth cue of the retinal image size.

- **Shading and shadowing.** The amount of light from a light source illuminating a surface is inversely proportional to the square of the distance from the light source to the surface. Hence, surfaces of an object that are further from the light source are darker (shading), which gives cues of both depth and shape. Shadows cast by one object onto another (shadowing) also give cues to relative position and size.

- **Aerial perspective.** Distant objects tend to be less distinct, appearing cloudy or hazy. Blue, having a shorter wavelength penetrates the atmosphere more easily than other colours. Hence, distant outdoor objects sometimes appear bluish.

- **Interposition.** If one object occludes, hides or overlaps (interposes) with another, we assume that the object doing the hiding is closer. This is one of the most powerful depth cues.

- **Retinal image size.** We use our knowledge of the world, linear perspective, and the relative sizes of object to determinate relative depth. If we view a picture in which an elephant is the same size as the human being, we assume that the elephant is further away since we know that the elephants are larger than human beings.

- **Texture gradient.** We can perceive detail more easily in objects that are closer to us. As objects become more distant, the texture becomes blurred. Texture in brick, stone, or sand, for example, is coarse in the foreground and grows finer as the distance increases.

- **Colour.** The fluids in the eye refract different wavelengths at different angles. Hence, objects of the same shape and size and at the same distance from the viewer often appear to be at different depths because of differences in colour. In addition, bright-coloured objects will appear to be closer than dark-coloured objects.

The human visual system uses these entire cues to determine relative depths in a scene. In general, depth cues are additive; the more cues the more apt is the viewer to determine the depth. However, in certain situations some cues are more powerful than others, and this can produce contrasting depth information. Our interpretation of these scenes and our knowledge of what we perceive as depth correlations can override binocular disparity.

2.6 Summary

This chapter presented the already excised technologies for three-dimensional presentation. There are also presented the principle of work of autostereoscopic displays, based on parallax barrier mask and lens-raster glass. They are used in PhD thesis. At end are presented the ways of the volumetric visual perception of the human eyes and brain.

3. Device components, design and processing

3.1 Introduction and uses of Organic Light Emitting Diode (OLED)

3.1.1 Introduction

Since the report of high efficiency electroluminescence from evaporated organic molecular films in 1987 [24], organic electroluminescent thin films have raised a huge interest amongst the display community and several laboratories, SMEs or large companies around the world have initiated the production of flat panel displays based on their use. An organic light emissive diode OLED schematically consists of a stack of organic materials sandwiched between two adequately chosen electrodes. Electrons are injected from one electrode into the holes of the other one; they recombine in the organic material generating excitations, which then decay in a radiation, producing visible photons.

Pioneer produced the first commercially available low-information content displays based on OLEDs. These early products have already proved that the high contrast of self-emitting displays offers a superior alternative to liquid crystal displays in applications with changing lighting conditions and the need for a wide viewing angle as in the automotive and the steadily growing mobile phone and personal digital assistant (PDA) market. Consequently, following an order 70 company worldwide conduct research and development in the field of OLED. Display development ranges from low-content monochrome passive-matrix displays to active-matrix full-colour displays and XGA and higher resolution microdisplays.

Most of the materials useful in light-emitting structures employ amorphous thin films, which may be deposited on any flat substrate. Crystalline materials are, however, useful for charge-transport and/or protection layers [30], and there is ample evidence that under appropriate growth conditions, crystalline order can be achieved in such films by quasiepitaxy deposition, even on highly lattice-mismatched or amorphous substrates [31], [32]. The key properties of vacuum deposited organic semiconductors, which allow for realization of light emitting device structures difficult or impossible to create with other material systems are as follows:

- **Transparency.** Most charge transport and luminescent layers are transparent to their own luminescence. This high transparency extends across the visible spectral region and has been utilized to make transparent OLEDs (TOLEDs) [33], [34] which are 70% transparent when turned off and emit light from both surfaces when turned on.

- **High purity.** Low molecular weight organic materials are typically purified first by recrystallization, with several subsequent purifications by vacuum sublimation. Extremely high purity starting materials are therefore available. Such structural and chemical purity is difficult to obtain with polymeric systems.

- **Epitaxy-free growth.** Both amorphous and crystalline, van der Waals bonded organic solids readily form thin films with a high degree of structural order by vacuum deposition on a wide range of substrates. Flat, uniform thin films are formed regardless of lattice-match or even substrate crystallinity. In particular, vacuum deposition allows for the creation of complex multi-layer heterostructures while maintaining excellent layer uniformity and sharp interfaces between adjacent layers [32].

- **Flexibility.** The relatively weak Van der Waals force dominates the intermolecular binding of non-polar organic molecular materials. Small-molecule OLEDs deposited on ITO-coated polyester substrates [35] have therefore been shown to be extremely flexible and can be bent around a radius of curvature of 8 mm with no degradation of device properties.

- **Durability.** A life of the functioning unit must be as long as possible, without alteration of the optical and electrical parameters. The common defects, evinced usually after 10000 h of work are loss of illumination and black points in the polymer layer (owing to a diffusion of oxygen molecules across glue material). The requirements for passivity film for OLED are as follows. On the first place, the deposition temperature for making the passage film should be low, because OLED is not immune to high temperature. On the second place, low film stress is needed, if the passage film stress is high, the organic layer may easily peel off. On the third place, the passage film should work as a good barrier against moisture and oxygen in order to stop expansion of dark spots. On the fourth place, as the panel is not flat for it has cathode separators in the shape of a reverse tapered cross section, a passage film must cover the cathode separators thoroughly.

- **Homogeneity.** The luminance must be balanced in the whole surface of the display.

All these properties together make vacuum-deposited, low molecular weight, organic semiconductors ideal candidates for fabricating multi-layer heterostructures with a high degree of optical and structural perfection on a variety of low-cost substrates. The substrates are typically kept close to room temperature during deposition, making film growth possible even on such substrates as plastic. Furthermore, the organic film deposition and device fabrication processes are compatible with conventional semiconductor processes.

Lots of efficient light-emitting structures using spin-coated polymeric materials have also been demonstrated, which exhibit some of the above properties. However, polymerbased devices have two key disadvantages. On the first place, control of purity (both chemical and structural) is more difficult for solution-processed polymers than for vacuum-deposited small molecules since the latter can be rendered extremely pure by repeated vacuum-sublimation. On the second place, complex multilayer structures with sharp interfaces between several different polymers require each polymer to be cast from a solvent in which the others must be insoluble. In contrast, vacuum-deposition can be used to grow complex structures regardless of the chemical compatibility between the various layers.

3.1.2 Structure of an OLED

A schematic cross section of a typical OLED is shown in Fig. 3.1. Variations on this basic structure have now demonstrated green, red, blue, orange, white OLEDs with operating voltages below 10 V, luminosities in excess of 230 000 cd/m² and operational lifetimes in excess of 25 000 h (although not in the same device). Blue

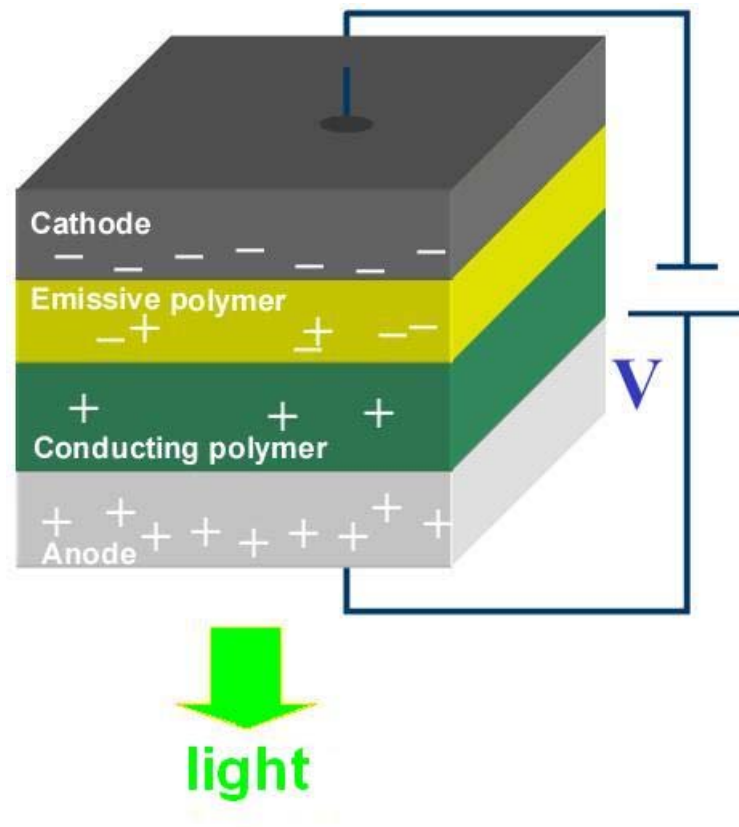


Fig. 3.1 Schematic cross-section of a single colour organic light emitting device (Source: OSRAM)

and red OLEDs have somewhat inferior, though still useful, characteristics. It has also been shown that this well-known structure may be rendered transparent by reducing the thickness of the MgAg to below ~ 100 Å and using a cap layer of sputter-deposited indium tin oxide (ITO) to protect and provide bulk to the thin metal cathode [34]. There are many potential applications for TOLEDs²⁶, including head-up or windshield mounted displays.

3.1.3 Working principle of OLED

When a voltage is applied to the electrodes the charges start moving in the device under the influence of the electric field. Electrons leave the cathode and holes move from the anode in opposite direction. The recombination of these charges

²⁶ Transparent Organic Light Emitting Display

leads to the creation of a photon with a frequency given by the energy gap ($E = h\nu$) between the LUMO²⁷ and HOMO²⁸ levels of the emitting molecules. Therefore, the electrical power applied to the electrodes is transformed into light (Fig. 3.2).

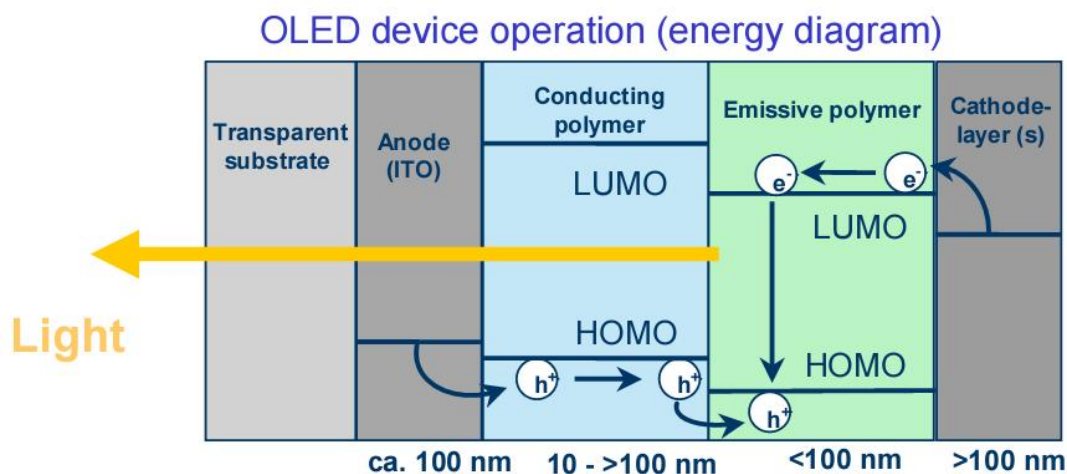


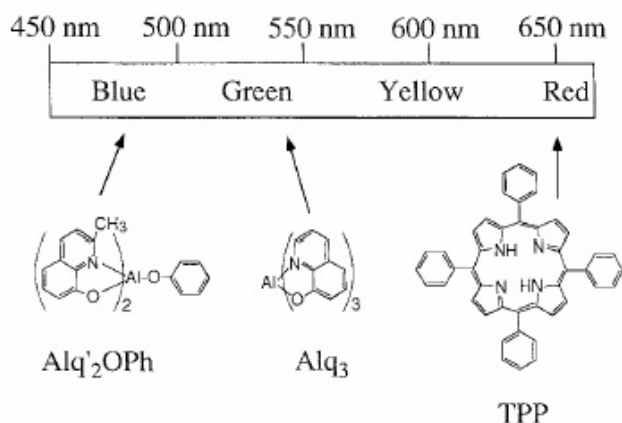
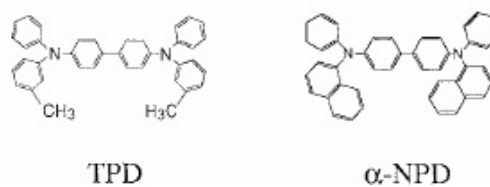
Fig. 3.2 Charge transport and light generation in OLED's (Source: OSRAM)

HOMO and LUMO are acronyms for highest occupied molecular orbital and lowest unoccupied molecular orbital, respectively. The difference of the energies of the HOMO and LUMO, termed the band gap can sometimes serve as a measure of the excitability of the molecule: the smaller the energy, the easier it will be excited. When the molecule forms a dimer or an aggregate, the proximity of the orbitals of the different molecules induce a splitting of the HOMO and LUMO energy levels. This splitting produces vibrational sublevels which each have their own energy, slightly different from one another. There are as many vibrational sublevels as there are molecules that interact together. When there are enough molecules influencing each other (e.g. in an aggregate), there are so many sublevels that we no longer perceive their discrete nature: they form a continuum. We no longer consider energy levels, but energy bands [76].

Different materials and dopants can be used to generate different colors and the combination of them allows building up a white light source (Fig. 3.3).

²⁷ Highest occupied molecular orbital

²⁸ Lowest unoccupied molecular orbital

Light Emitting MoleculesHole Transporting Molecules**Fig. 3.3 Materials used in OLED's****3.1.4 Comparison between LED and OLED working principles**

The radiative recombination of electron-hole pairs can be used for the generation of electromagnetic radiation by the electric current in a p-n junction. This effect is called electroluminescence. (Fig. 3.4) In a forward-biased p-n junction fabricated from a direct band gap material, such as GaAs or GaN, the recombination of the electron-hole pairs injected into the depletion region causes the emission of electromagnetic radiation. Such a device is called a Light Emitting Diode (LED). If mirrors are provided (usually by cleaved crystallographic surfaces of the semiconductor) and the concentration of the electron hole pairs (called the injection level) exceeds some critical value, this device may function as a

semiconductor laser that emits a coherent electromagnetic radiation with all photons in phase with each other.

As in other diodes, when this structure is forward biased, holes from the p-region are injected into the n-region, where electrons are the majority carrier. Similarly, electrons from the n-region are injected into the p-region, where holes are the majority carrier. When an electron and a hole are present in the same region, they may recombine by spontaneous emission—that is, the electron may re-occupy the energy state of the hole, emitting a photon with energy equal to the difference between the electron and hole states involved. These injected electrons and holes represent the injection current of the diode, and spontaneous emission gives the laser diode below lasing threshold similar properties to an LED. Spontaneous emission is necessary to initiate laser oscillation, but it is a source of inefficiency once the laser is oscillating.

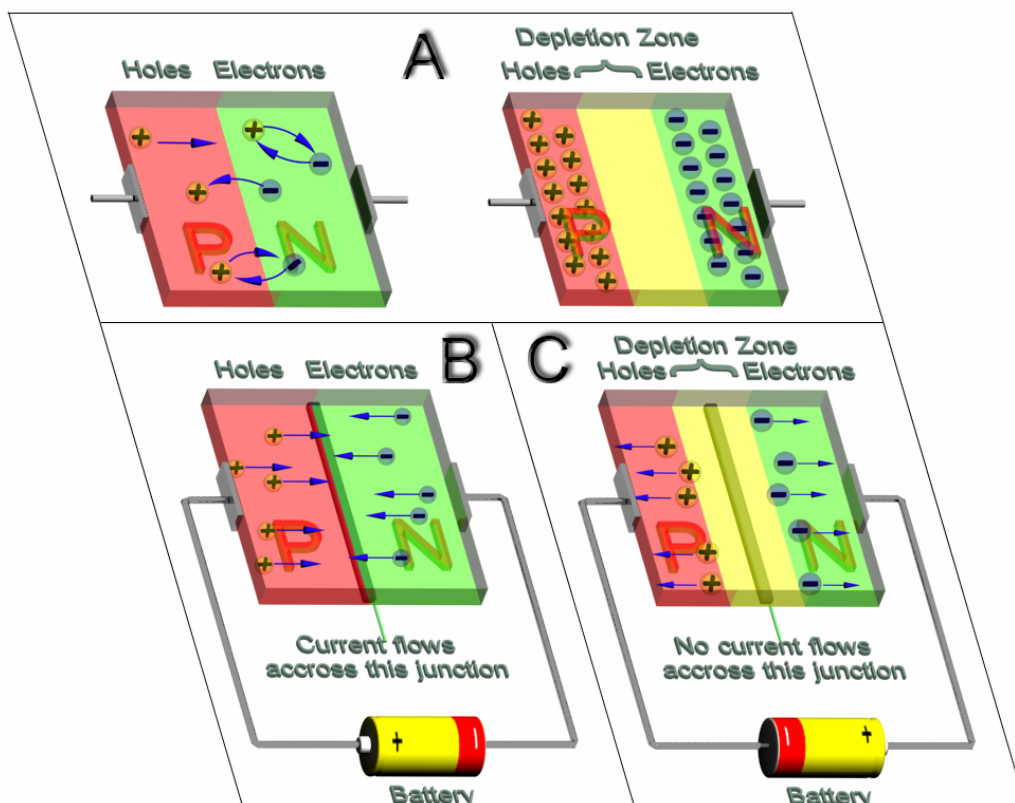


Fig. 3.4 A) At the junction, free electrons from the N-type material fill holes from the P-type material. This creates an insulating layer in the middle of the diode called the depletion zone. **B)** When the negative end of the circuit is hooked up to the N-type layer and the positive end is hooked up to P-type

layer, electrons and holes start moving and the depletion zone disappears. C) When the positive end of the circuit is hooked up to the N-type layer and the negative end is hooked up to the P-type layer, free electrons collect on one end of the diode and holes collect on the other. The depletion zone gets bigger.

Under suitable conditions, the electron and the hole may coexist in the same area for quite some time (on the order of microseconds) before they recombine. Then a nearby photon with energy equal to the recombination energy can cause recombination by stimulated emission. This generates another photon of the same frequency, travelling in the same direction, with the same polarization and phase as the first photon. This means that stimulated emission causes gain in an optical wave (of the correct wavelength) in the injection region, and the gain increases as the number of electrons and holes injected across the junction increases. The spontaneous and stimulated emission processes are vastly more efficient in direct bandgap semiconductors than in indirect bandgap semiconductors, thus silicon is not a common material for laser diodes.

As in other lasers, the gain region is surrounded with an optical cavity to form a laser. In the simplest form of laser diode, an optical waveguide is made on that crystal surface, such that the light is confined to a relatively narrow line. The two ends of the crystal are cleaved to form perfectly smooth, parallel edges, forming a Fabry-Perot resonator. Photons emitted into a mode of the waveguide will travel along the waveguide and be reflected several times from each end face before they are emitted. As a light wave passes through the cavity, it is amplified by stimulated emission, but light is also lost due to absorption and by incomplete reflection from the end facets. Finally, if there is more amplification than loss, the diode begins to "lase".

Some important properties of laser diodes are determined by the geometry of the optical cavity. Generally, in the vertical direction, the light is contained in a very thin layer, and the structure supports only a single optical mode in the direction perpendicular to the layers. In the lateral direction, if the waveguide is wide compared to the wavelength of light, then the waveguide can support multiple lateral optical modes, and the laser is known as "multi-mode". These laterally multi-mode lasers are adequate in cases where one needs a very large amount of

power, but not a small diffraction-limited beam; for example in printing, activating chemicals, or pumping other types of lasers.

LEDs fabricated from different semiconductors cover a broad range of wavelengths, from infrared to ultraviolet.

The HOMO level is to organic semiconductors what the valence band is to inorganic semiconductors. The same analogy exists between the LUMO level and the conduction band. The energy difference between the HOMO and LUMO level is regarded as band gap energy.

3.1.5 OLED display technologies

There are some different technologies to produce monochrome and full colour OLED displays. The main difference is the way of coating the lighting substrate on the carrier pad.

Basically, the colour filter technology can be adopted from LCD technology. On a glass substrate usually a black matrix is produced by photolithography as a first layer to avoid optical crosstalk between colour subpixels. The RGB subpixels are produced in three subsequent steps by photolithographic patterning of RGB colour filter coatings. As the colour filter pixels are about 1 to 1,5 μm high an additional planarization coating is necessary prior to ITO sputtering. The entire colour filter stack is now 2 to 2,5 μm high and planarization ratios of 70 to 80% are necessary to achieve well- performing OLEDs on top of the colour filter stack. Crucial is the angle of the top coat edge which has to be adjusted carefully to assure proper deposition of ITO with adequate conductivity (Fig. 3.5).

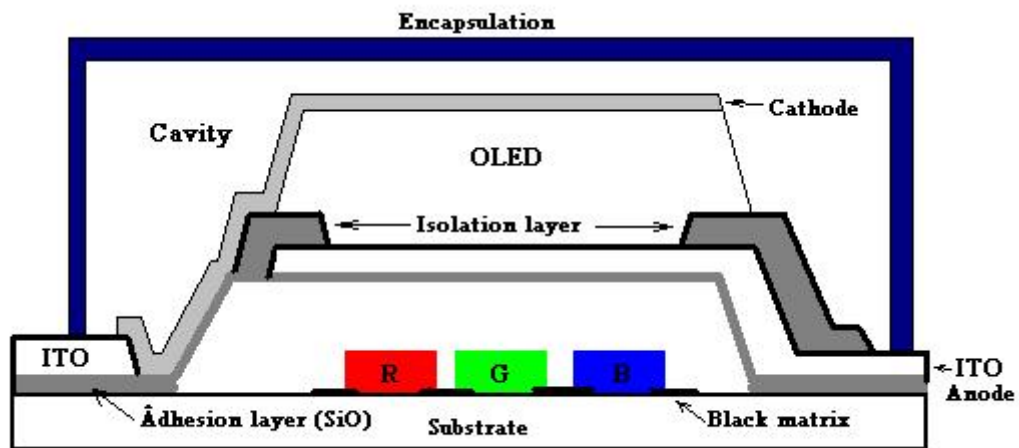


Fig. 3.5 Schematic of OLEDs with Color Filter Setup (source: [36])

Full colour displays are produced on colour filter substrates on which each pixel of the display matrix consist of three separately addressable RGB subpixels. On this colour filter substrates the same processes as for monochrome displays are carried out. This means that the only emitter polymer can be processed with moderate resolution requirements. Besides spin coating, this gives access to fast and economic area printing processes as e.g. screen-printing.

The screen-printing process needs a special screen pattern to deposit the polymeric solutions only on the active area of the display and to prevent precipitation of the polymers on non-active areas as for example the contact pads. To achieve this, the screen has open meshes, where the polymeric solution can wet the substrate, whereas a plastic film covers the remaining screen. For the printing process the screen is aligned to the substrate to ensure the exact print pattern. The polymer is applied on the screen and a rubber squeegee is flooding the open meshes with the polymer solution. At the same time the squeegee is presenting the screen to the substrate and the solution is transmitted to the active area (Fig. 3.6) [37], [38].

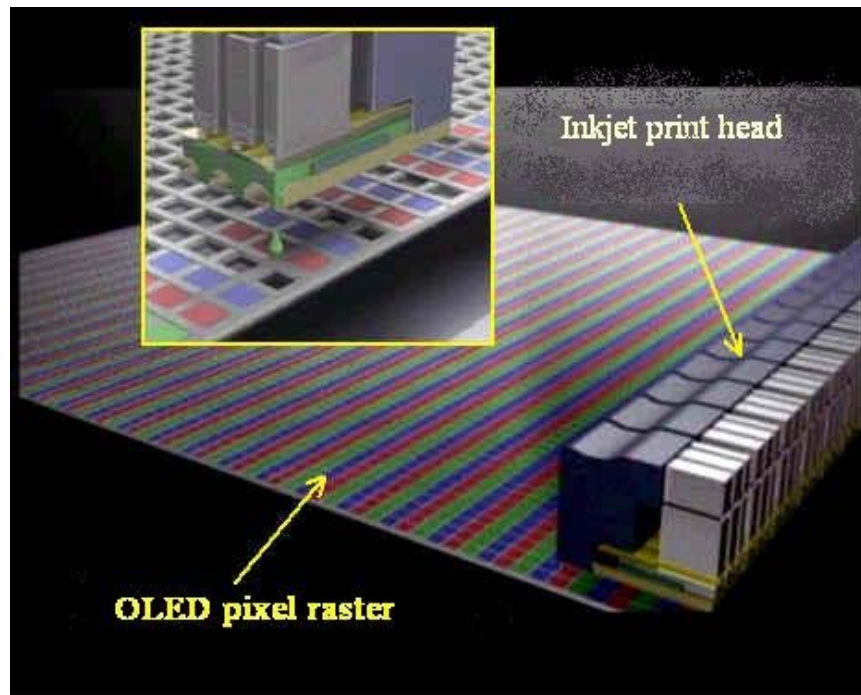


Fig. 3.6 Schematics of Screen Printing Process

For OLED application printing of extremely homogenous layers with a thickness of about 100nm is very critical. To match these requirements an adjustment of several printing parameters is necessary. Very important for good results are low viscosities and quite high boiling point solvents, well-balanced squeegee pressure, printing speed, snap off distance and adequate screen characteristics.

The development of full colour displays was carried out by screen printing an 80nm thick buffer layer of PEDOT:PSS (H.C. Stark) and a 60nm emitter layer of the white emitting polyspiro copolymer from Covion [39].

Spin coating has some drawbacks. One issue is the coverage of the whole substrate with polymer, which poses the need for complicated processes to remove the polymer from contact pad and seal frame areas. Material waste is another item where screen offers much better process.

On the other hand, spin coating advantages are high layer homogeneity and an easily adjustable layer thickness.

When the screen-printing process is compared to the spin coating alternative, the screen-printed displays reach approximately 75% of the performance of the screen coated ones. The efficiency of the screen-printed display is presently at 4,2 Cd/A,

displays produced by spin coating using the same polymer show an efficiency of 6,2 Cd/A.

In contrast to polymer devices, which are fabricated by dipping or spin-on techniques, OLEDs consisting of molecules with low molecular weight are processed in high or ultrahigh vacuum systems. The complete organic molecular beam deposition (OMBD) system is depicted in Fig. 3.7. Following the concepts of inorganic semiconductor MBE²⁹ systems, it consists of two organic growth chambers (base pressure approx. 10^{-9} mbar), a metallization chamber, a sputter chamber and a substrate pretreatment chamber, connected by a vacuum transfer system. The organic source materials are sublimated from effusion cells. Cell temperatures can range from 100 to 450⁰C, while growth rates are kept rather low in order of 2–8 nm/min to achieve smooth and homogenous thin films on an ITO-coated glass substrate, which can be cooled. Layer thickness is monitored with a quartz oscillator. Co-evaporation of organic molecules for doped layers is feasible.

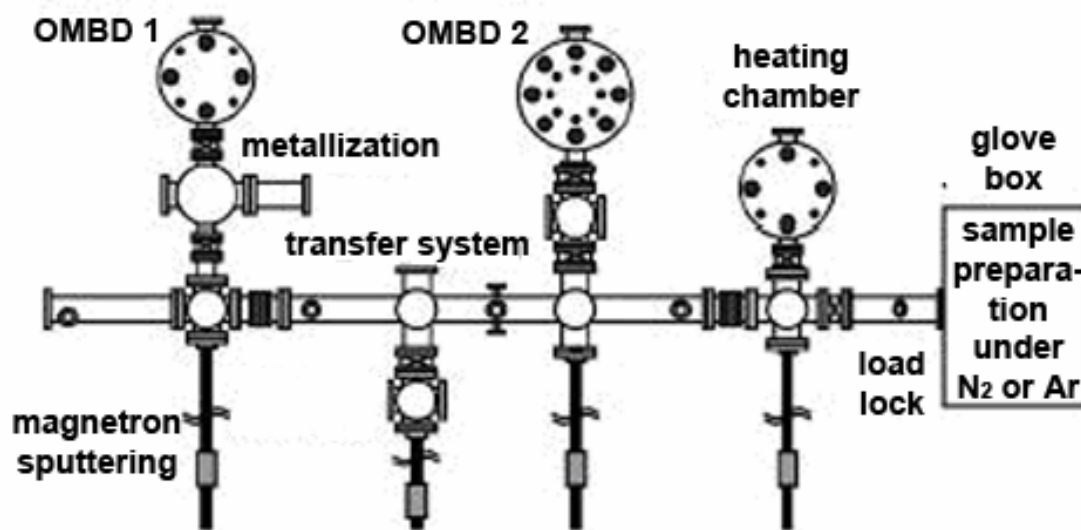


Fig. 3.7 OMBD System (source: T. Dobbertin et al. / Thin Solid Films 442 (2003) 132–139)

The conventional OMBD technology is not easily scalable to meet production requirements. It is more promising to follow a different approach that is comparable to previously suggested concepts [25], [26]. Fig. 3.8 shows an in-line

²⁹ Molecular Beam Epitaxy

OMBD system. Samples are advanced through the vacuum system, which consists of several evaporation chambers. Each of these chambers contains one or two evaporation sources, so that co-evaporation of guest–host systems is possible and certain flexibility in the layer and material sequence in the OLED production is maintained. The final evaporation process is the contact metallization. For substrate preparation, the OMBD³⁰ system includes an evaporation chamber equipped with sputter and e-beam sources.

Advancing a substrate over an evaporation source which emits a molecular beam through a narrow slit rectangular to the direction of substrate movement, will principally result in a superior homogeneity of layer thickness. The variation in the film thickness is well below 5% over a substrate width of 160 mm. The length of the substrate is determined by the carrier transport capability. Further, the source material yield is very good. Care has to be taken to avoid organic layer build-up on the sample guiding system. Finally, the processing time per sample for such a system is much lower in comparison to evaporation systems featuring a single (Fig. 3.7) or cluster evaporation chambers. The processing time can further be reduced if a second load lock is implemented at the end of the in-line system or if the system exhibits a ‘circular’ shape, so that the samples return to the starting point after layer deposition.

³⁰ Organic molecular beam deposition

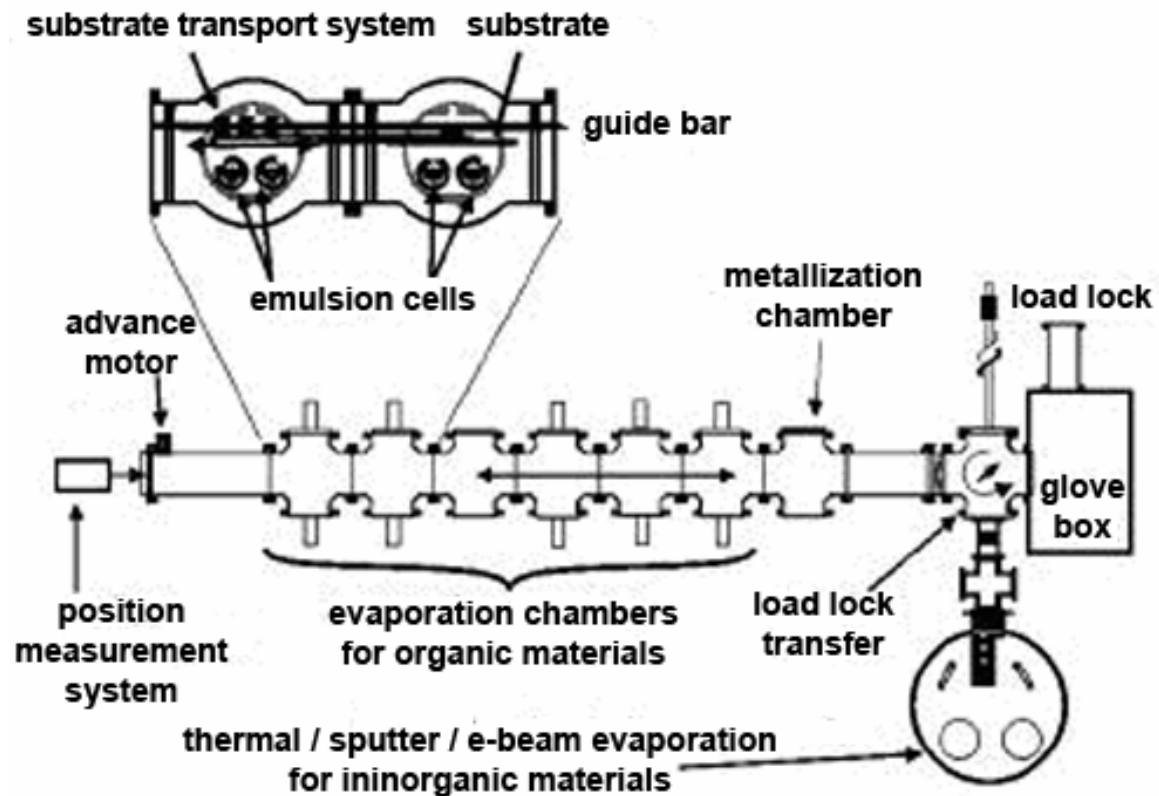


Fig. 3.8 In-Line OMBD System (source: T. Dobbertin et al. / Thin Solid Films 442 (2003) 132–139)

The fabrication process is based on ITO coated glass substrates. The pixels are obtained by etching the lithographically patterned ITO layer. Since the sensitivity of the organic layers to chemicals and humidity does not allow patterning of the metallic top contact after deposition, a different approach has to be used. Due to the desired high resolution and the resulting small pixel pitch, the adjustment of a shadow mask is too error-prone, especially if one does not want to break the vacuum between organic and metal layer deposition. Instead, we use photoresistant barriers to separate adjacent rows. The barriers are 20 times higher than the organic films and metal layer. Furthermore, the photoresistant forms a distinct undercut, leading to a reliable separation of the evaporated layers into single columns.

3.2 Introduction and Uses of Indium-Tin Oxide (ITO)

As is mentioned above, the OLED displays are based on the luminous polymer and conductive layer - ITO. The ITO layer forms the pixel structure on the carrying substrate – usually transparent material (glass, quartz, etc.).

Interest in transparent conductors can be traced back to 1907 when reports of transparent and conductive cadmium oxide (CdO) films first appeared. Since then there has been a growing technological interest in materials with these unique properties as evidenced by not only their increased numbers but also the large variety of techniques that have been developed for their deposition. It is now known that non-stoichiometric and doped films of oxides of tin, indium, cadmium, zinc and their various alloys exhibit high transmittance and nearly metallic conductivity is achievable [40]. However, tin doped indium oxide (ITO), with reported transmittance and conductivity as high as 95% and $1 \times 10^4 \text{ W}^{-1}\text{cm}^{-1}$ respectively, is among the most popular of these thin films which have found a host of electronic, optoelectronic and mechanical applications. Hence, some of the physical and technological aspects behind ITO films will now be reviewed and discussed.

Uses of ITO have traditionally ranged from transparent heating elements of aircraft and car windows, antistatic coatings over electronic instrument display panels, heat reflecting mirrors, antireflection coatings and even in high temperature gas sensors. Early electro-optic devices using ITO include OLED displays, liquid crystal displays, CCD³¹ arrays and as transparent electrodes for various display devices. More recently, ITO has been used as a transparent contact in advanced optoelectronic devices such as solar cells, light emitting and photo diodes, photo transistors and lasers - some for the first time as a result of this investigation [41]. Thus it is soon becoming an integral part of modern electronic technology wherever there is a potential for improving quantum efficiency of light emitting devices or optical sensitivity of light detecting devices.

³¹ Charge-coupled device

3.2.1 Patterning ITO

Patterning ITO is necessary not only for appraising the quality of the film, but also for fabricating useful micro-contacts to devices. As for metals and semiconductors, there are two potential methods of patterning ITO:

- Etch lithography;
- Lift-off lithography.

In my case the building of the pixel structures is done through the use of etch lithography process, and the chromium contact pads are done by means of lift-off lithography.

3.2.2 Spin-On Method

Spin-on is a process to put down layers of dielectric insulators and organic materials. The equipment of this method is simple and requires a variable-speed spinning table with appropriate safety screens. A nozzle dispenses the material as a liquid solution in the centre of the wafer. Spinning the substrate at speeds of 500 to 5000rpm for 30 to 60 seconds it spreads the material to a uniform thickness.

Photo-resists and polymers are common organic materials that can be spin on a wafer with a typical thickness between 0.5 and 20 μm , though some special purpose resists can exceed 200 μm . The organic polymer is normally in suspension in a solvent solution; subsequent baking causes the solvent to evaporate, thus forming a firm film.

Thick (5-100 μm) spin-on glass (SOG) has the ability to uniformly coat surfaces and smooth out underlying topographical variations, effectively planarizing surface features. Thin (0.1-0.5 μm) SOG have been widely investigated in the integrated circuit industry as an interlayer dielectric between metals for high-speed electrical interconnects; however, its electrical properties are considered poor compared to thermal or CVD³² silicon oxides. Spin-on glass is commercially available in different forms, commonly siloxane- or silicate based. The latter type allows water absorption into the film, which results in a higher relative dielectric constant and a tendency to crack. After deposition, the layer is typically made thick at a

³² Chemical vapor deposition

temperature between 300^o and 500^oC. Measured film stress is approximately 200MPa in tension but decreases substantially with increasing anneal temperatures.

3.2.3 Photolithography

Patterning ITO is necessary for getting of desired structure on the substrate, creating a contacts, conductivity wires i.e. all the stuff needed for creating of one full functionality device based on transparent conductor. As is mentioned above for metals and semiconductors, there are two potential methods of patterning ITO:

- lift-off lithography
- etch lithography

Lithography involves three sequential steps:

- Application of photo-resist (or simply “resist”), which is a photosensitive emulsion layer;
- Optical exposure to print an image of the mask onto resist;
- Immersion in an aqueous developer solution to dissolve the exposed resist and render visible the latent image.

The mask itself consists of a patterned opaque chromium (the most common), emulsion, or iron oxide layer on a transparent fused-quartz or soda-lime glass substrate. The pattern layout is generating, using a computer-aided design (CAD) tool and transferred into the opaque layer at a specialized mask-making facility, often by electron-beam or laser-beam writing. A complete microfabrication process normally involves several lithographic operations with different masks.

Positive photoresist is an organic resin material containing a sensitizer. It is spin-coated on the wafer with a typical thickness between 0.5 μ m and 10 μ m. Special types of resist can be spin to thickness of over 200 μ m, but the larger thickness poses significant challenges to exposing and defining features below 25 μ m in size. The sensitizer prevents the dissolution of unexposed resist during immersion in the developer solution. Exposure to light in the 200-nm range (ultraviolet to blue) breaks down the sensitizer, causing exposed regions to immediately dissolve in developer solution. The exact opposite process happens in negative resists – exposed areas remain and unexposed areas dissolve in the developer.

Optical exposure can be accomplished in one of three different modes: contact, proximity, or projection. In contact lithography, the mask touches the wafer. This normally shortens the life of the mask and leaves undesired photoresist residue on the wafer and the mask. In proximity mode, the mask is brought to within 25 to 50 μm of the resist surface. By contrast, projection lithography projects an image of the mask onto the wafer through complex optics.

Resolution, defined as the minimum feature the optical system can resolve, is seldom a limitation for two-dimensional display devices, but the need of considerable higher resolution for three-dimensional ones makes this problem important. For proximity systems, it is limited by Fresnel diffraction to a minimum of about 5 μm , and in contact systems it is approximately 1 to 2 μm . For projection systems, it is given by $0.5 \times \lambda / NA$, where λ is the wavelength (~400nm) and NA is the numerical aperture of the optics. Resolution in projection lithography is routinely better than micrometer. Depth of focus, however, is a more severe constraint to lithography, especially in light of the need to expose thick resist or accommodate geometrical height variations across the wafer. Depth of focus for contact and proximity systems is poor, also limited by Fresnel diffraction³³. In projection systems, adjusting the focus settings can move the image plane, but once it is fixed, the depth of focus about that plane is limited to $\pm 0.5 \times \lambda / NA^2$. Depth of focus is typically limited to few microns.

Projection lithography is clearly a superior approach, but an optical projection system can cost significantly more than proximity or contact system.

For our 3D OLED display, conventional photolithography is used as patterning technology employed in the manufacturing. It uses photomask and photoresist. The resist is positive, type AZ 1518, Clariant.

3.2.4 Etching of ITO

In etching, the objective is to selectively remove material using imaged photoresist as a masking template. The pattern can be etched directly into the glass substrate or into a thin film, which may be used as a mask for subsequent etches. For a

³³ Fresnel diffraction or near-field diffraction is the diffraction pattern of an electromagnetic wave obtained close to the diffracting object (often a source or aperture).

successful etch, there must be sufficient selectivity (etch-ratio) between the material being etched and the masking material.

Etching process, like metallization, is an integral part of fabricating semiconductor devices on wafers with epitax grown active layers. These vertically stacked layers have to be defined by mesa etching in order to make contacts to underlying layers or simply to electrically isolate a working device to restrict undesirable leakage currents. In addition, certain metals and compounds can also be defined by etching after deposition. Chemical etching is one of the more convenient ways of achieving this [44]. In its simplest mode, chemical etching involves the dissolution of the material without any change in the chemical nature of the dissolved species. Factors affecting etch rates include temperature, humidity, strength of the etching solution as well as the morphology and the cleanliness of the surface being etched. In addition, given the tendency of different crystallographic planes to etch at dissimilar rates, various orientations of single-crystal substrates may etch very differently in a given etchant [45].

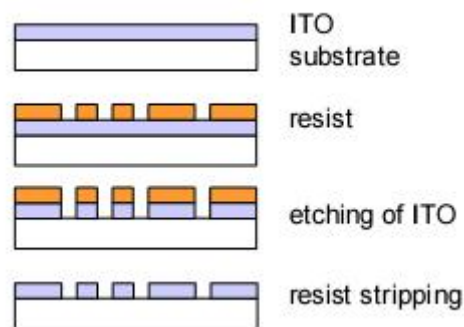


Fig. 3.9 High-resolution ITO structuring

We used two step etching process. First was dry etching step and the second a wet etching step. During the first step high pattern definition was obtained and all possible resist residues have been removed. In the second step we used standard etching solution (HCl:HNO₃:H₂O), completely removing all remainders of ITO at the substrate – ITO interface that survived the dry etching process, thereby avoiding "parasitic" contacts in the insulation spacer areas between two adjacent

ITO conducting lines, causing either shorts between two adjacent lines or "parasitic" light emission. There are some shortcomings such as isotropic under cutting of the mask during the wet etching step, which must be considered and compensated in the final display design.

Another possibility for etching is plasma³⁴. Plasma etching is relatively new technique in the fabrication of integrated circuits and microsystems. It was introduced in the seventies, mainly for stripping resists. In the eighties, plasma etching became a mature technique to etch layers and was introduced in the production of integral circuits. Reactive Ion etching was the main technology, but new techniques were developed. In the nineties new techniques, such as electron cyclotron resonance (ECR), and inductively coupled plasmas (ICP), were introduced, with mixed success.

3.2.5 Metallization and Ohmic Contacts – Lift-off Process

Making metal contacts practically is the first step of producing an OLED sample, based on ITO substrate. These chrome contacts ensured low impedance between the contact socket and ITO layer.

³⁴ Typically an ionized gas, and is usually considered to be a distinct phase of matter in contrast to solids, liquids, and gases because of its unique properties.

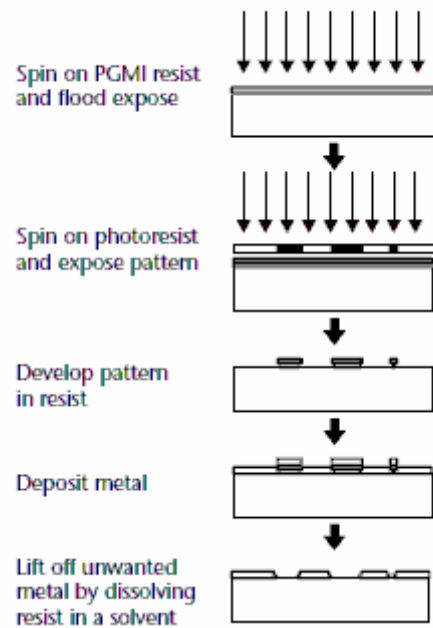


Fig. 3.10 Process flow for lift-off

Lift-off is a simple method for patterning, usually metallic layers. It is used for metals that are difficult to etch or where etching might damage other materials already on the substrate. A typical process is as follows Fig. 3.10. On the first place a resist is deposited and patterned with an image of contacts where the areas intended to have metal are cleared by the developer. On the second place metal is deposited by evaporation or sputtering. Finally, the resist is removed in a solvent such as acetone that takes away the resist and lifts off the unwanted material. In order to achieve best results the pattern may have undercut edges. This can be achieved by soaking the resist in chlorobenzene. Depending on the exposure time, this penetrates only a certain depth into the resist, causing the surface of the resist to develop at a slower rate than the resist in contact with the wafer. The process however is difficult to control and success is often only partial. Usually, the problems in combination: ITO and chrome, deposited by lift-off process are small chrome particles (in micrometer order), making foul the sample. For our 3D OLED display a negative photo resist type (ma-N 420, MRT) is used so as to lift-off the metal contacts.

3.2.6 Measurement and Analysis techniques

A schematic diagram of a semiconductor with ohm contact pads is shown in Fig. 3.11. Metal pads of finite width, w , and length, s are then deposited on mesa at a linearly increasing pad spacing, L , such as $L_1 < L_2 < L_3$. A constant current is passed between two adjacent pads through two probes; a second set of probes is then used to measure the voltage drop using a voltmeter, enabling the total resistance between the pads to be obtained. Separate current source and voltmeter are preferred to a single ohm meter because of the latter's relatively low impedance which may lead to inaccuracies. The process is repeated and the total resistance is plotted on a linear graph as a function of pad spacing.

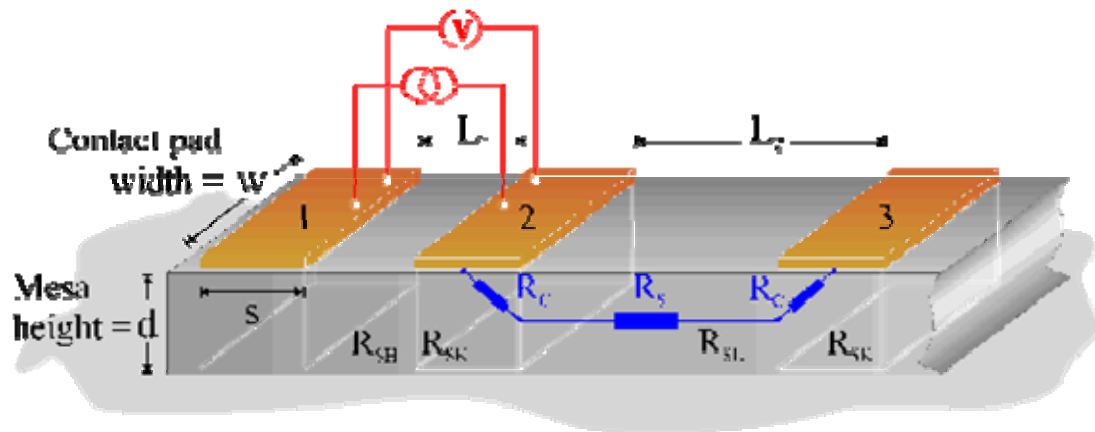


Fig. 3.11 Schematic diagram of a semiconductor material with ohmic contact pads

From Fig. 3.11, it is seen that resistance, r , between two adjacent pads, is given by:

$$r = 2R_c + R_s \quad (3-1)$$

where,

R_c – resistance due to the contact

R_s – resistance due to the semiconductor material

R_s is given by:

$$R_s = \frac{\rho L}{dw} \quad (3-2)$$

where,

r – resistance of the semiconductor material.

But, since the sheet resistance, R_{sh} , of the semiconductor is given by ρ/d , we can re-write (3-1) as:

$$r = 2R_c + R_{sh}\left(\frac{L}{w}\right) \quad (3-3)$$

Thus, (3-3) has gradient of R_{sh}/w and x and y axis intercepts at L_x and $2R_c$ respectively. In [42] is shown that R_c can be expressed as:

$$2R_c = \frac{2R_{sk}L_T}{w} \quad (3-4)$$

where,

R_{sk} – modified sheet resistance of the material directly underneath the pads

L_T - the transfer length related to the distance required for current to flow into or out of the ohmic contact.

$$L_T = \sqrt{\frac{\rho c}{R_{sk}}} \quad (3-5)$$

where,

$$L_x = \frac{2R_{sk}L_T}{R_{sh}} \quad (3-6)$$

After rearranging of (3-4) and (3-5):

$$L_T = \frac{R_c w}{R_{sk}} \quad (3-7)$$

$$\rho c = L_T^2 R_{sk} \quad (3-8)$$

Substituting (3-7) in (3-8):

$$\rho c = \frac{(R_c w)^2}{R_{sk}} \quad (3-9)$$

In practice, the resistance between two contact pads or respectively the current is calculated, using the specific square resistance of ITO. Typically the resistance is between 10 and 100 Ω .

3.3 Lens-raster glasses

Lenticular simply means “biconvex³⁵”. A lenticular lens is a single convex lens that magnifies light through a prism effect. It is also an array of magnifying lenses, designed so that when viewed from slightly different angles, different images are magnified. The simplest form of a lenticular lens is a bifocal, which has just two magnifying lenses. Typically lenticular lenses are used to make lenticular print, for transforming, moving images, or 3d-effects (Fig. 3.12).

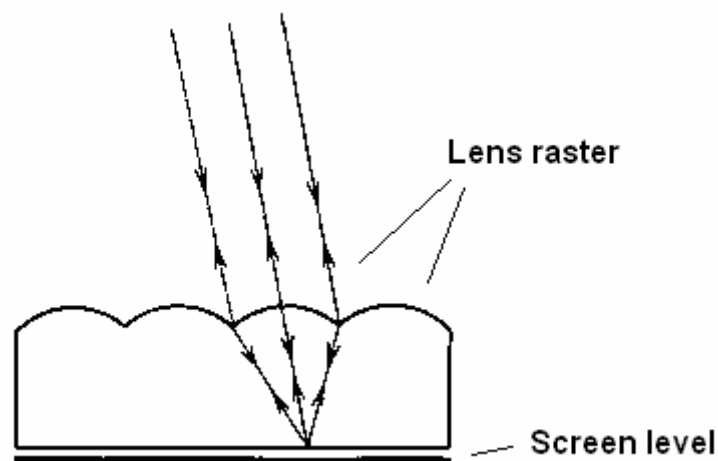


Fig. 3.12 Lenticular glass – cross section

The term Lenticular is often confused as a printed image that shows depth or motion as the viewing angle changes. But in general Lenticular is a term for the lens effect that creates a convex perspective of multiple images of light sources, but not necessary a physical printed image. This Lenticular technology can be used to create a lenticular image through the process of lenticular printing. This technology was created in the 1940s, but has evolved during the recent years to show more motion and increase the depth. Originally used mostly in novelty items, lenticular prints are now being used as a marketing tool to show products in three dimension and motion.

The key that makes a lenticular work is the plastic sheet that overlays the printed image. The sheet is moulded to have the form of dozens of tiny lenses or prisms

³⁵ Both surfaces are convex

per inch. There are actually two methods for printing the image. The first is printing the image on some material and then have the plastic lens properly overlaid. (Getting the lenticular lens lined up properly is referred to as "registration.") The second method is to print the image directly to the back of the lens itself.

The same sort of melded sheet is frequently used with projection television systems. In this case, the purpose of the lenses is to focus more of the light into a horizontal beam and allow less of the light to escape above and below the plane of the viewer. In this way, the apparent brightness of the image is increased.

The term "Lenticular" was used in the patent to describe linear lenses. Informally, lenticulars had been produced since the 1930s. The technology was not widely used until recent years as the cost of plastics (PVC³⁶) decreased and the new material PETG³⁷ emerged. The advancement of output, proofing and commercial printing also contributes to the mass production of lenticular products.

3.4 Summary

This chapter presented the basics concepts necessary for the study of the OLED devices with a description of the assumptions and limitations required in their development and applicability. There are also presented the main components and processes for building of an OLED unit.

³⁶ Polyvinyl chloride

³⁷ Polyethylene terephthalate

4. Multiperspective mixing algorithm. Digital and binary 3D sub-pixel arrangements.

4.1 Multiperspective mixing algorithm.

There is an algorithm used for mixing the source images. The algorithm computes the positions of the pixels from the input image, which must be placed on the output:

```

for( i = 0 ; i <= output_image_height_pixels ; i++ )
{
    row_new = i * lenses_per_inch / dot_per_inch ;
    if (row_new > input_image_height_pixels )
    {
        dst_height = i--;
        break;
    }
    if( row_new == row_old )
        perspective++;
    else
        perspective = 0;

    row_old = row_new;

    // Ceilenpositionen
    mix_mask[ (i * 2) + 0 ] = perspective;    // Pict. number
    mix_mask[ (i * 2) + 1 ] = row_new;       // Col. number
}
    
```

In the output array `mix_mask` are stored the sequences of input image number and input pixel address. The array's index coincides with the pixel number of the output image (Fig. 4.1). After the sequence generation, the values from the array are read and used as indexes for a simple copy operation:

$out_pixel = f(input_image_number, input_image_pixel)$

Img No.	Pix. No.	Img No.	Pix. No.	Img No.	Pix. No.	Img No.	---
1	2	3	4	5	6	7	---

Output image pixel sequence

Fig. 4.1 Sequence, generated from the mixing algorithm.

Such solution gives as flexibility - the algorithm can be used in different coding principles one changes and after pixel position determination, the process is simply copying.

4.2 Digital and binary 3D sub-pixel arrangements.

There are some possibilities to generate a picture for a different kind of displays:

- Controlling through pixel illumination
- Controlling through distribution of pixel sizes
- Controlling through dynamic pixel size variation

Each of them has some advantages and disadvantages. Below follows description of each type, and short description of algorithms, used for pixel control.

4.2.1 Controlling through pixel illumination

This is the most wide-spread principle for generating images on a conventional type of display (CRT; TFT; OLED). Usually there is a RGB matrix, arranged on a plane of display (Fig. 4.2).

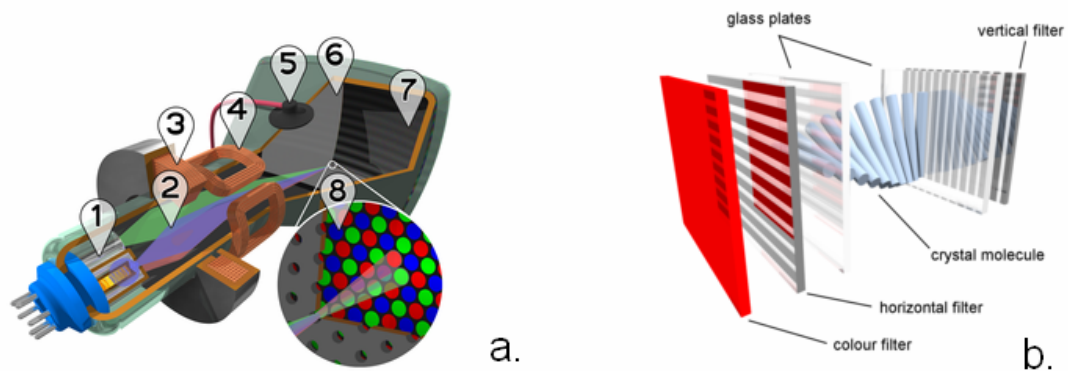


Fig. 4.2 Principle of CRT (a.) and TFT (b.) monitors functioning.

The main components of a CRT tube are (Fig. 4.2a):

1. Electron guns
2. Electron beams
3. Focusing coils

4. Deflection coils
5. Anode connection
6. Mask for separating beams for red, green, and blue part of displayed image
7. Phosphor layer with red, green, and blue zones
8. Close-up of the phosphor-coated inner side of the screen.

The electron beam source is the electron gun, producing the stream of electrons by thermionic emission and then focusing it into a thin beam. The gun is located in the narrow, cylindrical neck at the extreme rear of a CRT and has electrical connecting pins, usually arranged in a circular configuration, extending from its end. These pins provide external connections to the cathode, to various grid elements in the gun used to focus and modulate the beam, and, in electrostatic deflection CRTs, to the deflection plates. Since the CRT is a hot-cathode device, these pins also provide connections to one or more filament-type heaters within the electron gun. When a CRT is in operational mode, usually the gun heaters can be seen glowing orange through the glass walls of the CRT neck. It is the need for these heaters to achieve their effect that causes a delay between the times that a CRT is first turned on and the time that a display becomes visible; the CRT literally needs time to "warm up". In the older tubes, this could take fifteen seconds or more; modern CRT displays have fast-starting circuits that display an image within about two seconds, using either briefly increased heater current or elevated cathode voltage. Once the CRT has warmed up, the heaters stay on continuously to keep the cathode warm. The electrodes are often covered with a thermally black layer, a patented process used by all major CRT-manufacturers to improve electron density.

This kind of display has one big disadvantage – the geometry and the sub-pixels arrangement are non-homogeneous on the display surface, which means that it is impossible to mount a lenticular glass.

The liquid crystal display (LCD) (Fig. 4.2b) is a thin, flat display device made up of any number of colour or monochrome pixels arrayed in front of a light source or reflector. Engineers prize it because it uses very small amounts of electric power, and is therefore suitable for use in battery-powered electronic devices.

Each pixel consists of a layer of liquid crystal molecules suspended between two transparent electrodes, and two polarizing filters, whose axes of polarity are

perpendicular to each other. Without the liquid crystals between them, one of the layers would block the light passing through the other one.

Before applying an electrical charge, the liquid crystal molecules are in a relaxed state. Charges on the molecules cause these molecules to align themselves with microscopic grooves on the electrodes. The grooves on the two electrodes are perpendicular, so the molecules arrange themselves in a helical structure, or twist (the "crystal"). Light passing through one of the filters is rotated as it passes through the liquid crystal, allowing it to pass through the second polarized filter. The first polarizing filter absorbs half of the light, but otherwise the entire assembly is transparent.

When an electrical charge is applied to the electrodes, the molecules of the liquid crystal are pulled parallel to the electric field, thus reducing the rotation of the entering light. If the liquid crystals are completely untwisted, light passing through them will be polarized perpendicular to the second filter, and thus it will be completely blocked. The pixel will appear unlit. By controlling the twist of the liquid crystals in each pixel, light can be allowed to pass through in varying amounts, illuminating the pixel respectively.

It is normal to align the polarizing filters in a way that the pixels are transparent when relaxed and become opaque in the presence of an electric field; however the opposite is sometimes done for special effect.

There are also models with additional "white" sub-pixel³⁸.

The big advantage of TFT displays are the precise pixel (sub-pixel) sizes and arrangement on the display surface. This explains why most contemporary autostereoscopic displays are based on this principle.

4.2.2 Controlling through distribution of pixel parts

As is noticed above there is a possibility to control the sub-pixel illumination through distribution of the pixel parts.

The sub-pixel is divided in several parts. Each of them is identical. Usually the number of the parts is power of two. This is due to the easy generation and control

³⁸ The white sub-pixel is actually a clear area with no colour filter material; therefore the light transmission from the backlight is high. The use of white subpixels can therefore increase the total brightness of the display by 50% or more.

throw binary algorithms. (Fig. 4.3) Special controller can drive each of them independently. The luminance is function of the “lighting” parts. The number of the sub-pixel parts is as much, as are the colours that can produce the pixel.

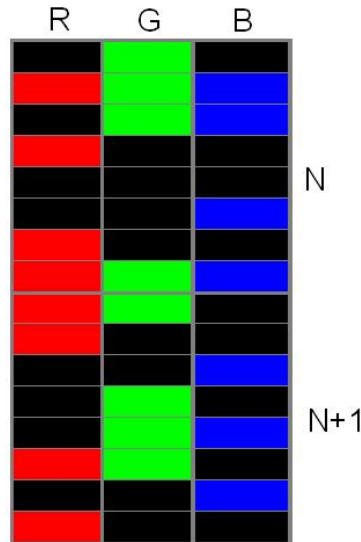


Fig. 4.3 Controlling trough distribution of pixel parts

There are some requirements in order to generate a better quality and clean picture. When the neighbouring parts of the pixel are with near or identical on-off characteristics the so-called moiré effect can be observed. The moiré pattern to some extent cannot be avoided, but in favourable circumstances the pattern is "tight;" i.e. the spatial frequency of the moiré is so high that it is not noticeable. In fact, the term moiré means an excessively visible moiré pattern. The visibility of moiré is not entirely predictable. The same set of part combinations may produce good results with some images, but visible moiré with others. To avoid such phenomenon it is enough to analyse the parts of the neighbour pixels and the current pixel to be generated with different stripes combination. For better quality results it is reasonable to generate the parts with some random function. It is a challenge to develop such a type of algorithm because on the first place a “random generator” consumes a lot of time and computing power and on the second place, each sub-pixel must be analysed and compared to its neighbours.

As I wanted to simulate such type of coding, it was enough to generate one single picture. The requirements are: fast and flexible algorithm for generating 3D

autostereoscopic images with possibilities to easy alter the pixel parameters, lens-raster glass parameters, and colour depth. The algorithm that meets those requirements is shown in Appendix 2.

This function has a possibility to code RGB and CMYK colour images. So it can be applied either on 3D images, generated for flat screens or high-resolutions printouts. For most efficiency and execution speed the following features have been implemented:

- Using a high-speed random generator that works independently from the RTC (Real Time Clock) of the computer. Such generator algorithm is more than one hundred times faster than the conventional, which used the RTC. The source code of random generation function is included in Appendix 2.
- There is a possibility to switch between RGB and CMYK colour spaces. As it was noted above, this gives us a possibility to use the algorithm flexible for flat panels – TFT, OLEDs or some type of high-resolution printouts.
- For better efficiency, the function is executed in own thread.

4.2.3 Controlling through dynamic pixel size variation

The next possibility for controlling the colour information is throwing that uses variable size of the emitting part of the sub-pixels. The pixel size is constant, but throw a sliding rules from both sides, the quantity of the emitting colour light is controlled (Fig. 4.4). On the image are presented the principle of function.

The algorithm, which calculates the pixel gaps, is shown in Appendix 2.

A configuration that simulates the function of such type of pixel coding is prepared as an experimental setup. It generates a very-high resolution 3D autostereoscopic image. For colour mask is used paper-printed RGB mask with 0.5mm pitch. A lens-raster glass, which separates the perspectives has been mounted at the front. Between the colour mask and the lens-raster glass is placed an image, which is coded. The horizontal coding represents mixing of the observer perspectives. The vertical coding is achieved through the dynamic pixel size. The image is printed on transparent folio. Two experiments are carried out – the one with resolution of the

image 5080dpi³⁹, and the other one with 2540dpi. The perspectives number is 100 for the 5080, respectively 50 for 2540dpi, and the observer's angle is 30°. Such characteristics give us a brilliant picture quality and very realistic 3D perception. As light source is used fluorescent lamp placed behind the colour mask. 3D modelling software or pictures from digital camera can generate the source images. It is also possible to use morphing algorithms for recovery of intermediate scenes, from two or more initial pictures. The setup configuration is shown on Fig. 4.5.

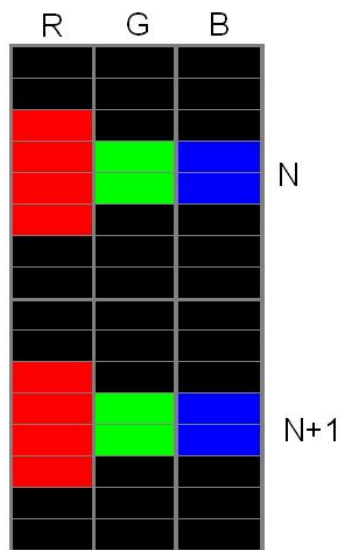


Fig. 4.4 Controlling trough dynamic pixel variation

³⁹ Measure of printing resolution, in particular the number of individual dots of ink a printer or toner can produce within a linear one-inch space. Printers with higher DPI produce clearer and more detailed output.

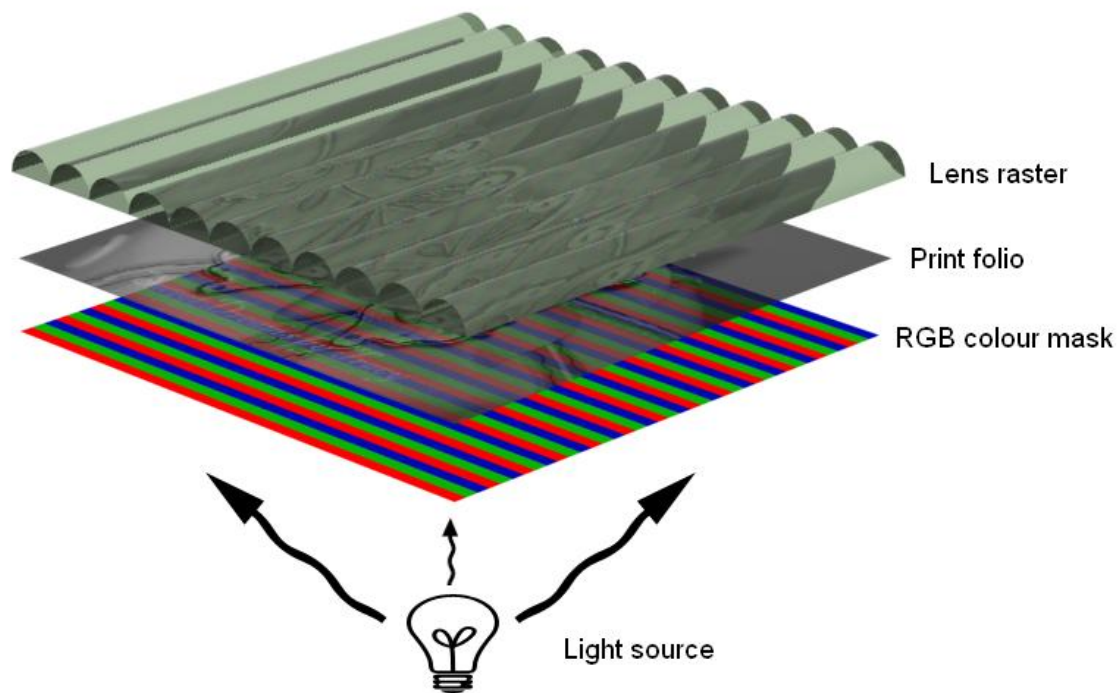


Fig. 4.5 Semi-holographic setup, based on RGB colour mask.

4.2.4 Controlling through brightness-groups

There are two types' photoreceptors in the eye - Rods and cones. The brain actually can detect one photon of light (the smallest unit of energy) being absorbed by a photoreceptor.

There are about 6.5 to 7 million cones in each eye, and they are sensitive to bright light and to colour. The highest concentration of cones is in the macula. The fovea centrals, at the centre of the macula, contain only cones and no rods. There are 3 types of cone pigments, each most sensitive to a certain wavelength of light: short (430-440 nm), medium (535-540 nm) and long (560-565 nm). The wavelength of light perceived as brightest to the human eye is 555 nm, a greenish-yellow.

There are about 120 to 130 million rods in each eye, and they are sensitive to dim light, to movement, and to shapes. The highest concentration of rods is in the peripheral retina, decreasing in density up to the macula. Rods do not detect colour. The rod pigment is most sensitive to the light wavelength of 500 nm. This

means that the ratio rods to cones are around 15:1 or proportion from 3:1 in horizontal and vertical directions. In case that a man has only rods, all subpixels of a display, independently from the colour can presented like a pixel, on condition that there are shined nearly equally. This means by a conventional TFT display a three times higher horizontal resolution. Therefore, the perceiving of the black-white transitions is better than between colours in some brightness.

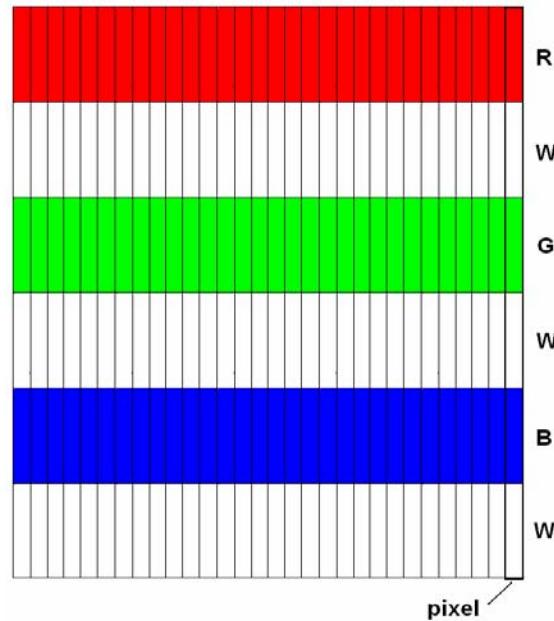


Fig. 4.6 RWGWBW Sub-pixel arrangement for optimal perception resolution in 3D scenes

Since succeeded with the perception-optimized coding to reduce black/white transitions to the sub-pixel level can increase the subjective resolution. Fig. 4.6 presented an arrangement with additional white sub-pixel, that increase the subjective resolution three times and brightness characteristics twice. In this case, the anyhow invisible monochromatic colour resolution decreases. Such vertical pixel arrangement especially reasonable because the higher horizontal resolution. Also with the following suggestion by inserting white sub-pixel will represent the red, green and blue monochromatic areas darker. However, such pixel pattern will present explicitly higher quality in natural pictures.

4.2.5 Controlling through time modulation

Response time of an OLED element of starting light emission after a voltage is applied is usually below $1 \mu\text{s}$. Due to the fast reaction, it is possible to control the luminance through change the time during the constant voltage is applied on a sub-pixel (Fig. 4.7). Such schema is use in plasma displays.

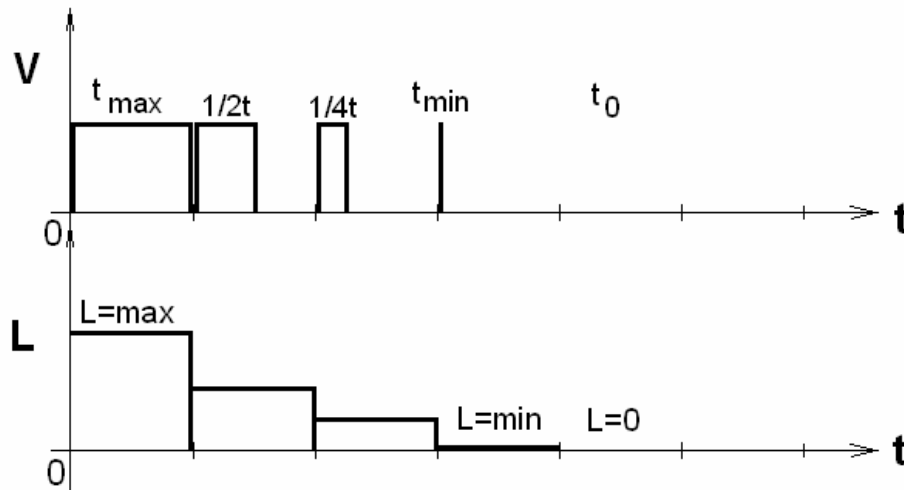


Fig. 4.7 Controlling sub-pixel luminance through time-modulation

A suggestion for refresh frequency 120Hz is, the times during the sub-pixels under voltage are, can vary from $8.3\mu\text{s}$ to 8.3ms – 10 bits coding and 1024 brightness-levels. Such wide range levels give us a possibility to obtain deeper colour depth compare to 256 levels coding.

4.3 Summary

This chapter presented the programming algorithms, including mixing of the images, and the way to coding the pixel colour information. At end is given the setup configuration for autostereoscopic three-dimensional display based on OLED and lens-raster glass.

5. Preparing of working samples and housing. Measurements and Analysis

5.1 Preparing of working sample

5.1.1 Sample for determination of the maximal Achievable resolution

It is important to define the limits of the physical parameters of the 3D display. Some of these parameters are pixel size, density of the light, clearness of the lighting surface, minimal distance between the pixels, optimal working voltage, consumption etc. It is also important to be familiar with the ITO-etch procedure. For the determination of the parameters, some steps are needed. As a base for our investigations are used 3.5" ITO wafers with different thickness.

There are some different methods for drawing of the pixel sequence – physical vapour deposition; lithography or printing with special “Ink” printer, where on the place of ink there is a very thin layer of polymer material used. In the following experiments the photolithography method is used.

At the first step is designed sample with special pattern structure for learning of the physical limits of the etch process and ITO wafer.

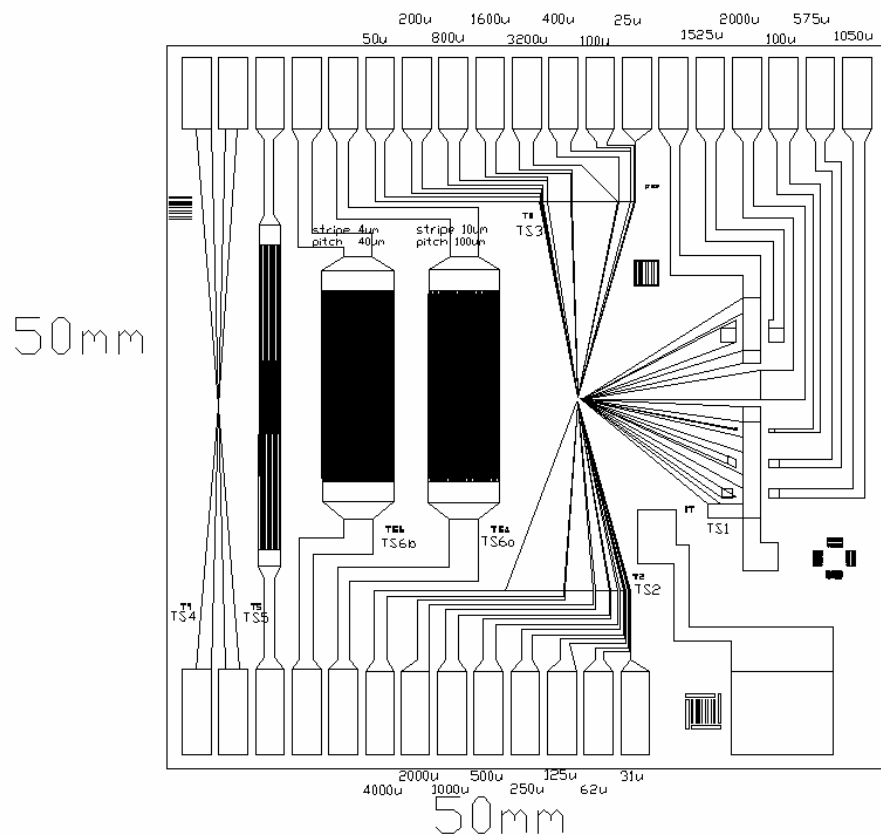


Fig. 5.1 Principal schema of OLED wafer for resolution determination

On Fig. 5.1 are shown the OLED wafer structures, for determination of the achievable resolution through wet-etch and plasma etch processes. For the process were ordered two glass masks. The first is mask, containing the structures i.e. “structures mask”. The second mask contains contact pads, used for connection between socket and glass material. This socket construction is used as a standard for furthers samples. It contains 36 contacts in number. The masks were produced on different materials, depending on the demands for accuracy. The first mask, containing structures information is filled on Quartz 4x4x0.06 inch. The minimal resolved structures are with width 0.5µm. The second mask, containing contact pads is filled on Sodalime glass 4x4x.06 inch. The masks are designed with AutoCad. The structures are projected in such a way in order to describe the all range of possible pixel sizes and distances between pixels. The detail description of the test sample is shown on Appendix A.1.

After preparing the contact mask some experiments are carried out, at first on silicon wafer (Fig. 5.2), and then on the ITO coated glass (Fig. 2.1).

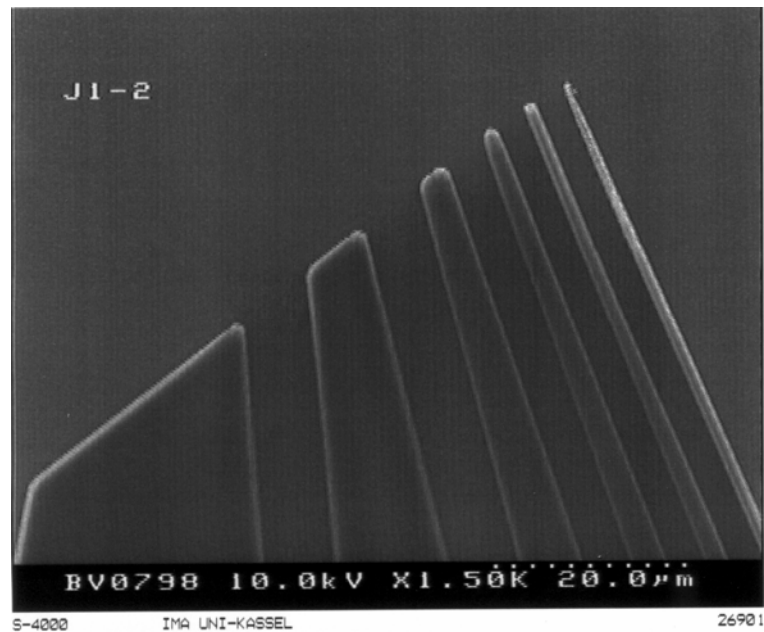


Fig. 5.2 Scan Probe Microscope photos of etch structures make on silicon wafer.

The results on silicon wafer shows that theoretically it is possible to produce with available technique structures with accuracy up to $1\mu\text{m}$. This accuracy is enough for further research work.

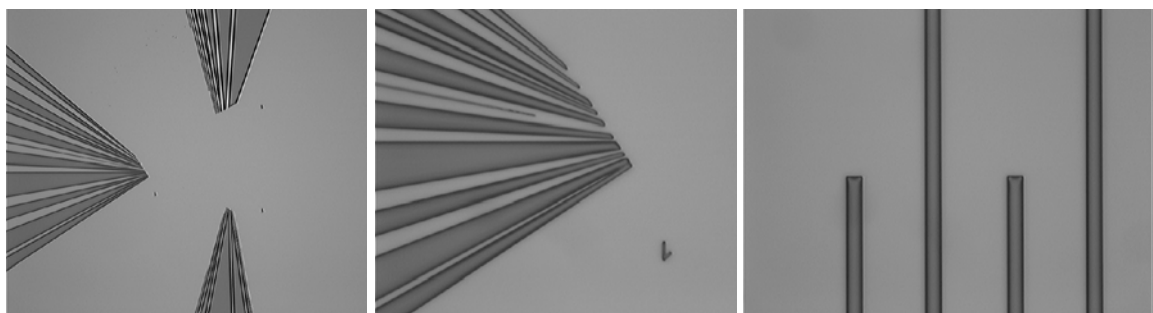


Fig. 5.3 Optical microscope photos of etch structures make on silicon wafer.

The process of etching includes the follow steps:

- cleaning of the wafer (critical because ITO is sensitive to acidity materials, that normally are used for cleaning of the wafers)

- Hexamethyldisilazane (HMDS) laying - used to improve photo-resist adhesion to oxides.
- laying photo-resist material on the wafer
- pre-bake of the photo-resist
- lithography
- post development
- post bake
- dry plasma etching
- cleaning of the rest resist (normally with acetone)

There are presented some pictures that show etched ITO structures under optical colour microscope. Some of images may have a red nuance. This is because in some of the wafers there is the rest of the resist material on it, i.e. for better optic control sometimes the last procedure (cleaning of the rest resist) is executed after optical measurement.

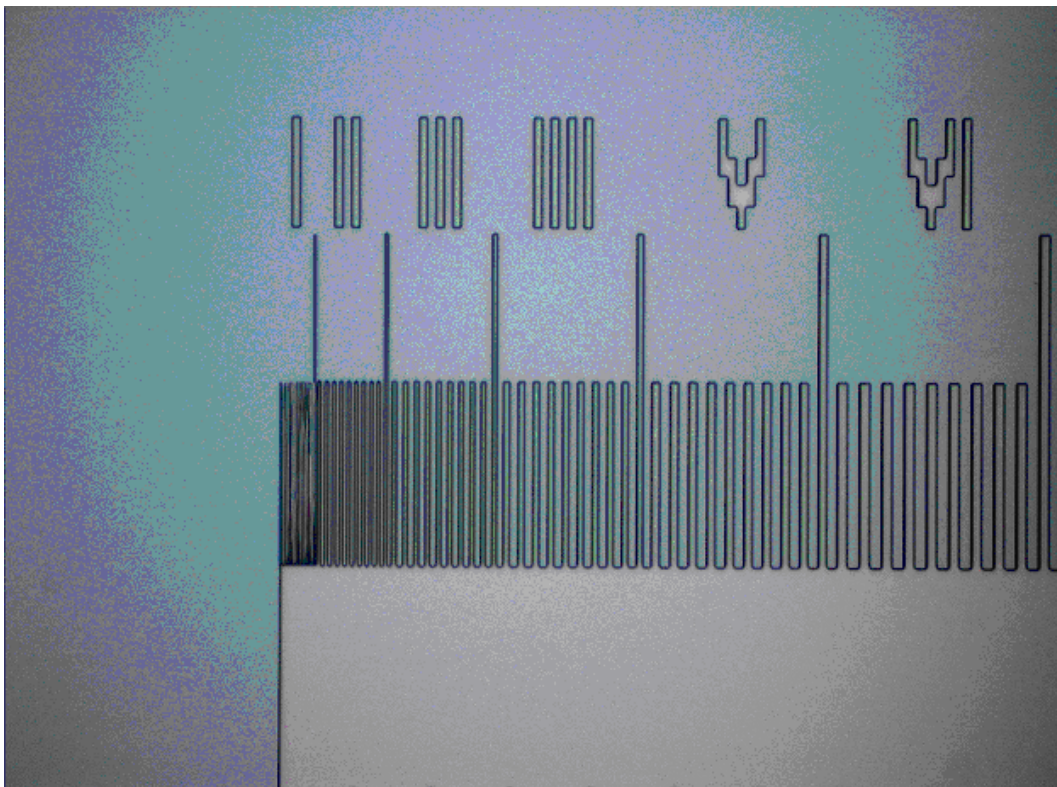


Fig. 5.4 Test structure with lines with ascending pitch in μm units.

In Fig. 5.4 is presented test structure with lines – alternated glass and ITO. In the upper site with roman digits is shown the bright of each line – glass or ITO. This means that the pitch of the first group is $1\mu\text{m}+1\mu\text{m}=2\mu\text{m}$. The first group (with pitch $2\mu\text{m}$) has bad quality – the lines are mixed and have short circuits between ITO lines. The second group – with pitch $4\mu\text{m}$ already have very good quality. The lines now are very clear and the ITO material is evenly distributed.

In Fig. 5.5 is presented the result after etching of the structure with 4 symmetric triangles going into the centre. Because the tips have extremely small size in the centre the lines stop at around $0.8\mu\text{m}$. There is no rest ITO material into the centre. Because of diffusion processes at etching, the tips are not smoothly cut, but have some small teeth.

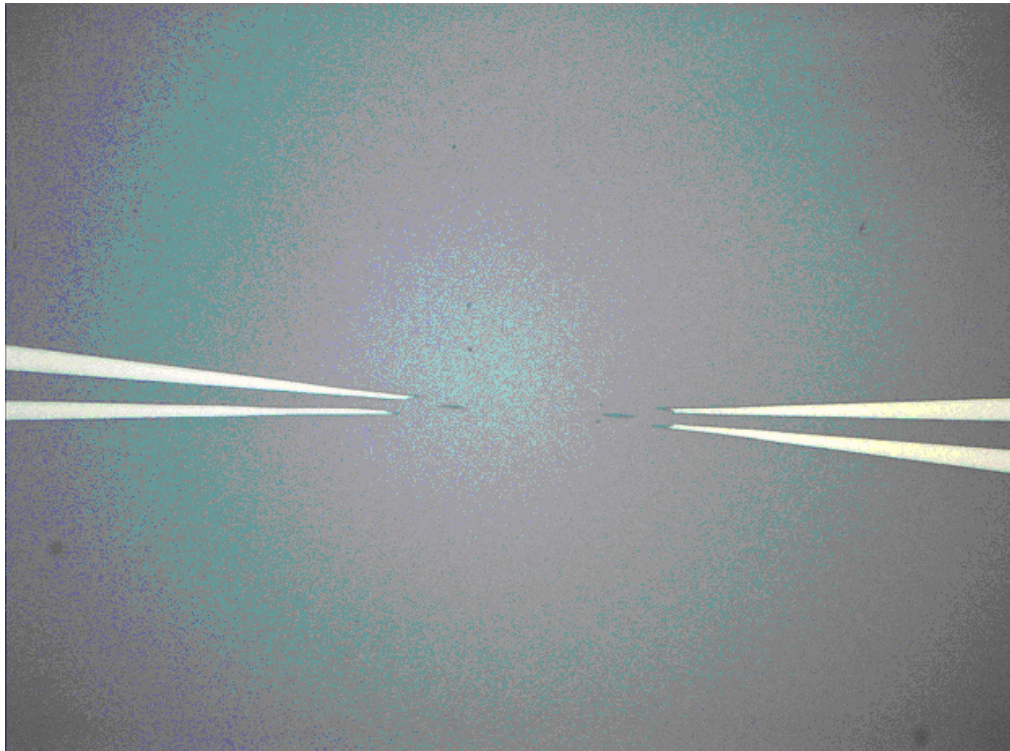


Fig. 5.5 Symmetric triangle stripes going to centre.

In Fig. 5.6 is presented a test structure for finding out the smallest distances between ITO stripes and smallest ITO stripes. Between the first and second stripe there is distance of $0.7\mu\text{m}$ which is under the resolution border for optical lithography and has got short circuit. The second distance between ITO stripes is

1,7 μm and the separation between the stripes now is very good. The smaller ITO stripe normally “printed” on this structure is with width 2 μm (the first from left), but because of the short circuit it is not easily noticed. The thinnest line is 0.2 μm – at the bottom of the picture.

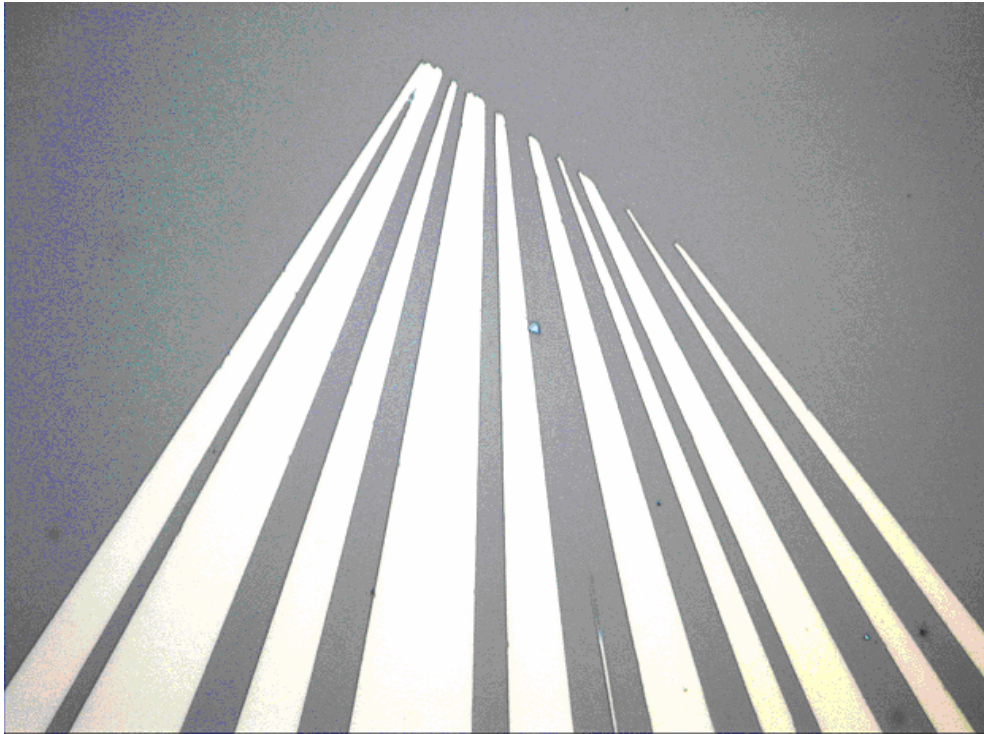


Fig. 5.6 Random arrangement test structure (from left to right) 2 μm , 3.7 μm , 2.3 μm , 5.9 μm , 3.6 μm , 0.2 μm , 4.6 μm , 3.4 μm , 6.7 μm , 3.9 μm , 6.8 μm .

In Fig. 5.7 is presented power of 2 – 8 mixed stripe arrangement. From the image it is visible that lines with widths of 3.8 μm , 3.6 μm and 1.2 μm are very clearly traced out. Lines with smaller widths on the vertexes started from minimal width of around 1.2 μm . Typical for this group structures is that in the most cases the lines are with extremely small gauges. This is the reason why so little lines are visible in comparison to the desired test structure.

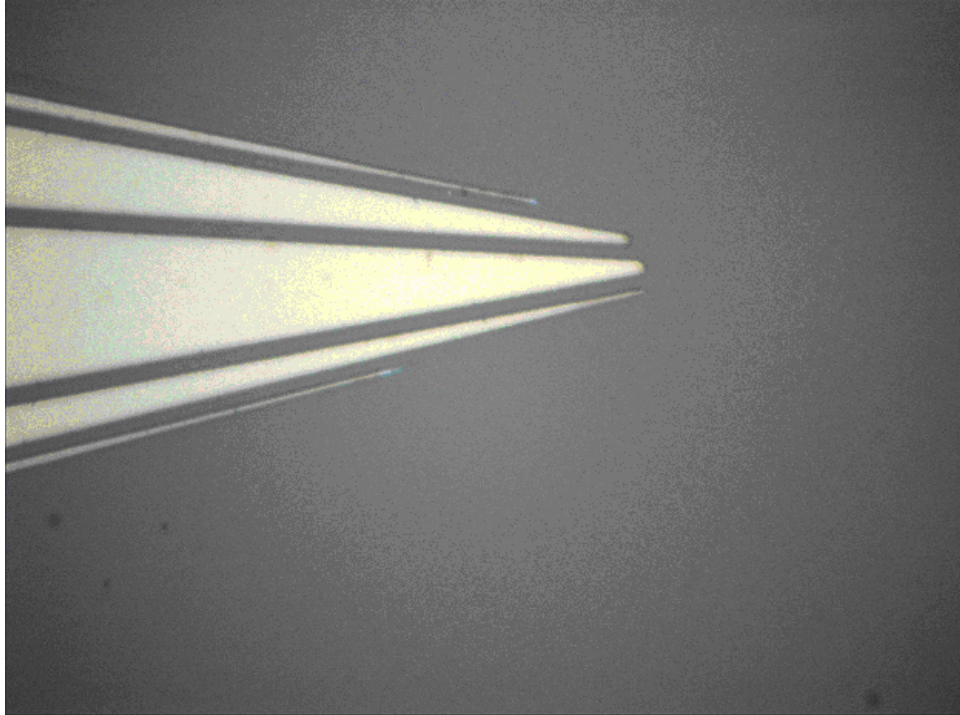


Fig. 5.7 Power of 2 mixed stripe arrangement (from top to bottom) 1.1 μm, 3.8 μm, 3.6 μm, 1.2 μm, 0.4 μm.

In Fig. 5.8 is shown power of 2 stripes. The image indicates that, the critic line there is 1.6 μm. The next line with width 1 μm on the vertex is not etched to the end.

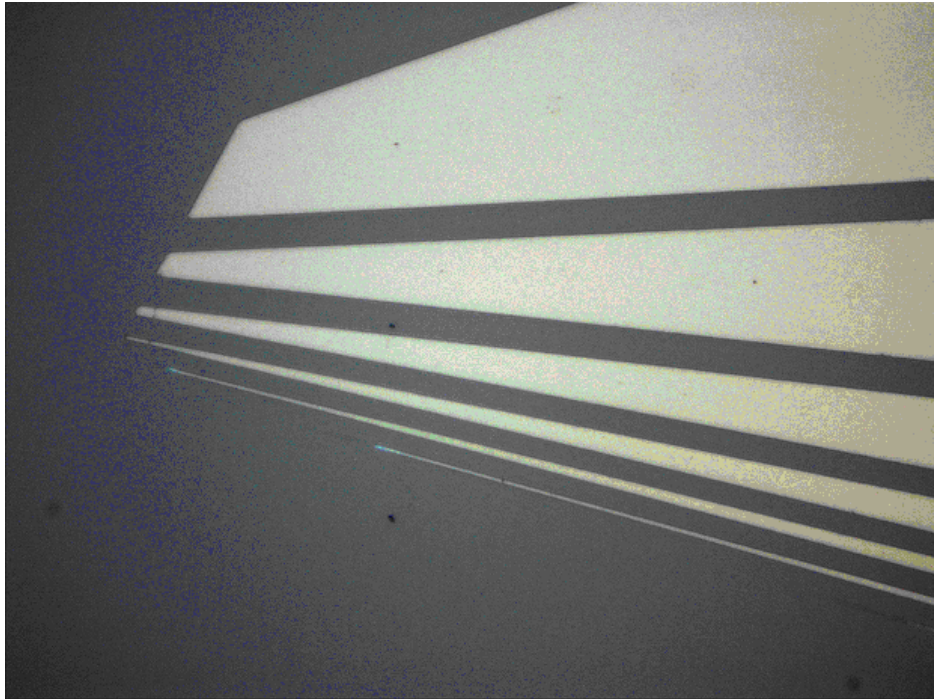


Fig. 5.8 Power of 2 stripe arrangement (from bottom to top) $1\mu\text{m}$, $1.6\mu\text{m}$, $3.4\mu\text{m}$, $7.4\mu\text{m}$, $28.1\mu\text{m}$.

After structuring the ITO layer, the ohm contacts are defined by deposition and lift-off of a metal layer (Cr/Au).

Process innovation has been achieved in the etching of ITO film which has an important role in the display manufacturing industries. As a patterning technology employed in the manufacturing is used the so-called conventional optical photolithography, which uses photo mask and photo resist. We use positive resist (AZ 1518, Clariant) for definition of ITO structures, and negative (ma-N 420, MRT) for lift-off of the metal contacts.

We used a two- step etching process. First was the dry etching step and the second was the wet etching step. During the first step high pattern definition was obtained and all possible resist residues are removed. In the second step we used standard etching solution ($\text{HCl}:\text{HNO}_3:\text{H}_2\text{O}$), completely removing all remainders of ITO at the substrate – ITO interface that survived the dry etching process, thereby avoiding "parasitic" contacts in the insulation spacer areas between two adjacent ITO conducting lines, causing either shorts between two adjacent lines or "parasitic" light emission. There are some shortcomings such as isotropic under

cutting of the mask during the wet etching step, which must be considered and compensated in the final display design.

The hole transporting layer (HTL) was polyethylenedioxythiophene doped with polystyrenesulphonic acid (Baytron® P CH8000) and drying at above 100 °C temperatures to remove the residual solvent. The emissive layers have been spin-coated from p-xylol solutions and tempered to eliminate solvent remains. The typical thickness was from 80 to 100 nm.

As a next step the so prepared ITO glass sample is coated with semiconductor-cathode-organic photopolymer. The emissive layer is organic compound. We have made experiments with two different kinds of light-emissive materials: based on Polymer OLEDs (P-OLED) and based on macromolecular layer OLED.

P-OLED device configuration was completed by thermal evaporation of cathode calcium/silver top electrodes (typical 200 nm) at pressures lower than 10^{-6} mbar. On Fig. 5.9 is shown a working structure under μm -scale. Voltage around 5V is applied. The light power is around 200cd/m^2 . After the measurements have been established, it became clear that the achieved resolution is under $1\mu\text{m}$ for lighting stripe and under $1\mu\text{m}$ for pause between two stripes. This means, the minimal theoretical pixel size, can be under $2\mu\text{m}$. The optical measurement shows that theoretical and practical can meet the requirements resolutions for projecting and producing one tree-dimensional sample, based on these technological processes. Extensive life-time tests have not been made, but a 4 week non-stop operation test was successfully completed, suggesting that the devices fabricated by our technology indeed would be reliable and stable in time.

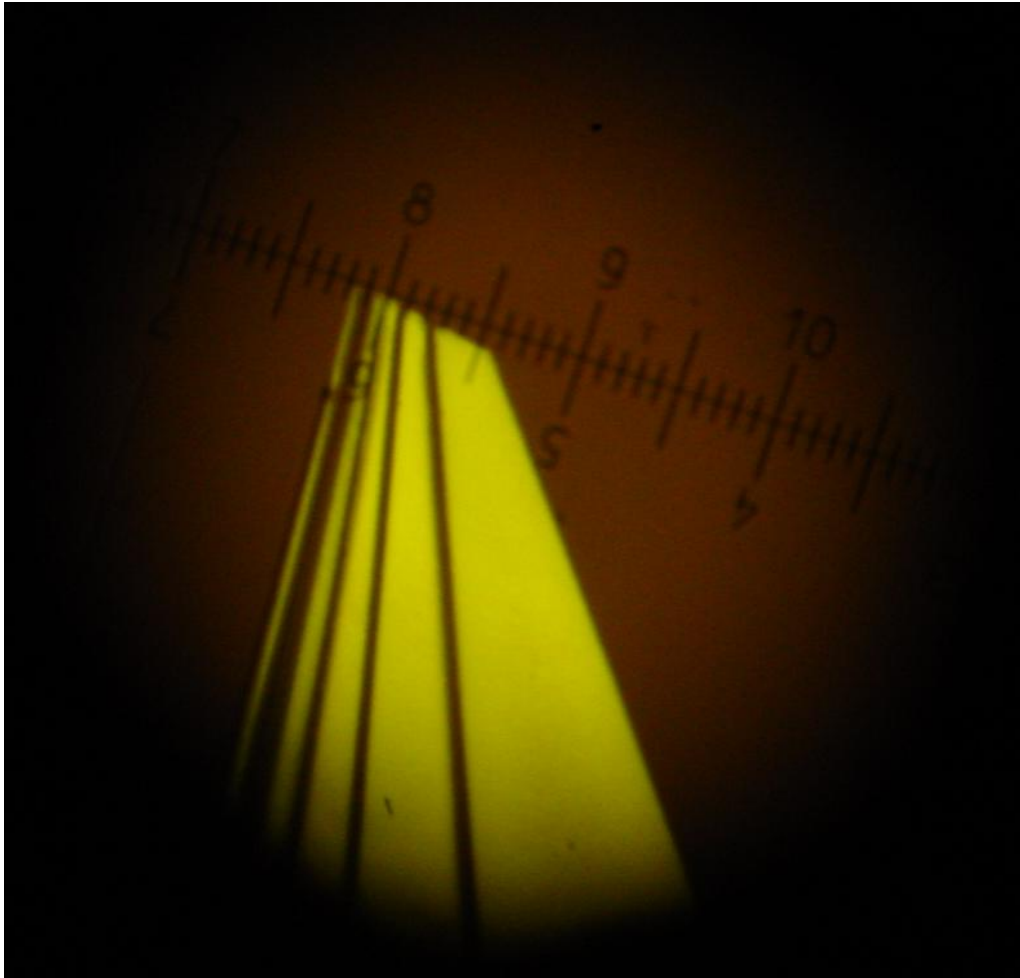


Fig. 5.9 Working P-OLED sample with μm -scale

In contrast to P-OLEDs, macromolecular OLEDs have to operate with a very low current. The used combination is [ITO (100nm) / CuPc (15nm) / Spiro-TAD (45nm) / Alq3 (35nm) / Mg:Al (200nm)] produce relative long lifetime and possibility to change the input voltage in the wide ranges. On Fig. 5.10 are shown parts of test sample with various magnifications. It is clearly obviously that even big defects in the supply circuit, the OLED diode continue its work.

On Fig. 5.11 the electrical and optical characteristics of the macromolecular OLED structure are shown. The optimal operating voltage for such type displays is around 15V.

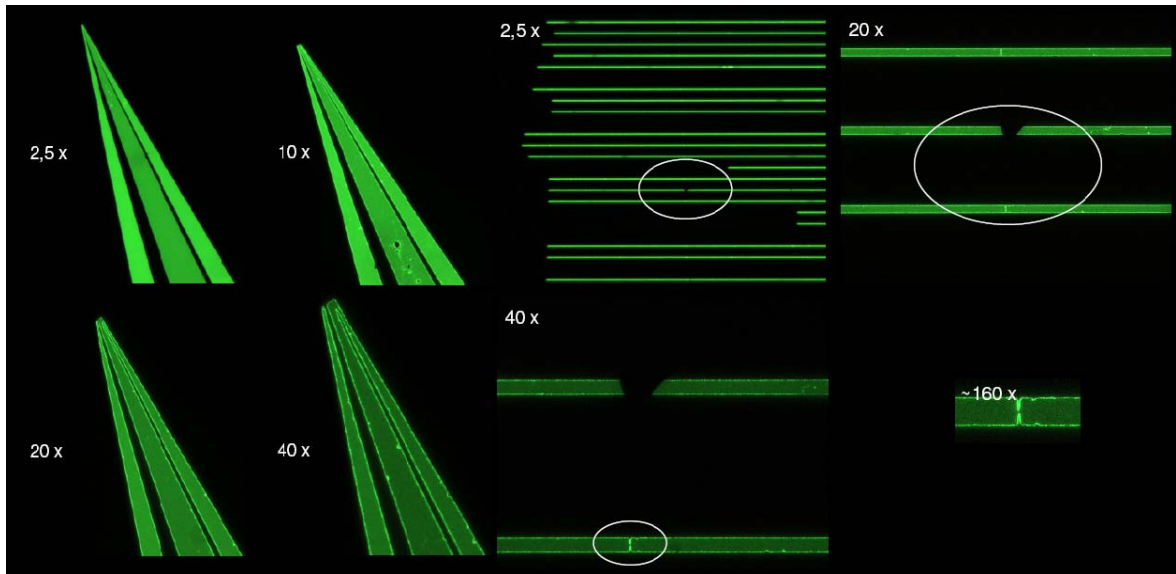


Fig. 5.10 Working OLED samples under optical microscope

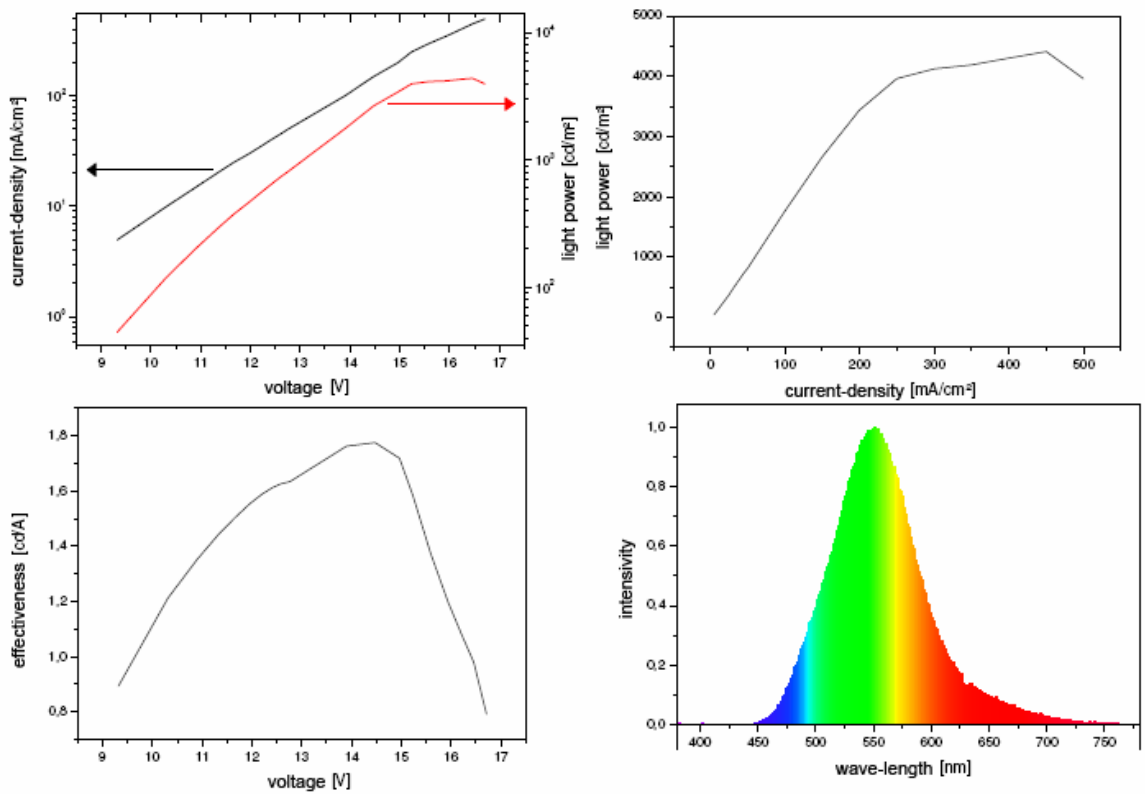


Fig. 5.11 Macromolecular OLED characteristics

As mention above a special contact socket is developed. With the aid of this socket it is possible for the glass to supply the given voltage. A typical setup for

optical measurements is shown on Fig. 5.12. The big advantage of such a standard socket is the possibility of easy replacement of the studded samples.

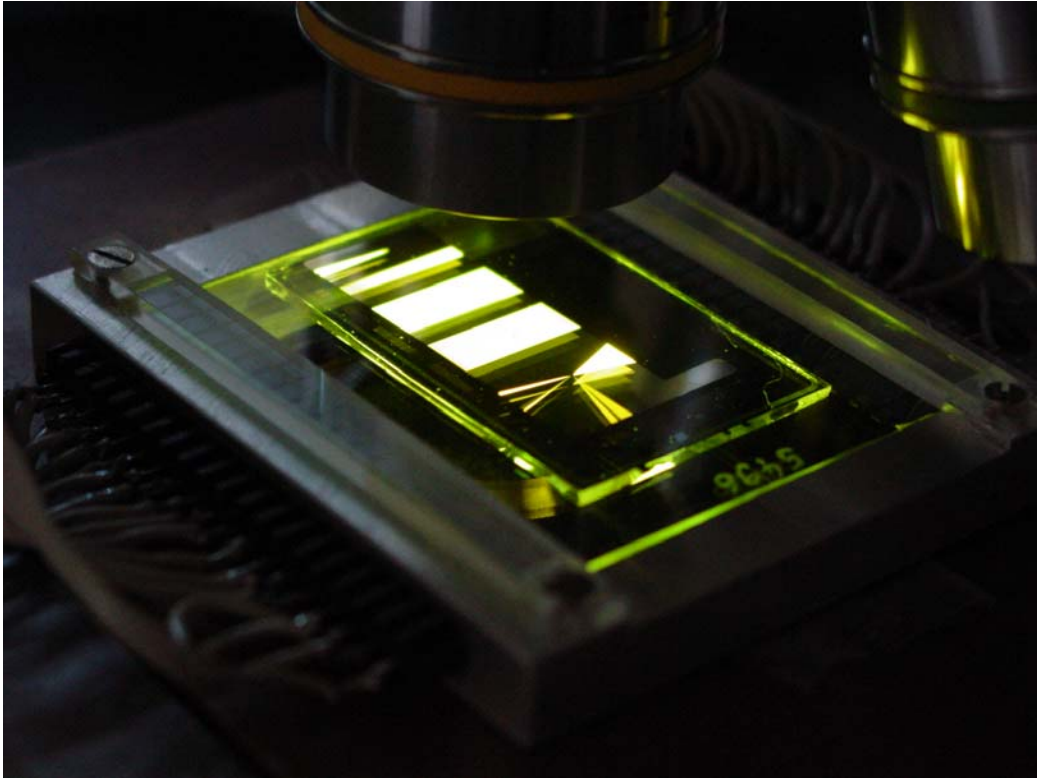


Fig. 5.12 Typical setup for optical measurements

After this first basic investigation is appointed, that with an achieved resolution of better than $2 \mu\text{m}$ pitch (equivalent to $1 \mu\text{m}$ lines and $1 \mu\text{m}$ spaces), the specifications for resolutions have been clearly surpassed by more than 100%. No cross-talk of any kind was observed at this pitch. Therefore, it can be concluded that the resolution limits for this type of display and the employed fabrication technology have not yet been exhausted.

It is proved that the fabrication of high resolution 3D-displays using the presented OLED technology is feasible. Technological limits for the resolution appeared to be much lower than the ones demanded by the specifications.

Furthermore, both brightness (200 cd/m^2) and power consumption (0.03 W/cm^2) already meet today's standards of another display technology.

5.1.2 Sample for determination of the structure homogeneity and reliability

After the determination of the basic parameters in the first step, is important to observe some more parameters. They are connected with surface constancy. For investigating of those parameters is next test sample developed Fig. 5.13.

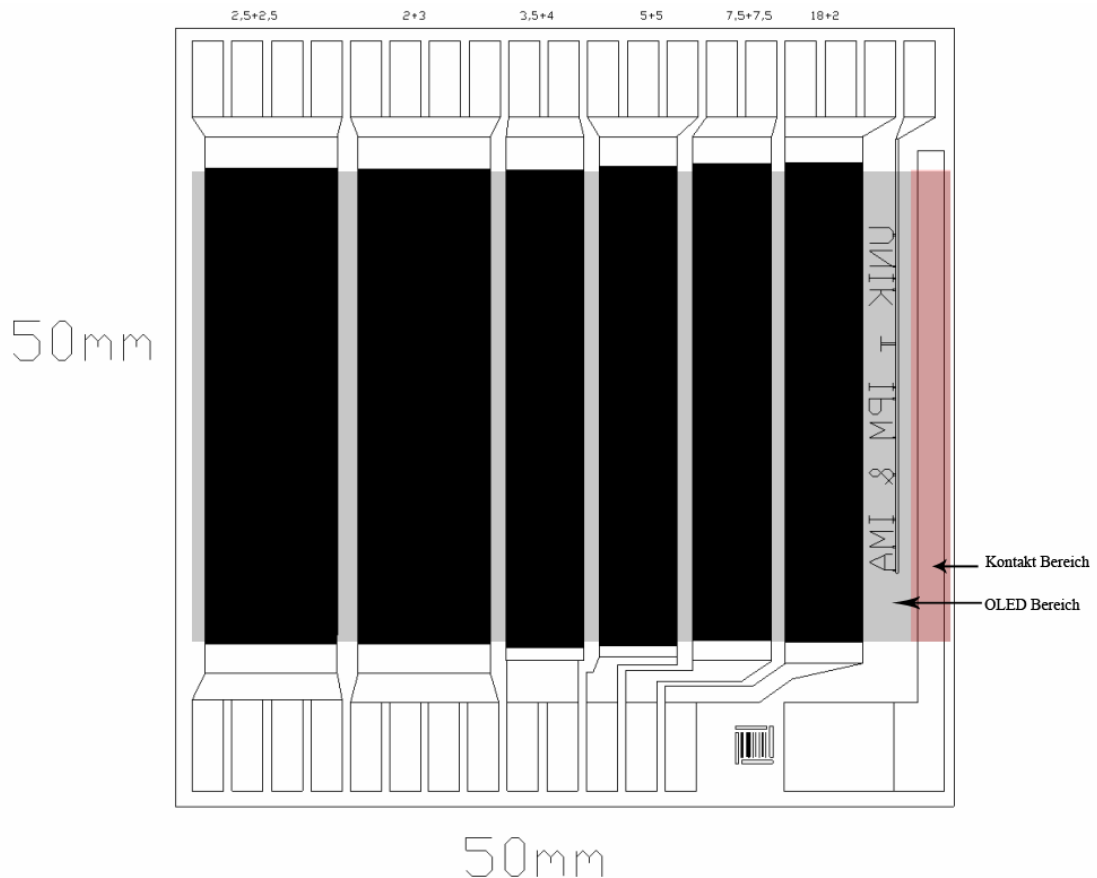


Fig. 5.13 Principal scheme of OLED wafer for surface cleanliness determination

The structures are selected in such a way to increase the sensitivity and detect easily the surface defects. Such defects can be:

- small particles – small pats of rest glass, not completely cleaned after wafer cutting process, particles from the ambiance of the clean room, etc. After cutting the glass in square form are glass particles on the borders of the sample. The cleaning process includes washing in supersonic tub (in Fig. 2.1b and Fig. 5.15d);

- defects of ITO layer – usually the ITO glass have thickness of around 100nm, but can be a little bit less (in Fig. 5.15 c);
- bursting on the structures;
- defects after the photolithography process;
- defects after etch process.

The structures on the sample wafer are designed in a way which enables the detection of defects.(Fig. 5.14). They give us information for the power consumption and the physical size of the supply busses.

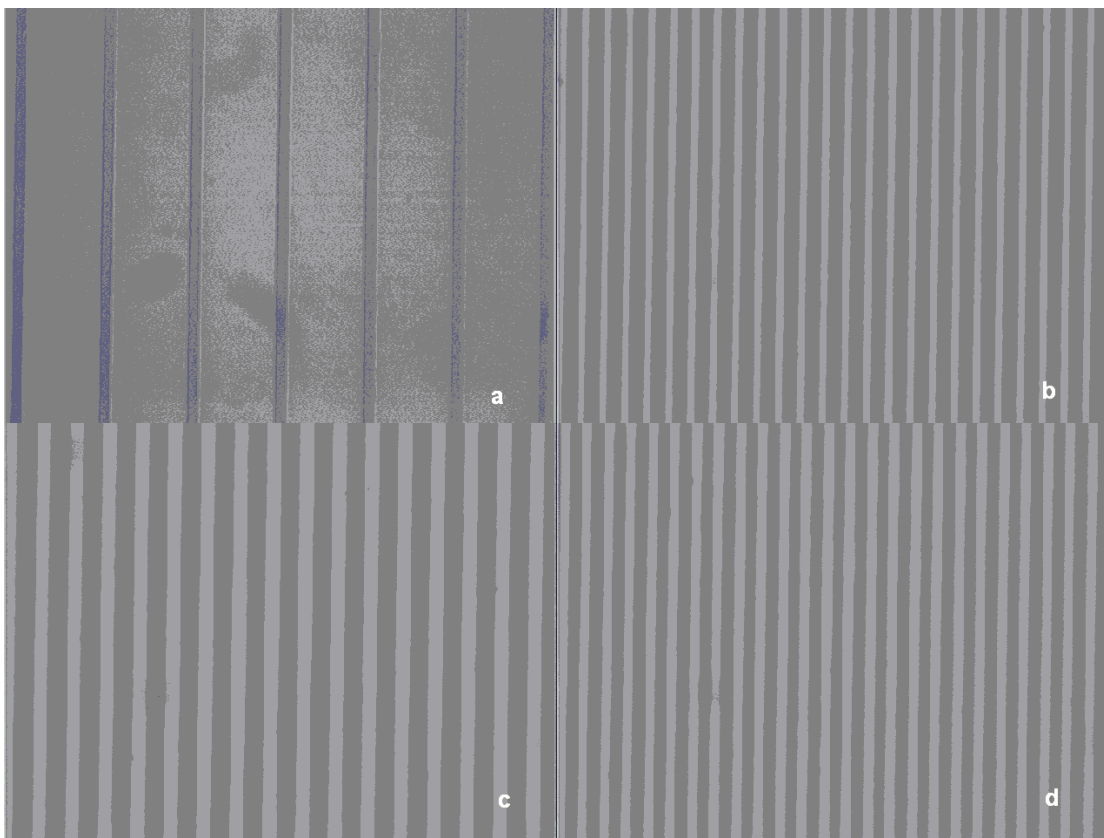


Fig. 5.14 Line structures with different pitches: a) 18µm ITO + 2µm gap; b)3µm ITO +2µm gap; c) 5µm ITO + 5µm gap; d) 2.5µm ITO + 2.5µm gap.

On Fig. 5.15 are shown some types of defects on the glass.



Fig. 5.15 Different types' defects on the test wafer: a) rest glass particle; b) an alien element on ITO; c) defect in ITO; d) glass particle.

5.1.3 3D-Sample – sub pixel arrangements

The next experiment is how to prepare a 3D stereoscopic scene etched on 3,5inch wafer. The scene is synthetic and this means abstract geometric objects are placed on the image. The scene itself is mathematically calculated and generated. The main goal is at first to observe the border limits of this technology regarding 3D human perceives – accommodation; convergence; binocular disparity; linear perspective. The next goal is to learn about the limitations in production process and possibly problems.

The scene parameters are defined at the beginning– number and placement of the objects (Fig. 5.16).

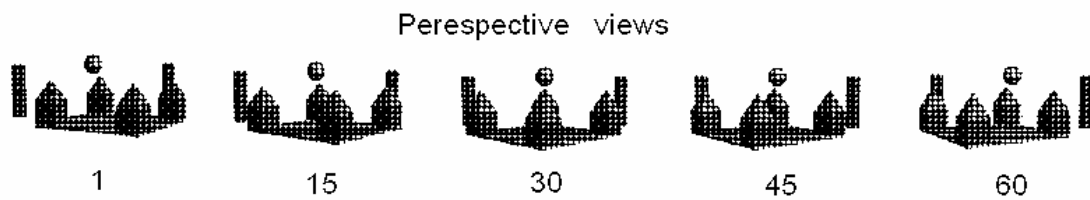


Fig. 5.16 3D scene, viewed from different observer angles (viewing way – from left to right).

They are placed on different distances from the level of the screen. The following measurements are given in the middle of the observer angle (Fig. 5.17):

- The front pyramid is placed 120mm in front of the screen level
- The middle pyramids are placed 20mm in front of the screen level
- The back pyramid is placed -120mm behind the screen level
- The pillars are placed -120mm behind the screen level
- The ball is placed -300mm behind the screen level. This object gives us an extremely big depth of 3D sense.

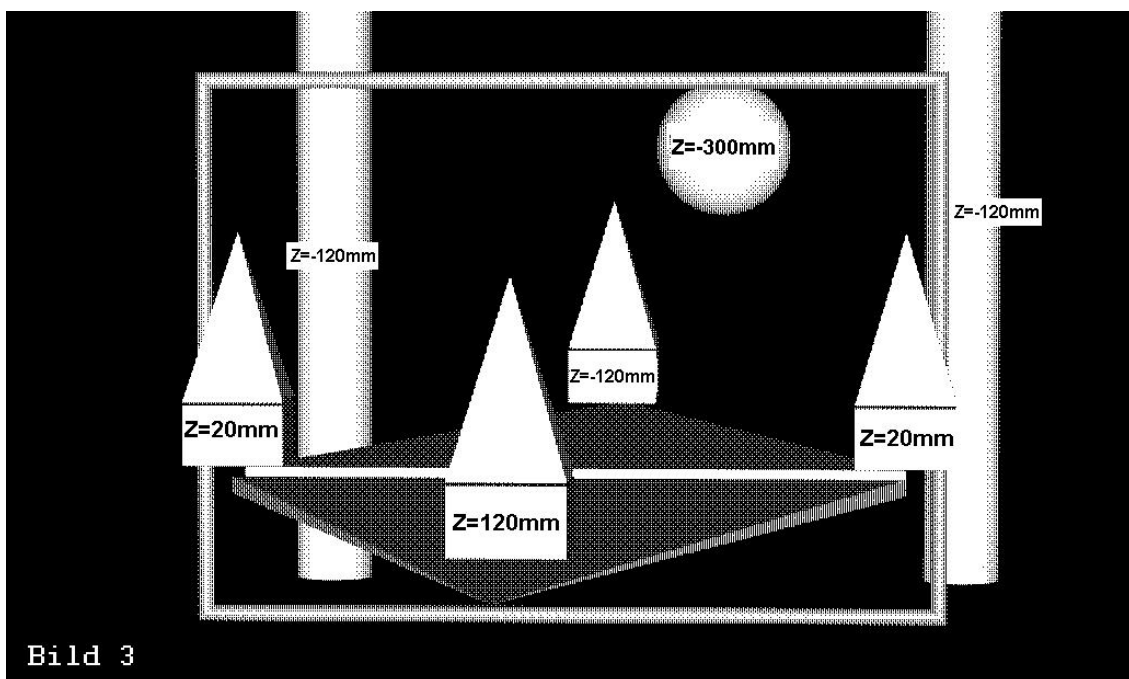


Fig. 5.17 Placement of the objects that are presented in 3D autostereoscopic scene.

The frame is placed exactly of the screen layer.

After the objects are determined, the 3D Studio max scene is designed. The observer angle is 15°, and the optimal distance for viewing is around 300mm.

The observer views are calculated, and with the mixing algorithm, described in chapter 4.1 a 3D autostereoscopic scene is generated.

The projected parameters of display model are:

- dimensions: 45x35 mm;
- pixel pitch: 2,5µm;
- observer angle: 30°;
- optimal distance between observer's eyes and the sample: 300mm;
- number of views: up to 112, situated on 0.25°.

I prepare a special algorithm for minimising of polygons number in the scene. This is necessary, because millions of polygons are generated, and this is a problem for future carrying out of the scene on ITO wafer. The algorithm is given in Appendix 2.

In this case after polygon-minimising algorithm the scene is imported in AutoCAD and is converted into .dxf format for generating a lithography contact mask (Fig. 5.18a).

As contact mask is used the standards socket (Fig. 5.18b), developed especially for this format wafers and described above.

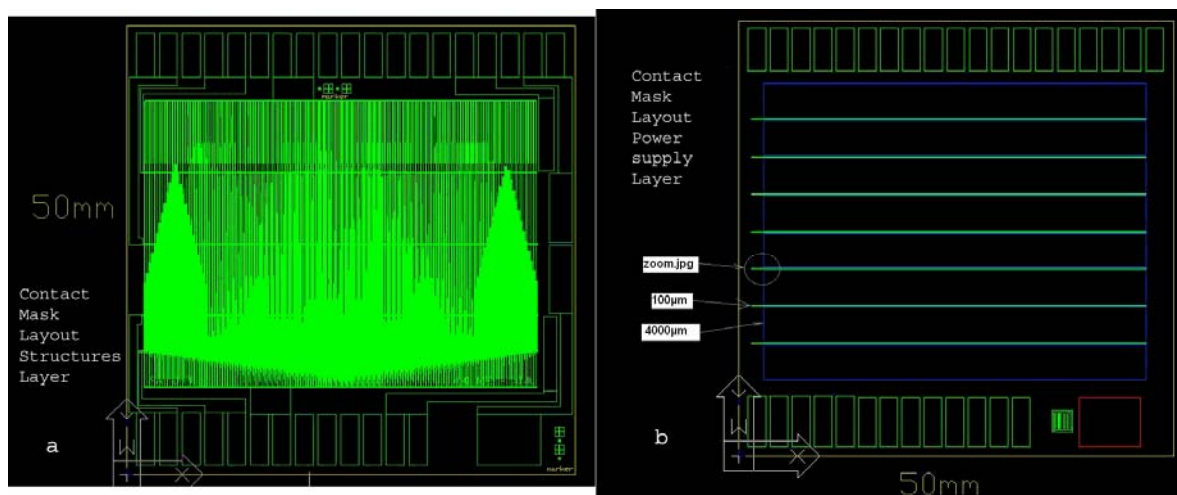


Fig. 5.18. 3D autostereoscopic OLED sample – lithography mask. a) 3D structure mask; b) contact mask.

The power supply lines are divided in five independent areas. These gives us a possibility the broken areas to be switched off by eventual short-circuit,. The next advantage of such a construction is a better distribution of the current. The current in this case is given with the following formula:

$$I = U \cdot y \cdot \int \frac{1}{R \cdot x} dx \quad (5-1)$$

Where:

R is resistance of the ITO layer and is given as (Ω/cm^2). The used from firma Merck ITO glass has impedance $15 \Omega/cm^2$;

- X is the length of the supply line
- Y is the width of the supply line
- U is the voltage, where: $U = 2.5 \div 10V$

There is algorithm for dynamical calculation of these values:

```
double OLED_Res = 15; // Ohm
double fTotalResistance = 0.0;
double fKoeffIncrease = ( BigSide - SmallSide + 1.10-6 )/BottomSide;

if ( ! (fKoeffIncrease <= 0) )
{
    for (int colRes = BottomSide; colRes > 0; colRes--)
    {
        fTotalResistance += OLED_Res / ( fKoeffIncrease * colRes
+ SmallSide );
    }
}
m_dResult = fTotalResistance;
```

Where:

- OLED_Res is the ITO resistance;
- BigSide and SmallSide are the width of the beginning and the end of the power supply line;
- BottomSide is the length of the power supply line;
- M_dResult is the result resistance of the power supply line.

The steps after that – photolithography, etching, metallization are identical as described in chapter 3.2.

The prepared 3D OLED sample is shown on Fig. 5.19.



Fig. 5.19 3D autostereoscopic OLED sample.

After the sample is ready a lenticular raster glass is mounted. There is also a power supply scheme provided, that gives us possibility to change the voltage and the active fields.

As a result a working portable sample kit is provided, that demonstrates a high resolution 3D autostereoscopic OLED display. The achieved resolution is a breakthrough in the 3D display technology. The impressive results show that there will be reasonable future investigations in this direction.

5.1.4 Pixel arrangements with using of additional passive layer

There is another possibility to generate an image with the aid of OLED technology. The working principle is as follows: the complete surface of the muster is covered with lighting substrate - OLED. Only the regions, which correspond to dark areas of the image, are covered with insulating layer. In this case there is no current and the areas stay dark. There is also a possibility to combine the two methods: sub-pixel arrangements and using of additional passive layer.

On the sample picture (Fig. 5.20) is shown the setup configuration. On a) and b) parts are represents ITO glass with etched structures (the vertical lines), and structures placed on additional photo resist layer (the horizontal lines). The result

is shown on c) and d) – the structures shine only where no resist layer is patterned.

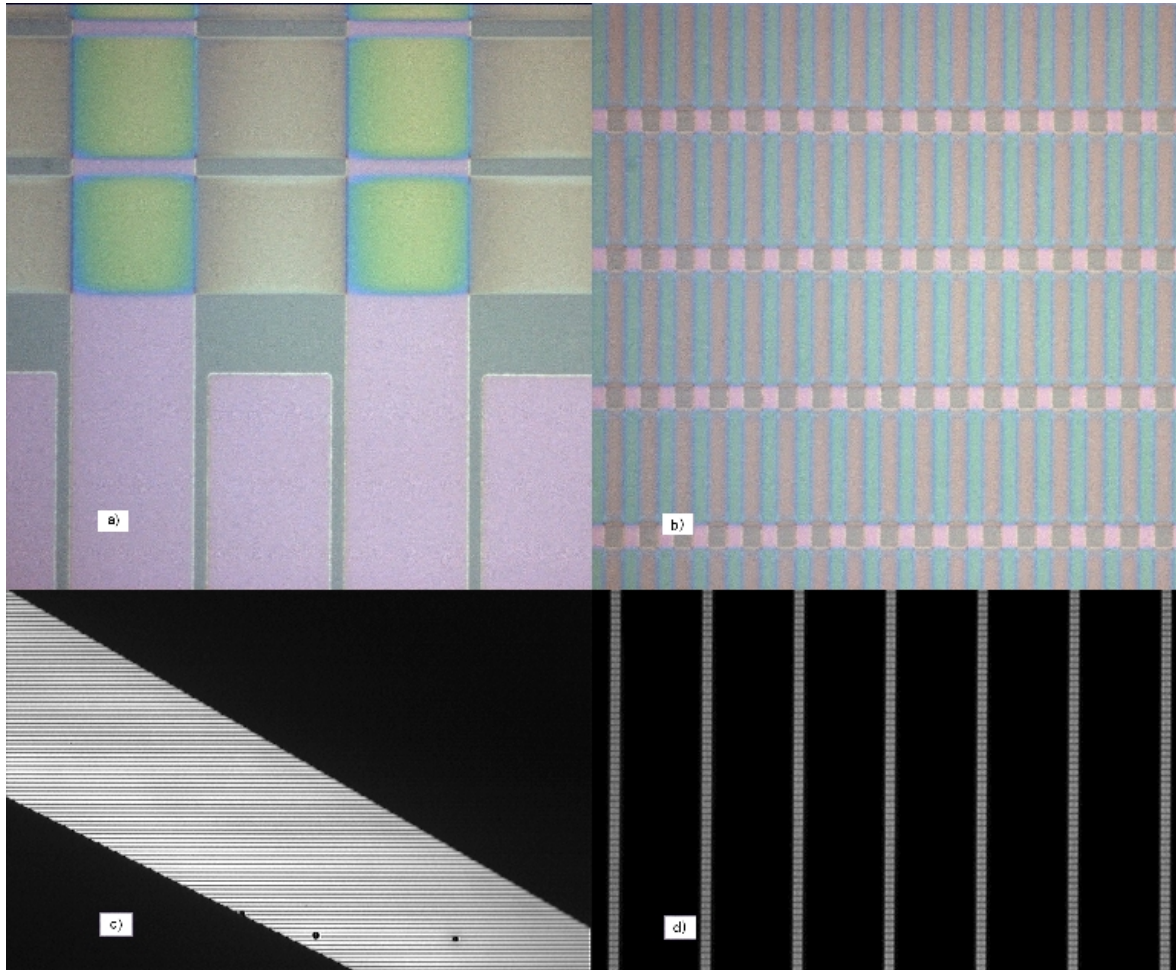


Fig. 5.20 Pixel representation, using additional passive layer. a), b) ITO pixels and additional resist layer; b) c) luminous sample, used passive layer.

5.2 Advantages, problems and limitations.

As has been already mentioned above, such techniques for 3D autostereoscopic image presentation have the advantages that the image is with very high resolution; relatively easy generation of the pixel sequence; very-high resolution, respective very small pixel size. Another advantage is the very easy control of the pixels, as the presented pictures are static or semi-static. It is only necessary a

few voltage-control lines to become a move picture. It is not needed to use a special external controllers and technique for generating the image. This advantages gives us the possibility to use such type of 3D image generation, based on OLED technology for instance in medicine (surgery, dentist-technique, learning processes), advertisement industry, entertainment industry.

On the other hand there are some problems and limitations, using such type of construction. There are two main types:

- problems conditioned from the resolution of the pixels;
- limitations conditioned from the used principle of the image generation.

In problems conditioned by the technology, we can include the possible appearance of moiré effect (chapter 4.2.2) of interference of emitting pixels. Such effects are relevant to human perception of the 3D image.

In limitations conditioned by the used principle of image generation, we can include the partial impossibility of generating movement scenes, or dynamic changes in the image.

5.3 Housing and control of OLED demonstrators.

A working sample of one autostereoscopic 3D display is prepared. At **Fig. 5.21** are shown the OLED samples, housed in transparent box. In a) is shown OLED stripe resolution demonstrator with different pitch distances. In b) is shown the 3D OLED sample with mounted lens-raster glass.

All stuff needed for demonstration and normal working is included inside. The power supply is 9V battery. Through potentiometer the voltage can be adjusted. There are also push-buttons, which switch the element combinations in the OLED samples.

The So -prepared transparent boxes can be carried and demonstrate the working of the system.



Fig. 5.21 a) OLED Stripe Resolution Demonstrator with different pitch distances. b) The 3D autostereoscopic display, housed in box with battery supply and buttons.

5.4 Summary

This chapter presented the basics components necessary for the functioning a OLED display, with a description of the problems and limitations their developement and applicatibility. At and is presented a working sample of 3D scene, and portable demonstrators.

6. Optimisations of the visual quality and suggestions for future development

In natural ambient light, the man's eye accepts better the horizontal and vertical structures as the diagonals. The reason is because the diagonals are seldom meted in nature.

6.1 Active Matrix Organic Light Emissive Diode

OLED technology is considered superior to LCD technology mainly because it's an emissive system, creating its own light rather than relying on modulating a backlight. This means higher contrast, truer colours, crisper motion, and potentially less power consumption. Products with OLED displays have been offered since 1999. However, those displays were all passive-matrix types. Such type passive-matrix OLED displays have one important limitation- they can be made with only a limited number of pixels, due to power-consumption issues.

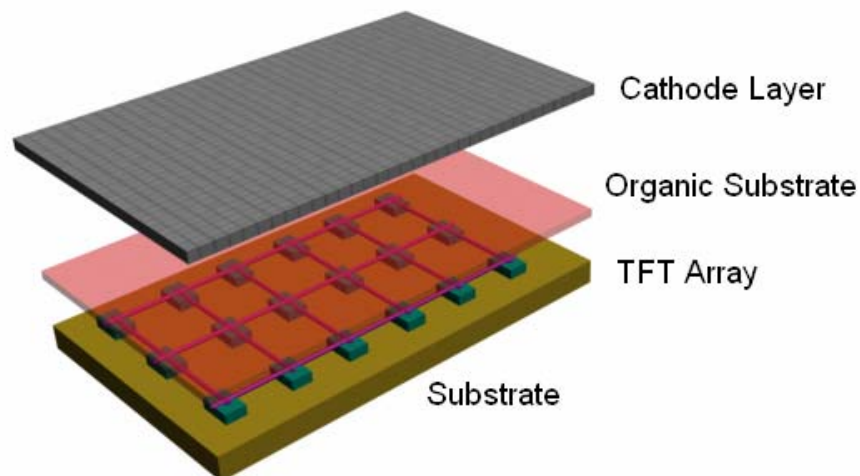


Fig. 6.1 Structure of an Active-matrix OLED Display

Such problem can be solved by using a next generation OLED displays Active-matrix Organic Light Emissive Diode – AMOLED (Fig. 6.1).

Active-matrix OLED displays provide the same beautiful video-rate performance as their passive-matrix OLED counterparts, but they consume significantly less power.

An active-matrix OLED (AMOLED) display consists of OLED pixels that have been deposited or integrated onto a thin film transistor (TFT) array to form a matrix of pixels that illuminate light upon electrical activation. In contrast to a PMOLED display, where electricity is distributed row by row, the active-matrix TFT backplane acts as an array of switches that control the amount of current flowing through each OLED pixel. The TFT array continuously controls the current that flows to the pixels, signalling to each pixel how brightly to shine. Typically, this continuous current flow is controlled by at least two TFTs at each pixel, one to start and stop the charging of a storage capacitor and the second to provide a voltage source at the level needed to create a constant current to the pixel. As a result, the AMOLED operates at all times (i.e., for the entire frame scan), avoiding the need for the very high currents required for passive matrix operation.

Two primary TFT backplane technologies, poly-Silicon (poly-Si) and amorphous-Silicon (a-Si) are used today in AMOLEDs. Next-generation technologies such as organic TFTs (O-TFTs) are also under development. While still in the research phase, O-TFTs are beginning to show promise for use with OLEDs.

- Poly-Silicon TFT Backplane Technology:

Poly-Silicon backplane technology is a technology-of-choice for OLEDs today because it provides excellent mobility that meet OLED current drive requirements. Poly-Si technology also allows for the integration of the drive circuitry directly onto the substrate. There are several key challenges, however, to address: reducing threshold voltage non-uniformities of poly-Si, installing additional manufacturing capacity, and demonstrating commercially-viable manufacturing yields. With these issues resolved, poly-Si AMOLEDs should offer excellent performance as some early-stage prototypes and products suggest.

- Amorphous-Silicon Backplane Technology:

Amorphous-Silicon backplane technology, until recently, had been dismissed as an acceptable backplane technology for OLEDs because the mobility of a-Si was considered too low to meet OLED current drive requirements. In large part due to the development of Universal Display Corporation's high-efficiency PHOLED technology, a-Si is now considered to be a viable backplane technology for

OLEDs. PHOLEDs' lower current density requirement, on the order of a few micro amps (μA) per pixel, makes this possible. The incorporation of red PHOLED pixels alone (with green and blue fluorescent OLED pixels) can reduce the power consumption by 42% compared with an otherwise equivalent all-fluorescent device.

While the long-term stability of a-Si TFTs needs further enhancement for use with OLEDs, a-Si technology offers several potential advantages over poly-Si technology. Existing a-Si capacity is significantly larger because the a-Si process is more mature and less costly. A-Si also currently supports larger substrate sizes (approaching 2 meters x 2 meters) compared with poly-Si capacity that today supports less than 1 meter x 1 meter substrates. Given these factors, a-Si backplanes may lead to less expensive AMOLED displays, particularly for larger size applications. A-Si also requires lower processing temperatures than poly-Si. This may help pave the way for building AMOLEDs on polymer-based flexible substrates earlier than is expected with poly-Si technology.

7. 3D Image coding for real time transmission - suggestion for coding algorithms

7.1 Introduction to media coding algorithms

Our brain acquires depth information from the subtle difference between the picture on the left retina and the picture on the right retina. It is well known that such a pair or multitude of pictures can be acquired with two or more cameras located at horizontally shifted positions. A very simple solution to stereoscopic video transmission is the “simulcast” technique that is based on independently coding between the views. Another possibility is to “group” the perspectives in one frame and after the transmission the perspectives must to be again separated. However, these requires twice or many times (depends from the perspectives number) the conventional monoscopic digital transmission bandwidth. On the other hand, stereoscopic video compression exploits the interrelationship between the views [23].

Efficient digital compression is one of the main issues of stereoscopic video so that a large volume of data can be easily stored or transmitted. Originally, the MPEG-2 video standard was primarily intended for coding of standard TV with good quality in the bit-rate range of 4 to 9 Mbit/sec. However, the scope of the MPEG-2 video standard was expanded to include stereoscopic video as well as video of higher resolutions. The MPEG-2 video standard is partitioned into “Profiles” and “Levels” to support applications for a variety of video signals. The “Profile” specifies tools used for coding and the “Level” specifies the numerical parameters such as image size.

The Multiview Profile (MVP), which is one of the profiles of MPEG-2 video, is the compression standard for stereoscopic video. One of the main features of the MVP is the use of scalable coding tools to guarantee compatibility with the MPEG-2 Main Profile (MP), which is one of the most popular video compression standards used for digital video broadcasting, DVD video, etc. Scalable coding means two or more layers of coding. It consists of a base layer and one or more enhancement layers that contain incrementally more information about the video. In MVP one base layer and one enhancement layer is used. The left eye view is coded as the base layer and the right eye view as enhancement layer. The base

layer video is coded in conformance with the Main Profile. The enhancement layer video is coded with scalable coding tools and exploits the correlation with the base layer video for efficient coding. Therefore, the conventional Main Profile decoder can decode the base layer video coded by a Multiview Profile encoder (backward compatibility), and Multiview Profile decoder can decode a bitstream coded by a Main Profile encoder (forward compatibility).

7.2 Codecs with quality damage

Codecs with quality damage or lossy data compression method is one where compressing data and then decompressing it retrieves data that may well be different from the original, but is "close enough" to be useful in some way.

There are two basic lossy compression schemes:

- In lossy transform codecs, samples of picture or sound are taken, chopped into small segments, transformed into a new basis space, and quantized. The resulting quantized values are then entropy coded.
- In lossy predictive codecs, previous and/or subsequent decoded data is used to predict the current sound sample or image frame. The error between the predicted data and the real data, together with any extra information needed to reproduce the prediction, is then quantized and coded.

In some systems the two techniques are combined, with transform codecs being used to compress the error signals generated by the predictive stage.

MPEG-2 video is optimized for coding of interlaced video adaptive frame/field algorithm is used to dynamically select frame or field mode or field mode for each macroblock. Frame mode has the advantage of coding efficiency for still image areas and the field mode has the advantage of coding efficiency for moving image areas.

In MPEG-2, two picture structures are prepared for coding of interlaced video. With "frame pictures", each interlaced field pair is interleaved together into a frame. With "field pictures", individual consistent fields are divided into macroblocks separately. One of the two picture structures is chosen for coding of each frame.

In frame pictures, frame-motion compensation and field-motion compensation can be chosen for each macroblock. In field pictures, only field motion compensation can be used. In both types of picture structures, two fields of a frame must be coded with the same picture-coding type. In I-field pictures, however, the second field of the frame can be coded as either an I-field picture or a P-field picture.

7.3 Codecs without quality damage

The advantage of lossy methods over lossless methods is that in some cases a lossy method can produce a much smaller compressed file than any known lossless method, while still meeting the requirements of the application.

Lossy methods are most often used for compressing sound, images or videos. The compression ratio (that is, the size of the compressed file compared to that of the uncompressed file) of lossy video codecs are nearly always far superior to those of the audio and still-image equivalents. Audio can be compressed at 10:1 with no noticeable loss of quality; video can be compressed immensely with little visible quality loss, e.g. 300:1. Lossily compressed still images are often compressed to 1/10th their original size, as with audio, but the quality loss is more noticeable, especially on closer inspection.

When a user acquires a lossily-compressed file, (for example, to reduce download-time) the retrieved file can be quite different from the original at the bit level while being indistinguishable to the human ear or eye for most practical purposes. Many methods focus on the idiosyncrasies of the human anatomy, taking into account, for example, that the human eye can see only certain frequencies of light. The psychoacoustic model describes how sound can be highly compressed without degrading the perceived quality of the sound. Flaws caused by lossy compression that are noticeable to the human eye or ear are known as compression artefacts.

8. Conclusions

High resolution 3D autostereoscopic sample based on OLED technology has been developed and demonstrated. In presented work includes the complete process, from the general concept to working prototype, including: a series novel original programming algorithms; generating the contact lithographic masks; patterning of the ITO layer; preparation of working model inclusive mount of suitable lens-raster glass. All results of the developed technology are included in it portable demonstrator.

There are programming algorithms developed for generating of completely new volumetric pixel generation and coding. They are presented in chapter four, and the programming realisations are located in Appendix. The algorithms are breakthrough in till now used for such operations. More at fifteen thousand lines of unique source code are created for solute of the problems. In comparison to the old existing algorithms, the calculation time is reduced up to 100 times. There are also additional supporting algorithms developed. Because of technological reasons is needed to calculate different parameters - minimal ITO receptivity, current in supply lines etc. It is also developed algorithm for generation of synthetic three-dimensional scenes, which are comfortable for analyse of the 3D OLED sample. To minimising of pixel number of an image scene is developed algorithm for analysing and group the proper pixels. Such algorithm reduces very strong the complexity of the lithographic masks i.e. the price and the development time.

For test and demonstrational purposes are make holographic scenes. The scenes are rendered with 3D Studio Max. The pictures, received from the program, are sources for the mixing algorithm.

Resolution of better than 2 μm pitch (equivalent to 1 μm lines and 1 μm spaces), the specifications for resolutions are demonstrated and clearly surpassed by more than 100%. No cross-talk between the pixels is observed. Therefore, it can be concluded that the resolution limits for this type of display and the employed fabrication technology is opening a new horizons for this OLED displays. However the practical needs are not yet exhausted.

It is proved that the fabrication of high resolution 3D-displays using the presented OLED technology is feasible. However, in the future applications this technology will play a key role in the development of new displays

Furthermore, both fundamental parameters of the display, brightness (200cd/m^2) and power consumption (0.03 W/cm^2) already meet today's standards of other display technologies. The relaxed voltage requirements (5 V DC) are very suitable for portable battery powered devices. This is emphasized by our ITO OLED display demonstrator which is powered completely by a standard 9 V dry battery.

Extensive life-time tests have not been fully completed by the time of writing, but a 4 week non-stop operation test was successfully completed, suggesting that the devices fabricated by our technology indeed would be reliable and stable in time.

The prepared 3D- OLEDs display can replace the current technology in many applications due to performance in greater cost-effectiveness.

In chapter eight are presented some suggestions for improving the quality of the display and the way to reduce the power consumption. The last point is significant advantage when the display is used in portable units such cell phones, PDAs, portable game consoles, portable TV sets, etc.

The working samples of this new technology are presented on SID 2005; SID 2006; Electronic Displays, Wiesbaden 2005.

9. Appendixes

Appendix 1 – Description of the test structures

Appendix 1.a. – Description of resolution test samples.

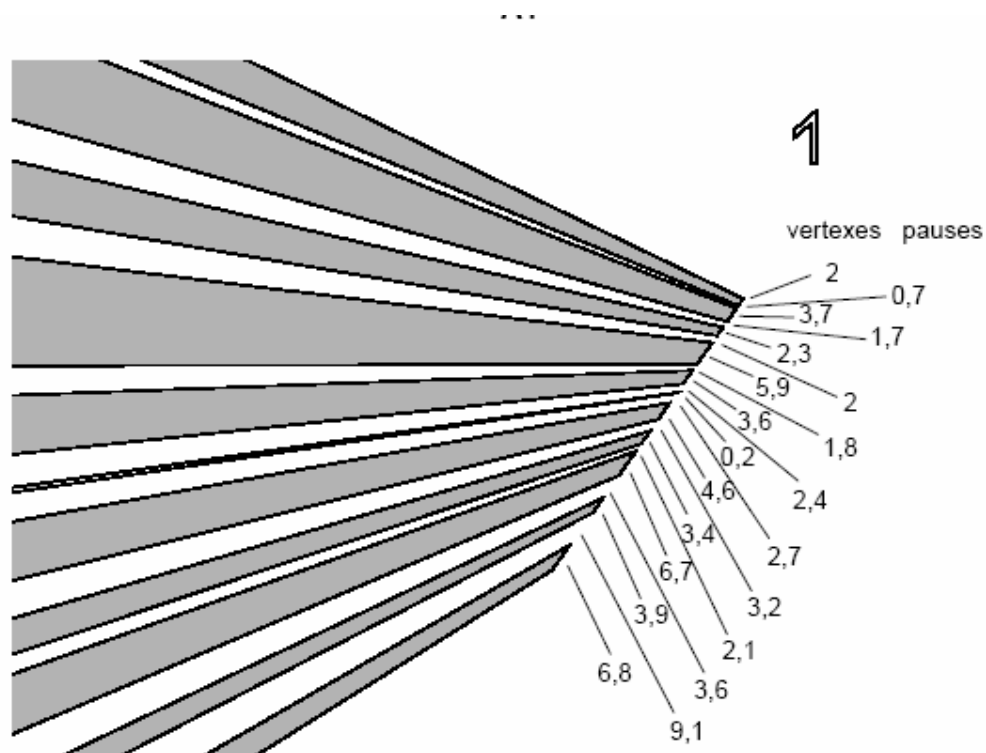


Fig. A 1 Test structure for finding minimal distance between pixels – type 1.

On Fig. A 1 is shown structure for finding out the smallest distances between ITO stripes and smallest ITO stripes. The centre has ITO. The triangles are with dimensions of the side on the border: 1525 μm ; 2000 μm ; 100 μm ; 575 μm ; 1050 μm . The borders around test triangles are with width 1000 μm . Width of “vertexes”, counted from 1 triangle: 2 μm ; 3,7 μm ; 2,3 μm ; 5,9 μm ; 3,6 μm ; 0,2 μm ; 4,6 μm ; 3,4 μm ; 6,7 μm ; 3,9 μm ; 6,8 μm .

Width of “pauses”, counted from 1 triangle: $0,7\mu\text{m}$; $1,7\mu\text{m}$; $2\mu\text{m}$; $1,8\mu\text{m}$; $2,4\mu\text{m}$; $2,7\mu\text{m}$; $3,2\mu\text{m}$; $2,1\mu\text{m}$; $3,6\mu\text{m}$; $9,1\mu\text{m}$.

The different angles toward middle axe determined different distances between sample triangles.

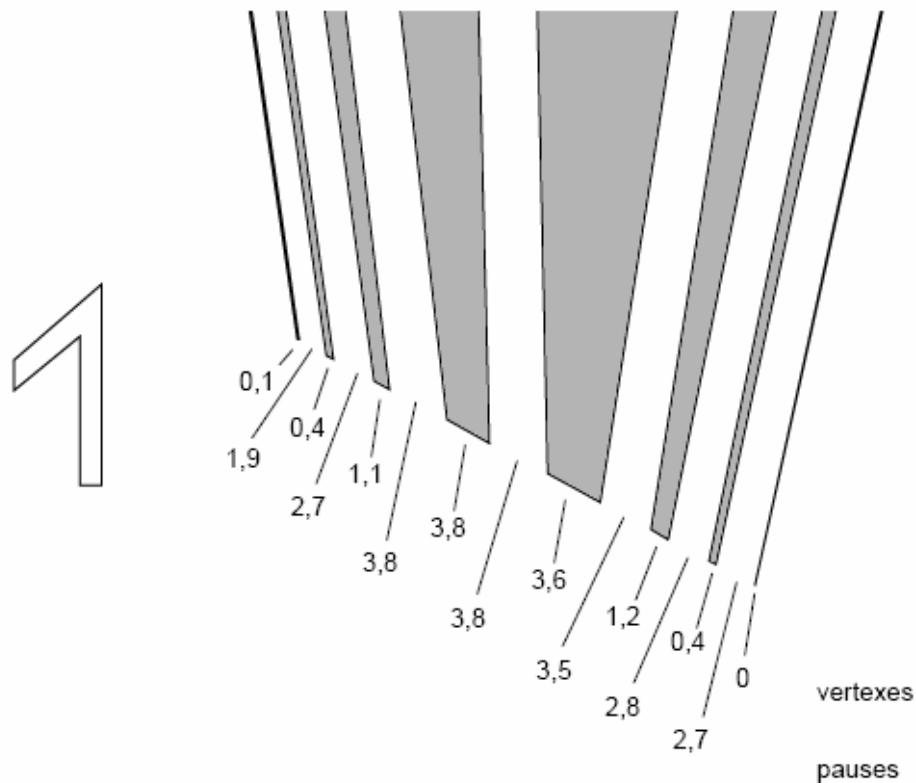


Fig. A 2 Test structure for finding minimal distance between pixels – type 2.

On Fig. A 2 the structures has arrangement Power of 2 - mixed stripe arrangement, going to centre. The width of triangle stripes in the beginning: $50\mu\text{m}$; $200\mu\text{m}$; $800\mu\text{m}$; $3200\mu\text{m}$; $1600\mu\text{m}$; $400\mu\text{m}$; $100\mu\text{m}$; $25\mu\text{m}$.

Width of “vertexes”, counted from 1 triangle: $0,1\mu\text{m}$; $0,4\mu\text{m}$; $1,1\mu\text{m}$; $2,9\mu\text{m}$; $3,6\mu\text{m}$; $1,2\mu\text{m}$; $0,4\mu\text{m}$; vertex.

Width of “pauses”, counted from 1 triangle: $1,9\mu\text{m}$; $2,7\mu\text{m}$; $3,8\mu\text{m}$; $3,8\mu\text{m}$; $3,5\mu\text{m}$; $2,8\mu\text{m}$; $2,7\mu\text{m}$.

Distance between stripes: on outside border - $50\mu\text{m}$.

On Fig. A 3 are shown structures, that hat Power of 2 arrangements. – no mixed stripe arrangement, going to centre. The width of triangle stripes in the beginning: 4000 μm ; 2000 μm ; 1000 μm ; 500 μm ; 250 μm ; 125 μm ; 62 μm ; 31 μm .

Width of “vertexes”, counted from 1 triangle: 28,1 μm ; 7,4 μm ; 3,4 μm ; 1,6 μm ; 1 μm ; 0,7 μm ; 0,3 μm ; vertex.

Width of “pauses”, counted from 1 triangle: 8,4 μm ; 7,3 μm ; 4,8 μm ; 3,7 μm ; 3,6 μm ; 3,3 μm ; 3,1 μm .

Distance between stripes: on outside border - 100 μm .

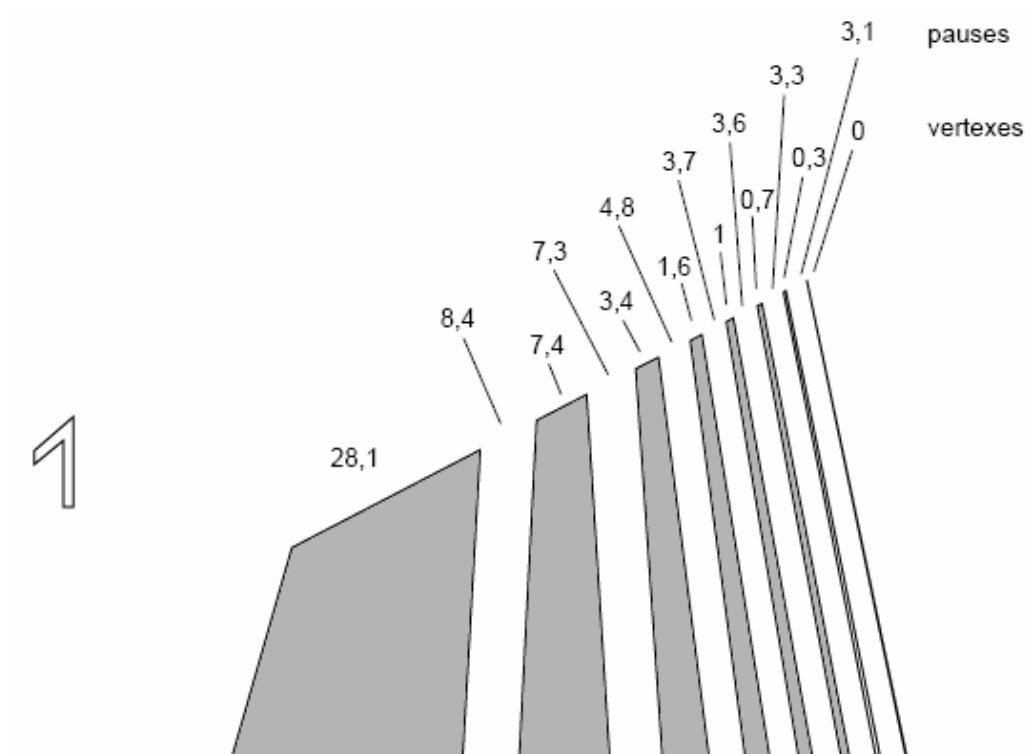


Fig. A 3 Test structure for finding minimal distance between pixels – type 3.

Appendix 1.B. – Description of surface homogeneity test sample.

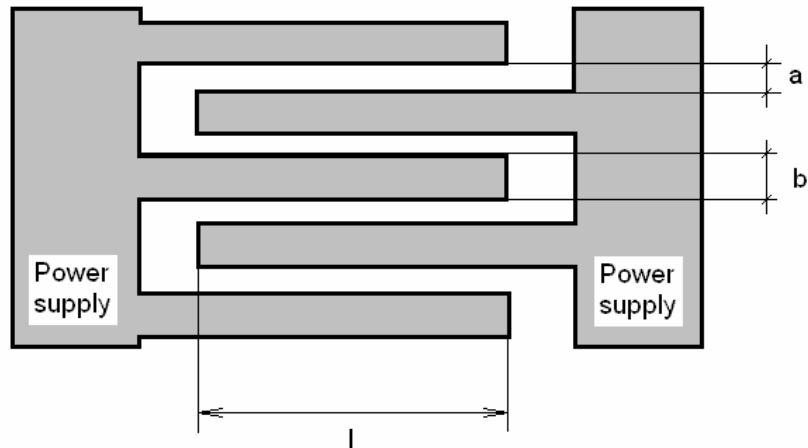


Fig. A 4 Test structure for testing of homogeneity light errors

On Fig A.4 are shown the structures, which examine the homogeneity and the possible mechanical defects, obtained in the produce processes. With “**a**” is mark the gap between ITO lines; “**b**” marks the ITO line width; “**l**” marks the active area length. The used measurements are as follow:

- 2,5 μm ITO + 2,5 μm gap
- 2 μm ITO + 3 μm gap
- 3,5 μm ITO + 4 μm gap
- 5 μm ITO + 5 μm gap
- 7,5 μm ITO + 7,5 μm gap
- 18 μm ITO + 2 μm gap

$l = 2,94 \text{ cm}$ – fixed for all structures.

Appendix 2 – Source codes of algorithms

Function – generating colour space through distribution of pixel parts:

```

----- BEGIN CODE -----

void CCodingThread::CalcBinaryPixels( int COLLENGHT )
{
    for (int k=0; k <= (NBCOL * IDPP); k++)
        for (int cl=0; cl<=4; cl++)
            CMYKBLLine[ICMYKBLLine(k, cl)]=0;

    for (int l=0; l<=(IDPP-1); l++)          //new
        for (int ll=0; ll<=3; ll++)
            IRDC[l][ll]=0;

    for (int k=0; k<=(COLLENGHT-1); k++)
    {

// --- RGB -> CMYK -----

        for (int l=0; l<=2;l++)
        {
            RGBT[l]=( pow ( rgbLine[IrgbLine(k, l)], 2 ) /
255*(1-LIN) + LIN * rgbLine[IrgbLine(k, l)]);
        }
        cmykLine[IcmykLine(k, 3)] = (int)(255 - RGBT[0]);
        for (int l=1; l <= 2; l++)
        {
            if ((255 - RGBT[l]) < cmykLine[IcmykLine(k, 3)])
cmykLine[IcmykLine(k, 3)] = (int)(255 - RGBT[l]);
        }
        for (int l=0; l <= 2; l++)
        {
            cmykLine[IcmykLine(k, l)] = (int)(255 - RGBT[l]-
cmykLine[IcmykLine(k, 3)]);
        }

// --- CODING !!! -----

        if (BLACKDOTS == false) IBLACKDOTS = 0;    else // black
dots ON or OFF
            IBLACKDOTS = (int)(cmykLine[IcmykLine(k,
3)]/255.0*IDPP);
        for (int l=0; l<=2; l++)
            //linear coding ON or OFF
            RGBT[l]=(int)(LIN*rgbLine[IrgbLine(k, l)]+(1-
LIN)* pow ( rgbLine[IrgbLine(k, l)], 2 ) / 255.0);
        for (int l=0; l<=2; l++)
            CD[l]=(255-RGBT[l])/255.0*IDPP-IBLACKDOTS;
        for (int l=0; l<=2; l++)
            IRD[l]=( Signum ( CD[l] - (int)( CD[l] ) -
genrand() ) + 1 ) / 2;
        for (int l=0; l<=2; l++)

```


Random Generator function:

----- BEGIN CODE -----

[randomGen.h]

```

#pragma once

/* A C-program for MT19937: Real number version */
/*  genrand() generates one pseudorandom real number (double) */
/*  which is uniformly distributed on [0,1]-interval, for each */
/*  call. sgenrand(seed) set initial values to the working area */
/*  of 624 words. Before genrand(), sgenrand(seed) must be */
/*  called once. (seed is any 32-bit integer except for 0). */
/*  Integer generator is obtained by modifying two lines. */
/*  Coded by Takuji Nishimura, considering the suggestions by */
/*  Topher Cooper and Marc Rieffel in July-Aug. 1997. */

/* This library is free software; you can redistribute it and/or */
/* modify it under the terms of the GNU Library General Public */
/* License as published by the Free Software Foundation; either */
/* version 2 of the License, or (at your option) any later */
/* version. */
/* This library is distributed in the hope that it will be useful, */
/* but WITHOUT ANY WARRANTY; without even the implied warranty of */
/* MERCHANTABILITY or FITNESS FOR A PARTICULAR PURPOSE. */
/* See the GNU Library General Public License for more details. */
/* You should have received a copy of the GNU Library General */
/* Public License along with this library; if not, write to the */
/* Free Foundation, Inc., 59 Temple Place, Suite 330, Boston, MA */
/* 02111-1307 USA */

/* Copyright (C) 1997 Makoto Matsumoto and Takuji Nishimura. */
/* Any feedback is very welcome. For any question, comments, */
/* see http://www.math.keio.ac.jp/matsumoto/emt.html or email */
/* matumoto@math.keio.ac.jp */

#include<stdio.h>

/* Period parameters */
#define N 624
#define M 397
#define MATRIX_A 0x9908b0df /* constant vector a */
#define UPPER_MASK 0x80000000 /* most significant w-r bits */
#define LOWER_MASK 0x7fffffff /* least significant r bits */

/* Tempering parameters */
#define TEMPERING_MASK_B 0x9d2c5680
#define TEMPERING_MASK_C 0xefc60000
#define TEMPERING_SHIFT_U(y) (y >> 11)
#define TEMPERING_SHIFT_S(y) (y << 7)
#define TEMPERING_SHIFT_T(y) (y << 15)
#define TEMPERING_SHIFT_L(y) (y >> 18)

static unsigned long mt[N]; /* the array for the state vector */
static int mti=N+1; /* mti==N+1 means mt[N] is not initialized */

```

```

class CRandomGen
{
public:
    CRandomGen(void);
    ~CRandomGen(void);

    void sgenrand(unsigned long seed);
    double genrand(void);
};

[randomGen.cpp]
#include "StdAfx.h"
#include "..\randomgen.h"
// #using <mscorlib.dll> // ???

CRandomGen::CRandomGen(void)
{
}

CRandomGen::~~CRandomGen(void)
{
}

// setting initial seeds to mt[N] using
// the generator Line 25 of Table 1 in
void CRandomGen::sgenrand(unsigned long seed)
{
    mt[0] = seed & 0xffffffff;
    for (mti=1; mti<N; mti++)
        mt[mti] = (69069 * mt[mti-1]) & 0xffffffff;
}

double CRandomGen::genrand(void)
{
    unsigned long y;
    static unsigned long mag01[2] = {0x0, MATRIX_A};
    /* mag01[x] = x * MATRIX_A for x=0,1 */

    if (mti >= N) { /* generate N words at one time */
        int kk;

        if (mti == N+1) /* if sgenrand() has not been called, */
            sgenrand(4357); /* a default initial seed is used */

        for (kk=0; kk<N-M; kk++) {
            y = (mt[kk]&UPPER_MASK) | (mt[kk+1]&LOWER_MASK);
            mt[kk] = mt[kk+M] ^ (y >> 1) ^ mag01[y & 0x1];
        }
        for (; kk<N-1; kk++) {
            y = (mt[kk]&UPPER_MASK) | (mt[kk+1]&LOWER_MASK);
            mt[kk] = mt[kk+(M-N)] ^ (y >> 1) ^ mag01[y & 0x1];
        }
        y = (mt[N-1]&UPPER_MASK) | (mt[0]&LOWER_MASK);
        mt[N-1] = mt[M-1] ^ (y >> 1) ^ mag01[y & 0x1];

        mti = 0;
    }

    y = mt[mti++];
}

```

```

y ^= TEMPERING_SHIFT_U(y);
y ^= TEMPERING_SHIFT_S(y) & TEMPERING_MASK_B;
y ^= TEMPERING_SHIFT_T(y) & TEMPERING_MASK_C;
y ^= TEMPERING_SHIFT_L(y);

return ( (double)y / (unsigned long)0xffffffff ); /* reals */
/* return y; */ /* for integer generation */
}
----- END CODE -----

```

Function – generating colour space through dynamic pixel size variation:

```

----- BEGIN CODE -----
void CCodingThread::run( void )
{
    ipm::CImage_TIFF dst;

    ipm::uint dst_width = as->_mixedImage->width();
    ipm::uint dst_height = as->_mixedImage->height();

    PRINTDPI = (double) theApp->getXResolution(); // Get Dpi resolution
    NBCOL = dst_width;

    dPapierColorPitch = 0.528188724; // Colour mask pitch
    iDotsPerColor = (int)( (dPapierColorPitch / 3) * (PRINTDPI / 25.4) ); // dots per color
    dRestDotsPitch = ((dPapierColorPitch / 3) * (PRINTDPI / 25.4)) - iDotsPerColor; // the rest after paper Pitch round

    ipm::uint _uiSlotDepth = 1;
    if( !dst.create( (int)((NBCOL * (iDotsPerColor + dRestDotsPitch) * 3)+1), ( dst_height ), ipm::CImage::BITMAP, _uiSlotDepth ) ) return;

    //create arrays
    rgbLine = new unsigned char[( NBCOL + 1 ) * ( 2 + 1 )];
    CMYKBLLine = new unsigned char[( NBCOL * 4 * (iDotsPerColor + dRestDotsPitch) + 1 ) * ( 3 + 1 )];

    _prgbProgress->setTotalSteps( as->_mixedImage->height() ); // Info for the progress bar

    // generate guide lines - bottom and left:
    for (ipm::uint LineCounter = 0; LineCounter <= as->_mixedImage->height(); LineCounter++)
    {
        TVal = as->_mixedImage->scanLine( LineCounter );

        for (ipm::uint j = 0; j < dst_width * 3; j+=3)
        {
            //if ( LineCounter < 1000 )
            if ( LineCounter < 1 ) // 10?
            {
                rgbLine[IrgbLine(j/3, 0)] = 0; //TVal[j+0]; //B
                rgbLine[IrgbLine(j/3, 1)] = 0; //TVal[j+1]; //G
                rgbLine[IrgbLine(j/3, 2)] = 255; //TVal[j+2]; //R
            }
        }
    }
}

```

```

        else
        {
            if ( j/3 < 1 ) // 15?
            {
                rgbLine[IrgbLine(j/3, 0)] = 0; // R
                rgbLine[IrgbLine(j/3, 1)] = 0; // G
                rgbLine[IrgbLine(j/3, 2)] = 255; // B
            }
            else
            {
                rgbLine[IrgbLine(j/3, 0)] = TVal[j+0]; //R
                rgbLine[IrgbLine(j/3, 1)] = TVal[j+1]; //G
                rgbLine[IrgbLine(j/3, 2)] = TVal[j+2]; //B
            }
        }
    }

    // now code!!
    CalcBinaryPixels( dst_width ); // look below for the
function implementation!

    // -- store row
    ipm::byte *tt; // pointer to target row
    ipm::byte buffer = 0; // buffer
    tt = dst.scanLine( LineCounter ); // all colors - mixed

    double      dCounterRestDotsPitch = 0.0;
    int         iDotsPerColorTemp = 0;
    unsigned int poscount = 0;
    int         bufcount = 0;
    for ( int k = 0; k <= NBCOL * iDotsPerColor - 1; k +=
iDotsPerColor )
    {
        for( int j = 0; j <= 2; j++ ) // color
        {
            // write each color to out picture
            iDotsPerColorTemp = iDotsPerColor;

            // add round error
            dCounterRestDotsPitch += dRestDotsPitch;
            if ( dCounterRestDotsPitch >= 1/*iDotsPerColor*/
)
            {
                dCounterRestDotsPitch--;
                iDotsPerColorTemp++;
            }
            for ( int m = 0; m < iDotsPerColorTemp; m++ )
            {
                CV = CMYKBLLine[ ICMYKBLLine( k + m, j ) ];
                //
                if ( ( CV < 0 ) || ( CV > 255 ) || ( CV ==
0 ) ) buffer = buffer << 1;
                else buffer = ( buffer << 1 ) + 1;

                if ( bufcount >= 7 )
                {
                    bufcount = 0;
                    // store out picture

```



```

        int iBegPosition = (int)((iDotsPerColor - cPixOppened)
/ 2);
        // distribute "transparent" pixels
        for ( int m = 0 ; m <= cPixOppened; m++ )
        {
            CMYKBLLine[ ICMYKBLLine( ( k * iDotsPerColor + m +
iBegPosition ), l ) ] = 0;
        }
        CMYKBLLine[ ICMYKBLLine( ((k+1)*iDotsPerColor-1 ), l ) ]
= 1; // add "black line" to the end of pixel_slot
    }
}

```

----- END CODE -----

Algorithm for converting of a bitmap 3D scene into contact mask script format:

----- BEGIN CODE -----

```

bool CPixel2Polyline::ConvertToPlyline ( void )
{
    bool                bNewPolygone = TRUE;
    double              dPixelSizeVerCounter = 0;
    unsigned int        iBlackPixelCounter = 0;        // count black pixel
sequence (define the polygone size)
    double              iPloygonBegin = 0;                // the
polygon start from iPloygonBegin position
    iNumberPolygons = 0;                // only for
statistik

    bNewPolygone = TRUE;
    for ( int i = 0; i < iColumns /** 8*/; i++ ) // (go to byte) // 8 -
no correction
    {
        unsigned char ucBuffArray = bTempArray[ i ];

        //for ( int j = 0; j < 8; j++) // read each bit in the
current byte
        //{
            if ( ucBuffArray != 255 ) // if it's a black pixel -
check how long is the sequence
            {
                if ( bNewPolygone == TRUE )
                    iPloygonBegin = dColumnsCounter; // <--
there is the problem !!!
                bNewPolygone = FALSE;
                iBlackPixelCounter++;
            }
            else // if it's a white pixel - check for end of
polygone and in case "YES" - write
            {
                if ( bNewPolygone == FALSE )
                {

```

```

        fprintf( ScriptFile, "_pline %.4f,%.4f
%.4f,%.4f %.4f,%.4f %.4f,%.4f Close\n",
                //dColumnsCounter,
                dRowsCounter,
                //dColumnsCounter,
                (dRowsCounter +
dPixelPitch),
                //( dColumnsCounter + dPixelPitch *
(double)iBlackPixelCounter ), (dRowsCounter + dPixelPitch),
                //( dColumnsCounter + dPixelPitch *
(double)iBlackPixelCounter ), dRowsCounter );
                iPloygonBegin,
                dRowsCounter,
                iPloygonBegin,
                (dRowsCounter +
dPixelPitch),
                ( iPloygonBegin + dPixelPitch *
(double)iBlackPixelCounter ), (dRowsCounter + dPixelPitch),
                ( iPloygonBegin + dPixelPitch *
(double)iBlackPixelCounter ), dRowsCounter );

                bNewPolygone = TRUE;
                iBlackPixelCounter = 0;
                iNumberPolygons++; // only
for info
        }
    }
    //ucBuffArray <= 1; // go to the next bit
    dColumnsCounter += dPixelPitch; // go to next column
    dPixelSizeVerCounter += dPixelPitch;
    //}
}

// if the last pixel was black - then close the polygone
if ( bNewPolygone == FALSE )
    fprintf( ScriptFile, "_pline %.4f,%.4f %.4f,%.4f %.4f,%.4f
%.4f,%.4f Close\n",
            iPloygonBegin,
            dRowsCounter,
            iPloygonBegin,
            (dRowsCounter + dPixelPitch),
            ( iPloygonBegin + dPixelPitch *
(double)iBlackPixelCounter ), (dRowsCounter + dPixelPitch),
            ( iPloygonBegin + dPixelPitch *
(double)iBlackPixelCounter ), dRowsCounter );

    dRowsCounter += dPixelPitch; // now go to the next row
    dColumnsCounter = 0; // and zero column in AutoCAD area
    iLineCounter++; // the next row in the input
picture

    return true;
}

```

----- END CODE -----

Appendix 3 Programs screenshots

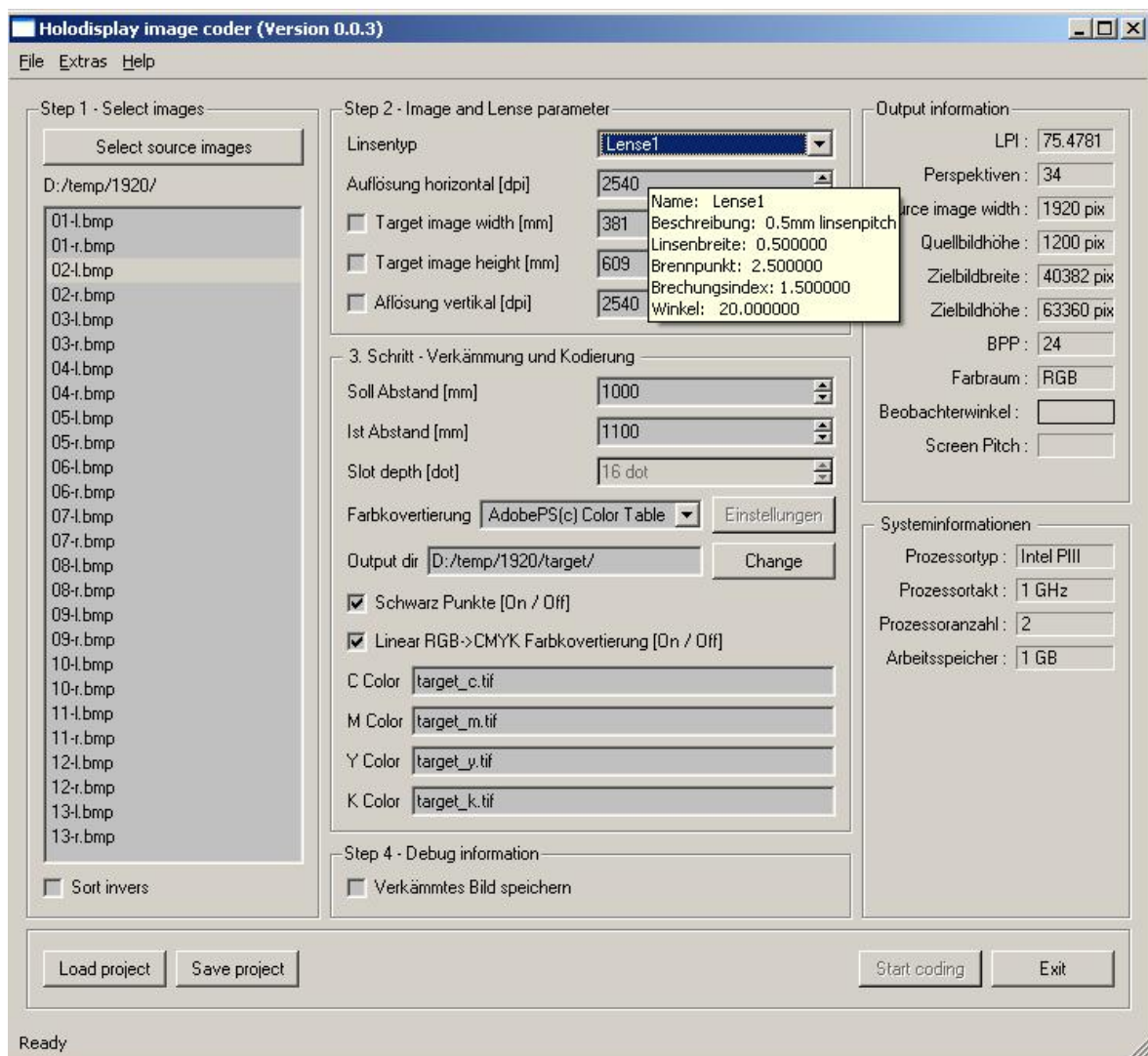


Fig. A 5 Program for generation of autostereoscopic 3D scenes – main screen.

Input parameters are given bitmap images; lens raster parameters; observing parameters.

As output is received either a colour separated scene – CMYK or black pixel coded image for RGB colour mask. The coding can be “dynamic pixel size variation” or “distribution of pixel parts”.

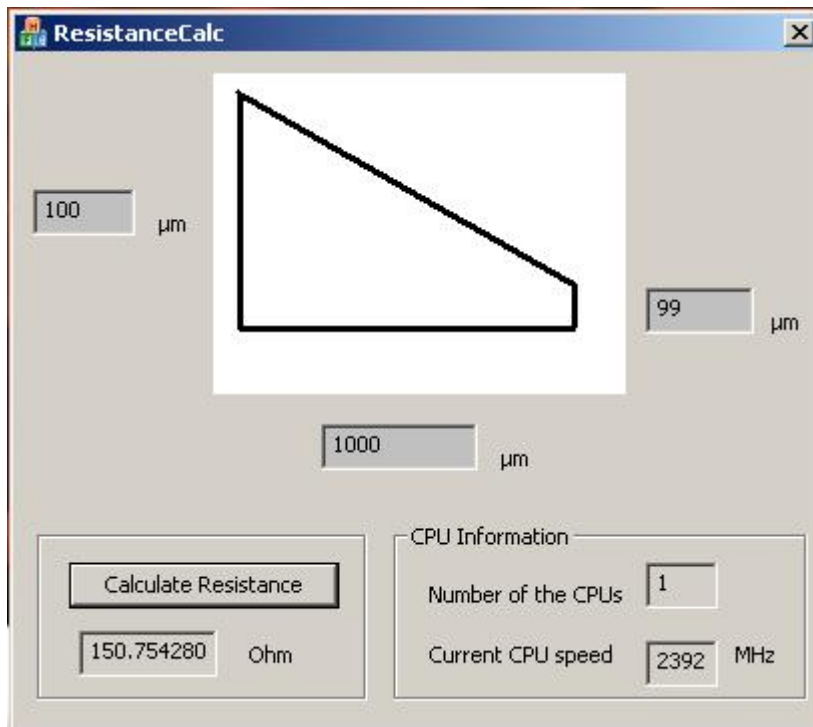


Fig. A 5 Program for calculation of ITO resistance of power supply lines on 3D sample – main screen.

The program calculates the resistance of ITO power supply lines.

Input parameters must be given: the typical resistance of the ITO substrate (given by the manufacture); the length of the line; width of the line. The width of the line can be with different width in the both sides.

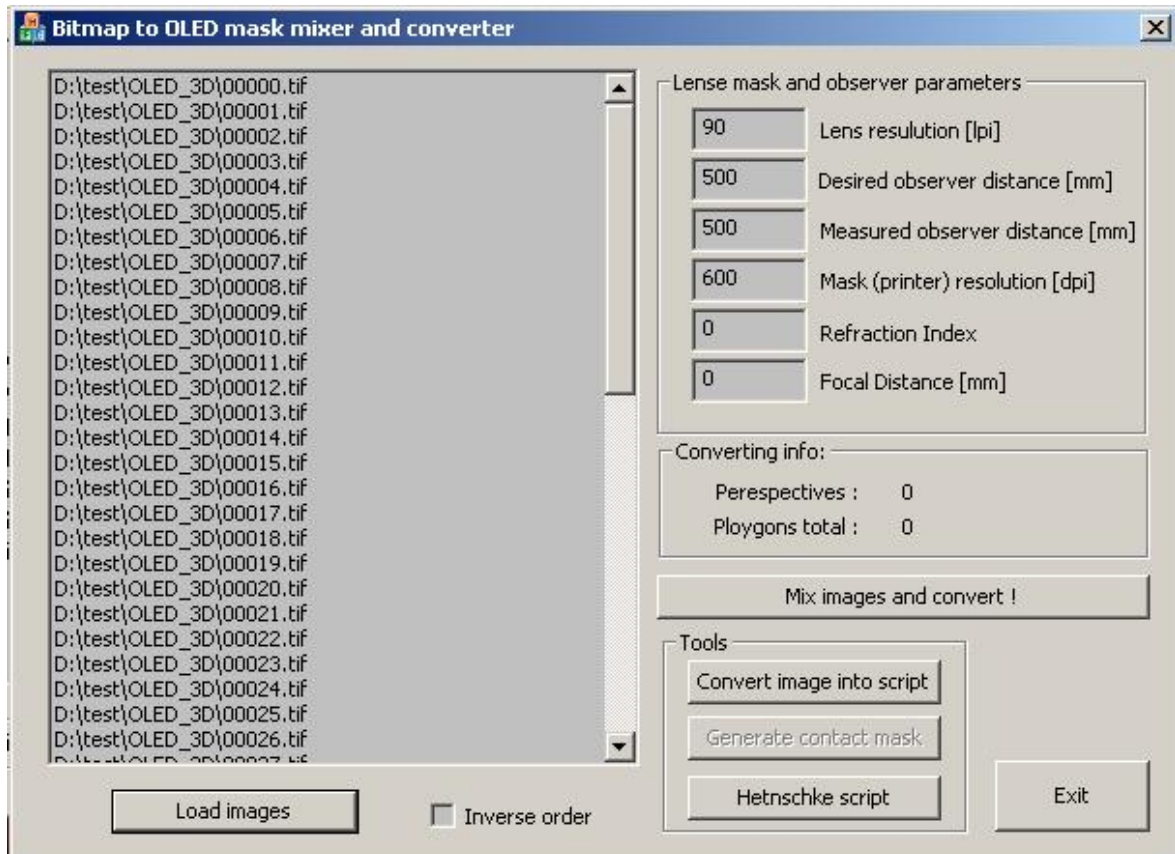


Fig. A 6 Program for calculation of ITO resistance of power supply lines on 3D sample – main screen.

The program imports observer views for generating of an AutoCAD script. The imported views at first are mixed in 3D scene. For mixing parameters are used number of perspectives, lens-raster parameters and observer parameters. After the scene is generated is coded into script. Special algorithm for minimising the number of polygons is implemented. So obtained script, imported in AutoCAD generates a contact photolithographic mask.

Abbreviations, used in the presented dissertation

2D	two-dimensional
3D	three-dimensional
CAD / CAM	Computer Aided Design / Computer Aided Manufacturing
DVD	Digital Versatile Disc
HDTV	High-Definition Television
ITO	Indium Tin Oxide
LCD	Low Consumption Display
MPEG-2	Moving Picture Experts Group
OLED	Organic Light Emissive Diode
PMOLED	Passive Matrix Organic Light Emissive Diode
AMOLED	Active Matrix Organic Light Emissive Diode
OMBD	Organic Molecular Beam Deposition
PLED	Polymer Light Emitting Display
PDA	Personal Digital Assistant
RGB	Red Green Blue
TFT	Thin Film Transistor
O-TFT	Organic Thin Film Transistor
CRT	Cathode Ray Tube
STN	Super-twisted nematic
CCD	Charge-coupled device
TOLED	Transparent Organic Light Emitting Display
XGA	eXtended Graphics Array
RTC	Real Time Clock

References

[1] David F. McAllister, „*Display Technology: Stereo & 3D Display Technologies*“

[2] J. Lipscomb, “Experience with stereoscopic display devices and output algorithms,” *Proc. SPIE: Non-Holographic True 3D Display Techniques*, 1083: pp. 28-34, 1989

[3] David F. McAllister, Ed. *Stereo Computer Graphics and Other True 3D Technologies*, Princeton U. Press, Princeton, NJ, 1993

[4] S. Hentschke, A. Herrfeld “*Hologram Display – Principle, 3-dimensional Representation and Sampling*”

[5] S. Hentschke, “*Stereo-Hologram-Display*” (HOLDISP), PCT/DE-97/02625, (1998).

[6] S. Hentschke, J. Nickel, A. Herrfeld: “*Person-Adaptive Autostereoscopic Shutter- Display (PAAS)*”, IEEE International Conference on Consumer Electronics, Chicago 1997.

[7] R. Börner, “*Autostereoscopic 3-D Imaging by Front and Rear Projection on Flat Panel Displays. Displays*”, Vol. 14, No.1 (1993), pp. 39-46.

[8] I.G. Kazantsev, V.V. Pickalov, “*On the accuracy of Line-, Strip- and Fan-Based Algebraic Reconstruction from Few Projections*”, *Signal Processing* 78, 1999, pp.117-126.

-
- [9] David F. McAllister, Ed., "*Stereo Computer Graphics and Other True 3D Technologies*", Princeton U. Press, Princeton, NJ, 1993
- [10] S. Pastor J. Liu, "*3-D Display and Interaction Technologies for Desktop Computing*", book: B. Javidi, F. Okano, "Three-Dimensional Television, Video, and Display Technologies", Springer (2002)
- [11] Ken Mashitani, Masutaka Inoue, Ryuhei Amano, Syugo Yamashita and Goro Hamagishi, "*15-in. XGA Non-Glasses 3-D Display and Application Systems*", Asia Display 98, pp. 151-156 (1998)
- [12] H. Morishima, H. Mose, N. Taniguchi, K. Inoguchi, S. Matsumura: Proc. SPIE 3295, 193 (1998)
- [13] G.Hamagishi, M. Sakata, A. Yamashita, K. Mashitani, E. Nakayama, S Kishimoto, K. Kanatani: *Proc. Of the 15th International Display Research Conference on Asia Display '95* 791 (1995)
- [14] S. Yano „*Visual Perception of Stereoscopic Images at the Point of Binocular Fusion*“, book: B. Javidi, F. Okano, "Three-Dimensional Television, Video, and Display Technologies", Springer (2002)
- [15] J.-Y. Son „*Autostereoscopic Imaging Systems Based on Special Optical Plates*“, book: B. Javidi, F. Okano, "Three-Dimensional Television, Video, and Display Technologies", Springer (2002)
- [16] H. Isono, M. Yasuda, H. Sasazawa: Japan Display '92 S9-3, 303 (1992)

-
- [17] G. Hamagishi, M. Sakata, A. Yamashita, K. Mashitani, M. Inoe: SID 00 Digest 54.3, 1216 (2000)
- [18] G.R. Ogram, "*Magical images, a handbook of stereo photography*", Stafford, UK (2001)
- [19] R. Börner: Displays 20, 57 (1999)
- [20] Valys N. A. „*Stereoscopy*“, Chapter III
- [21] H. von Helmholtz: *Handbuch der Physiologischen Optik*, Hamburg, Voss, 12866. Trans from 3rd German ed. By J.P.C. Southall, Optical Society of America, 1924/1925. New York: Dover (1962)
- [22] J. J. Gibson: *The Perception of the Visual World* (Houghton Mifflin, New York 1950)
- [23] Belle L. Tseng, Dimitris Anastassiou: „*Compatible video coding of stereoscopic sequences using MPEG-2's scalability and interlaced structure*“, Int. Workshop on HDTV'94, Toronto, (1994)
- [24] C.W. Tang, S.A. Van Slyke, Appl. Phys. Lett. 51 1987 913.
- [25] U. Hoffmann, P. Netuschil, P. Sauer, H.-G. Lotz, A. Koppel, M. Bender, J. Trube, SID International Symposium, Digest of technical paper, vol. 33, No. 2, Boston, USA, 22–23 May 2002, p. 891.
- [26] U. Hoffmann, A. Koppel, J. Trube, J. Schroder, Konferenzband, 16. Electronic Display 2001, No. 2, Wiesbaden, Germany, 6– 7 September 2001, p. 82.

-
- [27] J. B. Eichenlaub: Proc. SPIE 1256, 153 (1990)
- [28] T. Dobbertin, E. Becker, T. Benstem, G. Ginev, D. Heithecker, H.-H. Johannes, D. Metzdorf, H. Neuner, R. Parashkov, W. Kowalsky “*OLED matrix displays: in-line process technology and fundamentals*”, Thin Solid Films 442 (2003) p.132–139
- [29] P.E. Burrows, V. Bulovic, G. Gu, V. Kozlov, S.R. Forrest, M.E. Thompson “*Light emitting devices using vacuum deposited organic thin films*” Thin Solid Films 331 (1998) p.101-105
- [30] V. Bulovic, P. Tian, P.E. Burrows, M.R. Gokhale, S.R. Forrest, M.E. Thompson, Appl. Phys. Lett. 70 (1997) 2954.
- [31] S.R. Forrest, Chem. Rev. 97 (1997) 1793.
- [32] S.R. Forrest, P.E. Burrows, Supramolec. Science 4 (1997) 127.
- [33] V. Bulovic, G. Gu, P.E. Burrows, M.E. Thompson, S.R. Forrest, Nature 380 (1996) 29.
- [34] G. Gu, V. Bulovic, P.E. Burrows, S.R. Forrest, M.E. Thompson, Appl. Phys. Lett. 68 (1996) 2606.
- [35] G. Gu, P.E. Burrows, S. Venkatesh, S.R. Forrest, Opt. Lett. 22 (1997) 172.
- [36] K. Diekmann, W. Jakowetz, F. So, R. Gupta, A. Ingle, D. Henseler, K. Heuser, A. Hunze, G. Gieres, R. Gezzi, W. Rogler, D. Buchhauser, L. Rau, S. Vögele, H.

Becker, A. Büsing, A. Falcou „*Full Color Polymer OLED Displays*“ Displays And Vacuum Electronics 183 (2004)

[37] Brinstock, J et al.; Applied Physic Lett. 78, pp. 3905ff, (2001)

[38] Jabbour, G.E. et al.; Optics & Photonics News 12, pp. 27ff, 2001

[39] C. D. Müller, A. Falcou, N. Reckefuss, M. Rojahn, V. Wiederhirn, P. Rudati, H. Frohne, O. Nuyken, H. Becker, K. Meerholz, „Nature“ 421. pp. 829-833, 2003

[40] K. L. Chopra, S. Major and D. K. Pandya, "*Transparent Conductors - A Status Review*", Thin Solid Films, 102, 1983, pp. 1 – 46

[41] S. A. Bashar and A. A. Rezazadeh, "*Optically Transparent ITO Emitter Contacts in the Fabrication of InP/InGaAs HPTs*", IEEE Transactions on Microwave Theory and Techniques, MTT-43(9), 1995, pp. 2299-2303

[42] G. K. Reeves and H. B. Harrison, "*Obtaining the Specific Contact Resistance from Transmission Line Model Measurements*", IEEE Transactions on Electron Devices, EDL-3(5), 1982, pp. 111 – 113

[43] H. B. Harrison, "*Characterising Metal Semiconductor Ohmic Contacts*", Proceedings of IREE, 41, 1980, pp. 95 - 100

[44] R. E. Williams, "*Wet Etching in Gallium Arsenide Processing Technology*", (Published by: Artech House, Massachussetts) Chapter 5, 1984, pp. 101 - 123

[45] W. Kern and C. A. Deckert, "*Etching Processes in Thin Film Processes*" (Edited by: J. L. Vossen and W. Kern; Published by Academic Press, London) Part V, 1978, pp. 401 - 496

[46] Adrian Jacobs, Jonathan Mather, Robert Winlow, David Montgomery, Graham Jones, Morgan Willis, Martin Tillin, Lyndon Hill, Marina Khazova, Heather

Stevenson, Grant Bourhill, "2D/3D Switchable Displays", Sharp Laboratories of Europe, Ltd.

[47] J. Harrold, D. J. Wilkers, G. J. Woodgate, "Switchable 2D/3D Display – Solid Phase Liquid Crystal Microlens Array"

[48] Graham J. Woodgate, Jonathan Harrold, "Key design issues for autostereoscopic 2D/3D displays", Conference contribution – EuroDisplay 05, September 2005

[49] H. Y. Chen, W. Y. Lam, J. D. Luo, Y. L. Ho, B. Z. Tang, D. B. Zhu, M. Wong, H. S. Kwok, "Highly efficient organic light-emitting diodes with a silole-based compound", Applied Physics Letters, v.81, n.4, 2002

[50] C. F. Qui, L. D. Wang, H. Y. Chen, M. Wong, H. S. Kwok, "High-temperature ultraviolet emission from an organic light-emitting diode", Applied Physics Letters, v. 79, n.14, 2001

[51] H. Chen, J. Chen, C. Qui, B. Tang, M. Wong, Hoi-Sing Kwok, "Efficient and Bright OLED based on Hexaphenylsilole", SID 03 Digest p.509, 2003

[52] H. Riel, S. Karg, T. Beierlein, B. Ruhstaller, W. Riess, "Phosphorescent top-emitting organic light-emitting devices with improved light outcoupling", Applied Physics Letters, v. 82, n.3, 2003

[53] S. E. Shaheen, G. E. Jabbour, B. Kippelen, N. Peyghambarian, J. D. Anderson, S. R. Marder, N. R. Armstrong, E. Bellmann, R. H. Grubbs, "Organic light-emitting diode with 20 lm/W efficiency using a triphenylamine side-group polymer as the hole transport layer", Applied Physics Letters, v. 74, n.21, 1999

[54] K. R. Sarma, C. Chanley, S. Dodd, J. Roush, J. Schmidt, G. Srdanov, M. Stevenson, R. Wessel, J. Innocenzo, G. Yu, M. O'Regan, K. Long, H. Gleskova, S. Wagner, J. C. Sturm, "Active Matrix OLED using 150°C a-Si TFT Backplane Built on Flexible Plastic Substrate", SPIE Proc., Vol. 5080, paper 24, 2003

[55] S. A. Swanson, G. M. Wallraff, J. P. Chen, W. Zhang, L. D. Bozano, K. R. Carter, J. R. Salem, R. Villa, J. C. Scott, "Stable and Efficient Fluorescent Red and Green Dyes for External and Internal Conversion of Blue OLED Emission", Chem. Mater, 25, 2305-2312, 2003

- [56] C. Adachi, M. A. Baldo, M. E. Thompson, S. R. Forrest, "Nearly 100% internal phosphorescence efficiency in an organic light emitting device", *Journal of Applied Physics*, v. 90,n.10, 2001
- [57] R. S. Deshpande, V. Bulovic, S. R. Forrest, "White-light-emitting organic electroluminescent devices based on interlayer sequential energy transfer", *Applied Physics Letters*, v. 75,n.7, 1999
- [58] C. F. Magidan, M.-H. Lu, J. C. Sturm, "Improvement of output coupling efficiency of organic light-emitting diodes by backside substrate modification", *Applied Physics Letters*, v. 76,n.13, 2000
- [59] Z. Shen, P. E. Burrows, V. Bulovic, S. R. Forrest, M. E. Thompson, "Three-Color, Tunable, Organic Light-Emitting Devices", *Science*, vol.276, 1997
- [60] C. F. Lee, "Monolithic CMOS Power Supply for OLED Display Driver/Controller IC", Solomon Systech Ltd., <http://www.solomon-systech.com>
- [61] Z. Chen, B. Cotterell, W. Wang, "The fracture of brittle thin films on compliant substrates in flexible displays", *Engineering Fracture Mechanics* 69, 597-603, 2002
- [62] S. Camou, M. Kitamura, Y. Arakawa, T. Fujii, "Integration of OLED light source and optical fibers on a PDMS based microfluidic device for on-chip fluorescence detection", 7th International Conference on Miniaturized Chemical and Biochemical Analysis Systems, 2003
- [63] Z. Deng, S. T. Lee, D. P. Webb, Y. C. Chan, W. A. Gambling, "Carrier transport in thin films of organic electroluminescent materials", *Synthetic Metals* 107, 107-109, 1999
- [64] M.-H Lu, J. C. Sturm, "External efficiency in planar organic light-emitting devices", *Applied Physics Letters*, v. 78,n.13, 2001
- [65] T. Watanabe, K. Nakamura, S. Kawami, Y. Fukuda, T. Tsuji, T. Wakimoto, S. Miyaguchi, M. Yahiro, M.-J. Yang, T Tsutsui, "Optimization of emitting efficiency in organic LED cells using Ir complex", *Synthetic Metals* 122, 203-207, 2001
- [66] A. Nesterov, G. Paaschi, S. Scheinert, T. Lindner, "Simulation study of the influence of polymer modified anodes on organic LED performance", *Synthetic Metals* 130, 165-175, 2002

-
- [67] C. Qui, H. Chen, Z. Xie, M. Wong, H. S. Kwok, "*Praseodymium oxide coated anode for organic light-emitting diode*", Applied Physics Letters, v. 80,n.19, 2002
- [68] M. E. Thompson, P. E Burrows, S. R. Forrest, "*Electrophorescence in organic light emitting diodes*", Current Opinion in Solid State and Materials Science 2, 369-272, 1999
- [69] B. W. D'Andrade, M. A. Baldo, C. Adachi, J. Brooks, M. E. Thompson, S. R. Forrest, "*High-efficiency yellow double-doped organic light-emitting devices based on phosphor-sensitized fluorescence*", Applied Physics Letters, v. 79,n.7, 2001
- [70] D. Sweetman "*Organic Devices: A Review*", Microelectronic Engineering Research Conference, 2001
- [71] D. J. Millron, I. G. Hill, C. Shen A. Khan, J. Schwartz, "*Surface oxidation activates indium tin oxide for hole injection*", Journal of Applied Physics, v.87, n.1, 2000
- [72] Y. K. Lee, K. M. Kim, J. I. Ryu, Y. D. Kim, K. H. Yoo, J. Jang, H. Y. Jeong, D. J. Choo, "*Comparison Between a-Si:H TFT and Poly-Si TFT for a Pixel in AMOLED*", Journal of the Korean Physical Society, Vol.39, pp. S291-S295, 2001
- [73] D. A. Bernards, T. Biegala, Z. A. Samuels, J. D. Slinker, G. G. Malliaras, S. Flores-Tores, H. D. Abruna, J. A. Rogers, "*Organic light-emitting devices with laminated top contacts*", Applied Physics Letters, v. 84,n.18, 2004
- [74] C.-C Wu, C.-W Chane, Y.-T- Lin, H. L. Yu, J. H. Hsu, T. Y. Luh, "*Programmable organic light-emitting devices*", Applied Physics Letters, v. 79,n.19, 2001
- [75] H. J. Peng, M. Wong, H. S. Kwok, "*Design and Characterization of Organic Light Emitting Diodes with Microcavity Structure*", SID, P-78, 2003
- [76] Martin Pope et Charles E. Swenberg, "*Electronic Processes in Organic Crystals and Polymers*", 2nd ed., Oxford Science Publications, Oxford University Press, New York, 1999

List of publications

1. N. Abedinov, C. Popov, **Zh. Yordanov**, I. W. Rangelow, and W. Kulisch, "*Investigation of the sorption behavior of amorphous nitrogen-rich carbon nitride films as sensitive layers for cantilever-based chemical sensors*", **Applied Physics A 79**, 531-536 (2004).
2. N. Abedinov, C. Popov, **Zh. Jordanov**, Tzv. Ivanov, T. Gotszalk, P. Grabiec, D. Filenko, Yu. Shirshov and I. W. Rangelow, "*Chemical recognition based on micromachined silicon cantilever array*", **J. Vac. Sci. Technology B 21 (6)**, pp.2931-2936, (2003).
3. D. Müller, **Zh. Yordanov**, N. Babadzhanova, F. Müller, E. Fuchs, T. Elle and S. Hentschke "*Multi-user stereoscopic displays*", **Electronic Displays**, (2004)
4. D. Müller, T. Elle, E. Fuchs, F. Müller, **Zh. Yordanov** and S. Hentschke "*High resolution imaging for 3D multi-user displays*", **VDE - Displays and Vacuum Electronics**, (2003)
5. T. Elle, E. Fuchs, M. Steilmann, **Zh. Yordanov**, F. Müller and S. Hentschke „*3D-Displays für Echtzeit-Animationen und höchste Stereoauflösung*“, **CeBIT**, (2003)
6. K.Ivanova, Tzv.Ivanov, B.E. Volland, I.W.Rangelow, **Z.Yordanov**, F.Müller, N. Yordanova, S. Hentschke, A.Wedel, B.Fischer, A.Neugebauer, „*Microsystem Technology for OLED 3D-Displays*“, **Micro Systems, München**, (2005), Poster Award – 1-st place

7. S. Hentschke, F. Müller, **Zh. Yordanov**, N. Babadzhanova, K. Ivanova, Tzv. Ivanov, B.E. Volland, I. W. Rangelow, A. Wedel, B. Ficher, A. Neugebauer, „*High resolution OLED Structures for future 3D Displays*“, **SID** Boston (2005)
8. S. Hentschke, **Zh. Yordanov**, J. Börcsök, “High-resolution 3D OLED Demonstrator”, **SID** Boston (2006)
9. “*3D Monitors for Medicine*”, **CeBIT** 2004
10. 3D-Display des IPM der Universität Kassel auf der EUROMOLD 2003

Curriculum vitae

Name	Zhivko Yordanov
Date of Birth	29 September 1976, Kyustendil, Bulgaria
Family Status	Married Wife: Neli Yordanova Child: Silvia Yordanova
Nationality	Bulgarian
09.1991-05.1995	Technical School in Varna, Bulgaria, profile: Automatic in manufacturing.
09.1995-04.1997	Bulgarian navy.
09.1997-07.2002	Technical University of Varna, department: Computer science.
07.2002	Diploma thesis under the supervision of Prof. Dr. R. Kassing at University of Kassel, Germany. M.Sc. Eng. degree in Computer science from the Technical University of Varna, profiling in Hardware systems and Networks.
01.2003-08.2007	Institute of Peripheral Electronics, University of Kassel – PhD student in digital technique under the supervision of Prof. Dr.-Ing. S. Hentschke.
08.2005	Institute of Computer Architecture and System Programming, University of Kassel – Scientific employer, Prof.Dr.-Ing. J. Börcsök.

Acknowledgments

The printed pages of this dissertation hold far more than the culmination of years of study. These pages also reflect the relationships with many generous and inspiring people I have met since beginning my graduate work. The list is long, but I cherish each contribution to my development as a scholar:

To my advisor Prof.Dr.-Ing Siegbert Hentschke, a gracious mentor who demonstrates that rigorous scholarship can and must be accessible to everyone, that social change is central to intellectual work and, as such, scholars have a responsibility to use the privileges of academia to imagine and create a better world.

To my committee members Prof. Ivo W. Rangelow and Prof. Assen Nedev for their encouraging words, thoughtful criticism, and time and attention during busy semesters.

To my colleagues for sharing their enthusiasm for and help on my work: Thorsten Elle, Eduard Fuchs, Felix Müller, Neli Yordanova, Tzvetan Ivanov, Katerina Ivanova, Burkhard Volland, Chiraz el Borgi, Helmut Görlitz, Klaus Sindellar and Dirk Müller.

To my family, Neli and Silvia, my parents, Yordan and Silviya, and brother Nikolay for their love, support and understanding during the long years of my education.

Declaration: I confirm that I wrote this dissertation by myself and without illegal assistance. I have not used resources other than quoted. All materials taken verbally or logically from published or unpublished scripts are identified. No part of this work is related to another dissertation or attainment of academic rank.

Erklärung: Hiermit versichere ich, dass ich die vorliegende Dissertation selbständig und ohne unerlaubte Hilfe angefertigt und andere als die in der Dissertation angegebenen Hilfsmittel nicht benutzt habe. Alle Stellen, die wörtlich oder sinngemäß aus veröffentlichten oder unveröffentlichten Schriften entnommen sind, habe ich als solche kenntlich gemacht. Kein Teil dieser Arbeit ist in einem anderen Promotions- oder Habilitationsverfahren verwandt worden.